**UNIVERSITÄTSKLINIKUM HAMBURG-EPPENDORF**

Zentrum für Innere Medizin
III. Medizinische Klinik und Poliklinik

Prof. Dr. med Tobias B. Huber

# *Ex Vivo* Modelling of Prenatally Induced Oligonephronia

**Dissertation**

zur Erlangung des Grades eines Doktors der Medizin
an der Medizinischen Fakultät der Universität Hamburg.

vorgelegt von:

Lars Fuhrmann
aus Eutin

Hamburg 2021

**(wird von der Medizinischen Fakultät ausgefüllt)**

**Angenommen von der**

**Medizinischen Fakultät der Universität Hamburg am: 21.01.22**

**Veröffentlicht mit Genehmigung der Medizinischen Fakultät der Universität Hamburg.**

**Prüfungsausschuss, der/die Vorsitzende: Prof. Dr. Catherine Meyer-Schwesinger**

**Prüfungsausschuss, zweite/r Gutachter/in: Prof. Dr. Tobias B. Huber**

**Prüfungsausschuss, dritte/r Gutachter/in: Prof. Dr. Roland Schmitt**

## Table of Contents

International Journal of
*Molecular Sciences*

MDPI

*Article*

# Effects of Environmental Conditions on Nephron Number: Modeling Maternal Disease and Epigenetic Regulation in Renal Development

**Lars Fuhrmann [1], Saskia Lindner [2], Alexander-Thomas Hauser [3], Clemens Höse [2], Oliver Kretz [1], Clemens D. Cohen [4], Maja T. Lindenmeyer [1], Wolfgang Sippl [5], Manfred Jung [3,6], Tobias B. Huber [1] and Nicola Wanner [1,*]**

1 III Department of Medicine, University Medical Center Hamburg-Eppendorf, 20246 Hamburg, Germany; la.fuhrmann@uke.de (L.F.); o.kretz@uke.de (O.K.); m.lindenmeyer@uke.de (M.T.L.); t.huber@uke.de (T.B.H.)
2 Department of Medicine IV, Faculty of Medicine, University of Freiburg, 79106 Freiburg, Germany; saskia.lindner@googlemail.com (S.L.); clemens.hoese@uniklinik-freiburg.de (C.H.)
3 Institute of Pharmaceutical Sciences, University of Freiburg, 79104 Freiburg, Germany; alexander.hauser@pharmazie.uni-freiburg.de (A.-T.H.); manfred.jung@pharmazie.uni-freiburg.de (M.J.)
4 Nephrological Center, Medical Clinic and Policlinic IV, University of Munich, 80336 Munich, Germany; Clemens.Cohen@klinikum-muenchen.de
5 Institute of Pharmacy, Martin-Luther-University of Halle-Wittenberg, 06120 Halle (Saale), Germany; wolfgang.sippl@pharmazie.uni-halle.de
6 CIBSS—Centre for Integrative Biological Signalling Studies, University of Freiburg, 79104 Freiburg, Germany
* Correspondence: n.wanner@uke.de; Tel.: +49-474-103-5337



**Citation:** Fuhrmann, L.; Lindner, S.; Hauser, A.-T.; Höse, C.; Kretz, O.; Cohen, C.D.; Lindenmeyer, M.T.; Sippl, W.; Jung, M.; Huber, T.B.; et al. Effects of Environmental Conditions on Nephron Number: Modeling Maternal Disease and Epigenetic Regulation in Renal Development. *Int. J. Mol. Sci.* **2021**, *22*, 4157. https://doi.org/10.3390/ijms22084157

Academic Editor: Giuseppina T. Russo

Received: 23 March 2021
Accepted: 15 April 2021
Published: 16 April 2021



**Abstract:** A growing body of evidence suggests that low nephron numbers at birth can increase the risk of chronic kidney disease or hypertension later in life. Environmental stressors, such as maternal malnutrition, medication and smoking, can influence renal size at birth. Using metanephric organ cultures to model single-variable environmental conditions, models of maternal disease were evaluated for patterns of developmental impairment. While hyperthermia had limited effects on renal development, fetal iron deficiency was associated with severe impairment of renal growth and nephrogenesis with an all-proximal phenotype. Culturing kidney explants under high glucose conditions led to cellular and transcriptomic changes resembling human diabetic nephropathy. Short-term high glucose culture conditions were sufficient for long-term alterations in DNA methylation-associated epigenetic memory. Finally, the role of epigenetic modifiers in renal development was tested using a small compound library. Among the selected epigenetic inhibitors, various compounds elicited an effect on renal growth, such as HDAC (entinostat, TH39), histone demethylase (deferasirox, deferoxamine) and histone methyltransferase (cyproheptadine) inhibitors. Thus, metanephric organ cultures provide a valuable system for studying metabolic conditions and a tool for screening for epigenetic modifiers in renal development.

**Keywords:** renal development; nephron number; diabetic nephropathy; epigenetic regulation; iron deficiency; DNA methylation

## 1. Introduction

Fetal development is affected by the in utero environment, and an adverse milieu can predispose to diseases such as hypertension, cardiovascular disease and chronic kidney disease later in life [1–4]. A range of intrauterine disturbances can result in a reduction in nephron endowment and compromised renal function in the offspring. In rodents, conditions leading to reduced nephron numbers at birth include intrauterine growth restriction (IUGR), maternal low protein diet, medications (including corticosteroids or nonsteroidal anti-inflammatory drugs), monogenetic mutations and low vitamin A levels, as well as maternal diabetes and iron deficiency [5–10]. In humans, there is currently no

noninvasive method of measuring nephron numbers. However, postmortal studies have demonstrated a negative correlation between nephron numbers and blood pressure [4,11]. Additionally, intrauterine conditions associated with reduced nephron numbers such as IUGR are known to be are associated with increased rates of hypertension and CKD [12].

In vivo experiments where the adverse intrauterine conditions are artificially induced in pregnant animals have proven invaluable for the detection and description of the renal alterations induced in the offspring. However, any experimental intervention during gestation results in complex alterations in the maternal, placental and fetal physiology which may themselves affect the environment of the developing metanephroi. Ex vivo modeling techniques circumvent this by enabling the investigation of kidney development completely separated from the influence of the mother animal, the placenta or other organs of the fetus. Isolated cultures of metanephroi on a medium–air interface were initially performed by Trowell in 1950 [13] and have subsequently been refined by culturing of kidneys on filter membranes [14], providing a basis for single-variable culture conditions.

In summary, there is an increasing body of evidence suggesting that prenatal insults associated with low nephron numbers are relevant risk factors for hypertension and CKD. In order to develop preventative strategies to ensure adequate nephron endowment at birth, a mechanistic understanding of the factors influencing renal development and nephrogenesis is necessary. In the present work, metanephric organ culture was used to model different aspects of environmental regulation to study their effects on renal growth and possible implications for long-term renal function and used to screen for epigenetic regulators using FDA-approved small compounds.

## 2. Results

### *2.1. Use of Metanephric Organ Cultures to Study the Effect of Environmental Conditions on Renal Development*

To model adverse environmental conditions, kidneys from embryonic day (E) 12.5 embryos were cultured at the medium–air interface (Figure 1A). To facilitate monitoring of nephron and glomerular development, Six2.Cre and Pod.Cre dual-fluorescent reporter mice were used, respectively (Figure 1B,C). A common condition during pregnancy is fever, which affects more than 10% of pregnancies during the first 16 weeks of gestation [15]. Heat is a well-characterized teratogen, and hyperthermia during pregnancy has been shown to lead to fetal abortion, growth retardation and developmental defects, such as renal agenesis, hypoplasia and low birth weight in several species [16–21]. To assess the impact of prolonged, fever-range hyperthermic conditions on kidney growth and nephron formation, kidneys were isolated and maintained at either 37 or 40 °C (Figure 1D). After 7 days of culture, kidneys cultured at 40 °C were, on average, 18.36% smaller than their counterparts cultured under physiological conditions (Figure 1E). However, no significant difference in the number of glomeruli per kidney was found between the groups (Figure 1F). Nevertheless, the decreased overall growth of the kidneys demonstrates a negative effect of increased temperature on metanephric growth.

With an estimated 19% of pregnant women suffering from iron-deficiency anemia [22], iron deficiency is one of the most widespread conditions with the potential to disturb renal development [23]. In vivo data have shown that renal growth, glomerular numbers and renal iron uptake are reduced during pregnancies affected by maternal iron deficiency [24]. In order to assess the impact of reduced transferrin-bound iron supply on kidney growth and nephrogenesis, explants were cultured in medium containing 50 µg/mL of iron-saturated holo-transferrin or 50 µg/mL of iron-depleted apo-transferrin, respectively. Iron-restricted kidneys remained much smaller than their iron-sufficient counterparts and showed increased apoptosis in the ureteric buds and reduced ureteric bud branching and proliferation (Figure 1G, Supplementary Figure S1A–F). While the nephron population was morphologically unaffected, a decrease in the developing distal part of the nephron, as well as distal tubules, could be seen (Figure 1H,I, Supplementary Figure S1G–J). The iron-deficient kidneys were, on average, 47.9% of the size of their holo-transferrin cultured counterparts (Figure 1J) and showed a reduction in the overall number of glomeruli per

kidney of 69.9% after 7 days in culture (Figure 1K). Thus, iron depletion by apo-transferrin showed severe effects on kidney growth with an all-proximal nephrogenesis phenotype.

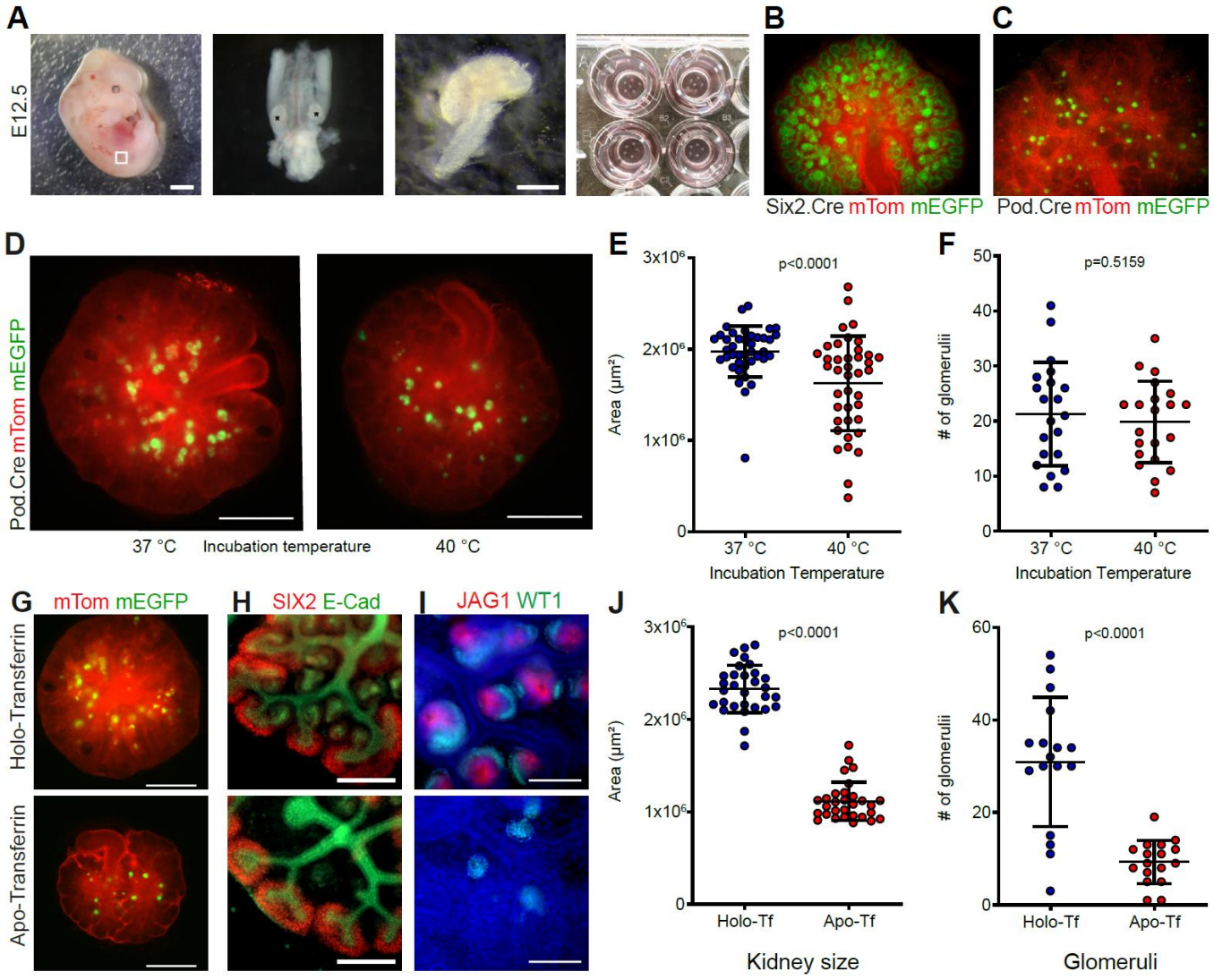


**Figure 1.** Use of metanephric organ cultures to study the effect of environmental conditions on renal development. (**A**) The urogenital ridge from E12.5 mouse embryos (left panel) was microsurgically extracted (second panel), and the kidneys were isolated (third panel) and placed on Transwell inserts (right panel). Scale bars: 1 mm (left panel), 500 µm (third panel). (**B**) Transgenic mice with dual Tomato/EGFP expression were used for conditional labeling of Six2-positive cells and their offspring using Six2.Cre or (**C**) podocin-positive cells using Pod.Cre mice. (**D**) Explants from the same embryo cultured for 7 days at 37 or 40 °C. Scale bars: 500 µm. (**E**) Surface areas of explants grown for 7 days at 37 or 40 °C. n = 40 pairs, paired *t*-test, mean ± SD. (**F**) Number of glomeruli in the explant groups after 7 days. n = 21 pairs, paired *t*-test, mean ± SD. (**G**) Explants from the same embryo cultured for 7 days in medium containing holo-Tf or apo-Tf. Scale bars: 500 µm. (**H**) Widefield images of holo-Tf and apo-Tf cultured explant pair stained against SIX2 and E-cadherin after 48 h of culture show normal progenitor cell pool and defects in early nephron morphology. Scale bar: 100 µm. (**I**) Widefield images of holo-Tf and apo-Tf cultured explant pair stained against WT1 and JAG1. Scale bars: 100 µm. (**J**) Surface areas of holo-Tf and apo-Tf cultured explants after 7 days. n = 30 pairs, paired *t*-test, mean ± SD. (**K**) Number of glomeruli in the explant groups after 7 days. n = 17 pairs, paired *t*-test, mean ± SD.

### 2.2. Ex Vivo High Glucose Exposure Leads to Diabetic Nephropathy-Associated Changes in the Developing Kidney

Maternal diabetes is another common condition during pregnancy, with a global prevalence of hyperglycemia in pregnancy of ~17% and over 20 million live births each year [25]. Diabetes induced in mouse and rat models has been shown to lead to offspring with a lower nephron number [10,26,27]. Metanephric organ culture has been used before to study the effect of high glucose on renal development [27–29]. Previously, we reported reduction in size, nephron number and DNA methylation under high glucose conditions of 55 mM [30]. In contrast to published data [28], no effect on explant size or glomerular number could be seen in our samples when cultured in different 30 mM glucose media compared to 5 mM control conditions after 7 days (Supplementary Figure S2A,B). Furthermore, no decrease in DNA methylation at LINE-1 and major satellite sites could be detected (Supplementary Figure S2C,D). The effect of 55 mM high glucose on renal development after a 7-day period culture was further analyzed, showing a decrease in the growth rate starting at day 3 in culture (Figure 2A,B). Immunofluorescence stainings showed no morphological defects of the SIX2-positive progenitor cell pool (Figure 2C) but showed reduced staining of podocyte marker podocalyxin (PODXL, Figure 2D). The glomeruli were found to contain a thickened glomerular basement matrix visible in histological stainings (Figure 2E). Similar findings were made in electron microscopy, showing an increase in glomerular basement membrane thickness (Figure 2F), one of the earliest markers of prediabetes and diabetic nephropathy (DN) [31,32], in five out of six kidneys and none of seven littermate control kidneys. To further unravel changes in the transcriptome, pairwise differential gene expression (DGE) analysis of kidney cultures from three litters was performed, with one kidney from each embryo cultured with high glucose and the other with control medium and the kidneys pooled for analysis (n = 3). DGE confirmed the upregulation of extracellular matrix components as the primary upregulated biological process (Supplementary Table S1). Downregulated genes were mainly involved in (immune) cell activation and exocytosis/secretion (Supplementary Table S1). Mammalian phenotype ontology indicated abnormal kidney cortex and renal corpuscle morphology due to downregulated genes such as Pdgfb, Podxl, Ren, Ptpro, Mafb and Vegfa (Supplementary Table S1). Renal expression of several genes, such as Angptl4, Spon2 (Mindin), Pappa and Txnip, which have been shown to be upregulated in diabetic nephropathy [33–36], was found to be increased under hyperglycemic conditions. To compare the high glucose kidney culture gene expression profile to human DN, the DGE data were matched to human data from microdissected glomeruli and tubules from diabetic nephropathy patient biopsies from the European Renal cDNA Bank (ERCB). From the 216 differentially regulated genes matched after batch analysis, 94 genes were correspondingly differentially regulated in the glomerular and/or tubular fractions (Figure 2G). The overlap of our model and human DN genes showed 40 out of 95 genes upregulated in the glomeruli and 34 genes in tubules (25 genes in common) (Figure 2H). The genes were mostly involved in extracellular matrix organization (COL4A5, COL4A6, COL8A2, LAMB3, LAMC3) and cell adhesion (ITGBL1, CLDN15). Additionally, diabetes-associated genes such as TXNIP, SPON2 and PAPPA were upregulated. Out of 120 downregulated genes from the kidney cultures, 22 were also downregulated in the glomeruli and 39 were also downregulated in the tubules (16 in common (Figure 2I). These genes were involved in response to endogenous stimulus (BMP2, KLF15, JUNB, CTSB), nephron epithelium development (PTPRO, PODXL, VEGFA) and positive regulation of endothelial cell chemotaxis (LGMN, P2RX4, VEGFA). Additionally, diabetes-associated genes such as RASGRP3, SIRPA, GATM and ESM1 were downregulated [37–39]. Differentially regulated genes not overlapping with ERCB data also reflected diabetes-associated changes, such as extracellular matrix (ANGPTL4, TNN, DPT, COL9A2) or gestational diabetes (LAT2, HP, CXCL10, CD86, CD68, REN, SLC2A3, VCAM1). Thus, renal development under high glucose conditions displayed remarkable similarities to human adult diabetic nephropathy.

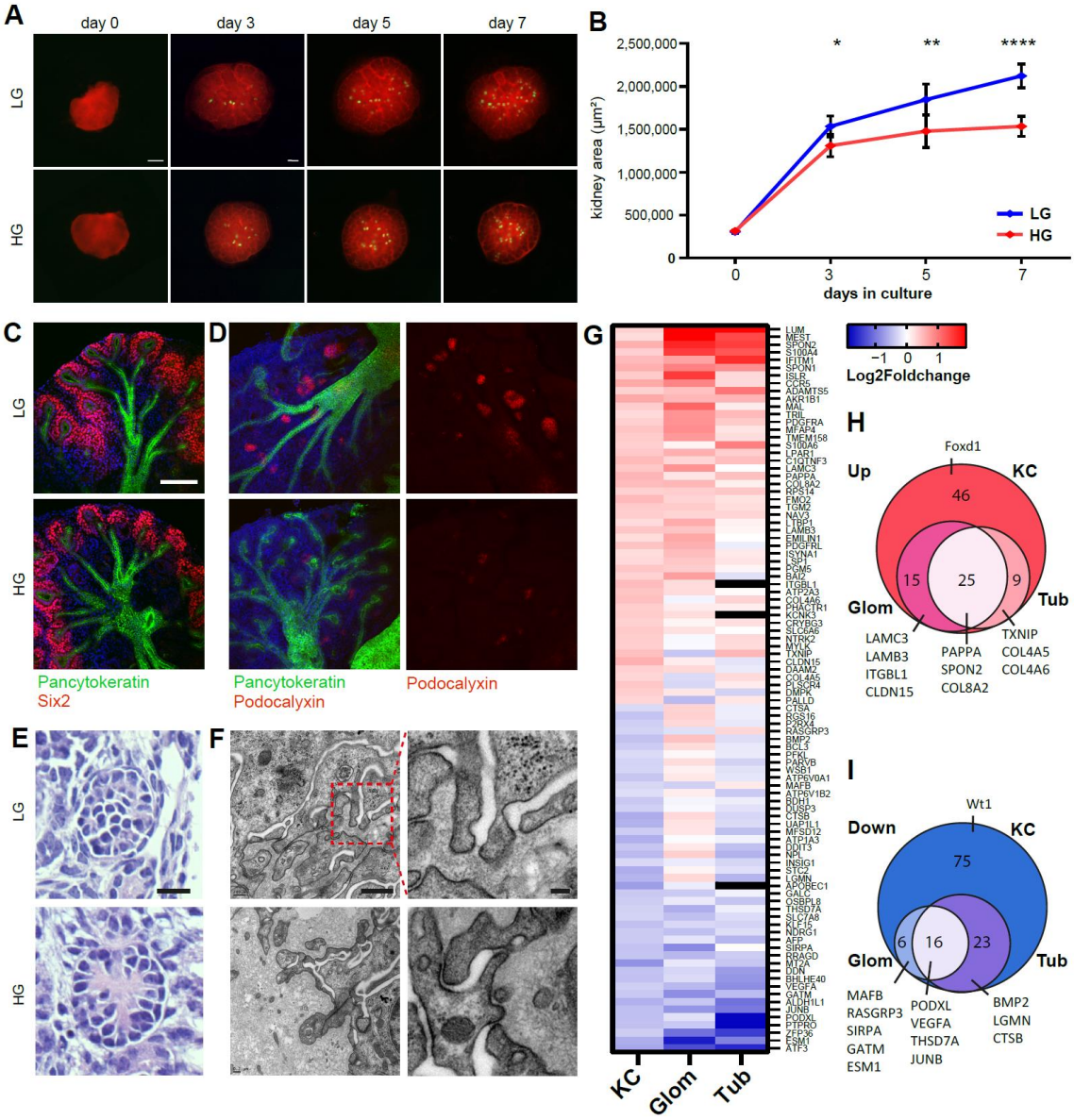


**Figure 2.** Ex vivo high glucose exposure leads to diabetic nephropathy-associated changes in the developing kidney. (**A**) Embryonic kidneys from Pod.Cre;Tomato/EGFP animals cultured for 7 days in low glucose (LG, 5.5 mM α-D-glucose, 55 mM mannitol) or high glucose (HG, 55 mM α-D-glucose) conditions. Scale bar: 500 µm. (**B**) Kidney surface area of HG and LG conditions. *, $p = 0.0474$; **, $p = 0.0052$; ****, $p < 0.0001$. Paired *t*-test, mean ± SD. (**C**) Confocal immunofluorescent stainings of day 7 kidney cultures against Six2 and (**D**) podocalyxin with pan-cytokeratin and Hoechst. Scale bar: 100 µm. (**E**) Stainings of 6 µm sections from day 7 kidney cultures. Scale bar: 20 µm. (**F**) Transmission electron microscopy of sections from day 7 kidney cultures. Glomerular basement membranes are thickened in kidneys exposed to high glucose conditions. Left column: magnification showing podocyte foot processes. Scale bars: 500 nm (left panels), 100 nm (right panels). (**G**) Fold change of RNA-seq data from HG compared to LG kidneys and ERCB diabetic nephropathy (DN) patient microarray data from microdissected glomeruli and tubules showing differentially expressed genes. (**H**) Genes upregulated in the kidney cultures (KC) overlapping with ERCB DN patient data and selected genes highlighted. (**I**) Genes downregulated in the kidney cultures (KC) overlapping with ERCB DN patient data and selected genes highlighted.

### *2.3. Ex Vivo High Glucose Exposure Influences to Long-Term Memory Formation via DNA Methylation*

To further understand the molecular changes mediated by a hyperglycemic environment, kidney cultures were grown at high glucose conditions for 3.5 days and then changed to low glucose conditions for the same amount of time (Figure 3A). Remarkably, incuba-

tion under physiological conditions after the shorter incubation period in high glucose medium did not reverse growth reduction after 7 days in culture with the cultures growing at the same rate as under continuous high glucose treatment (Figure 3B). Furthermore, DNA methylation showed hypomethylation of LINE-1 element and major satellite loci (Figure 2C,D), as well as sustained DNA hypermethylation of the Ppargc1a promoter, under both high glucose and reversed conditions (Figure 3E), indicating the formation of metabolic memory via DNA methylation due to the earlier adverse environmental conditions as a means of fetal programming.

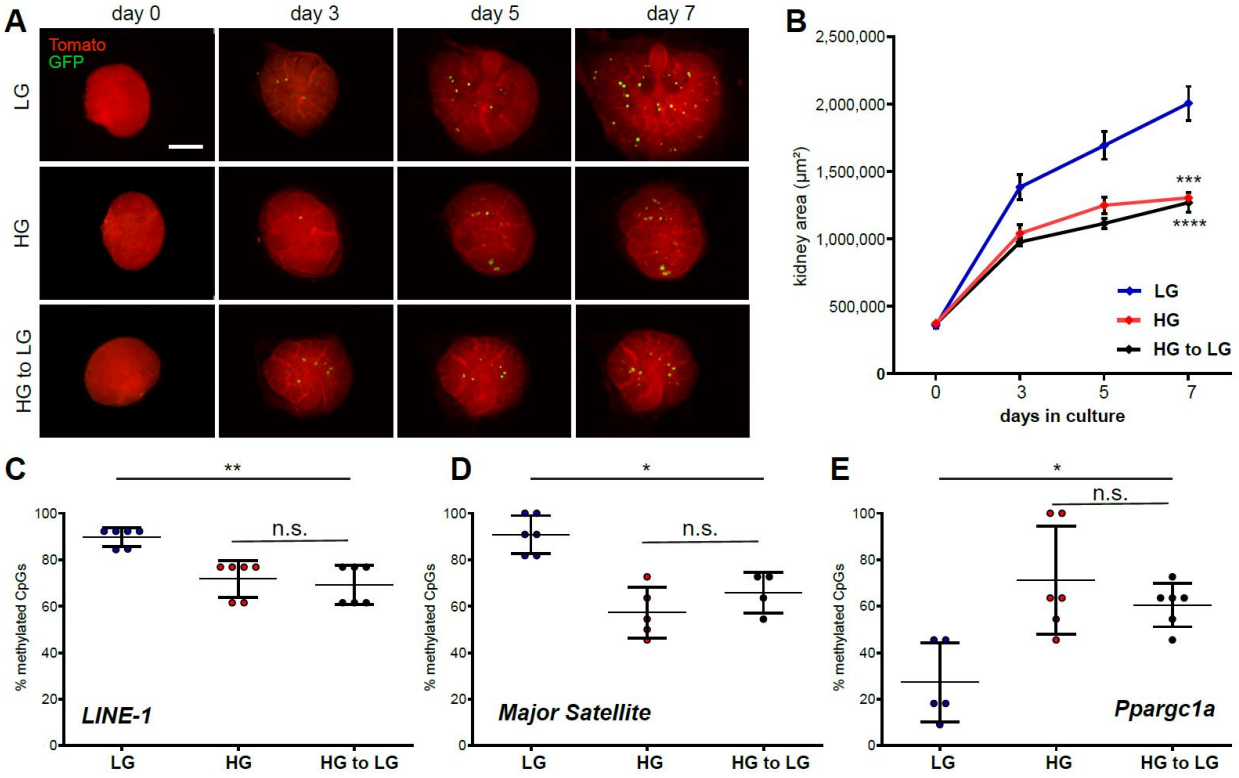


**Figure 3.** Ex vivo high glucose exposure influences long-term memory formation via DNA methylation. (**A**) Imaging of E12.5 embryonic kidneys from day 0 to day 7 in low glucose medium (5.5 mM), high glucose medium (55 mM) or high glucose medium for 3.5 days and reversal to low glucose medium for the remaining days. Scale bar: 500 µm. (**B**) Kidney surface area over 7 days. Mean ± SD. n = 36 kidneys. LG, low glucose treatment; HG, high glucose treatment; HG to LG, 3.5 days high and 3.5 days low glucose treatment. ***, LG–HG (unpaired *t*-test): $p = 0.0004$; ****, LG–HG to LG (paired *t*-test): $p < 0.0001$. (**C**) Analysis of the DNA methylation at *LINE*-1 and (**D**) *major satellite* loci shows continuous DNA hypomethylation in high glucose treated conditions. **, *p*-value = 0.0022. *, *p*-value = 0.0357. (**E**) Analysis of the DNA methylation at *Ppargc1a* locus shows continuous DNA hypermethylation in high glucose conditions. Mean ± SD. *, *p*-value = 0.0130.

### *2.4. Ex Vivo Small Compound Screen Identifies Epigenetic Regulators of Renal Development*

The results of this work as well as previous works suggest that epigenetic mechanisms play a role in kidney development [30,40–45]. Therefore, we wanted to systematically evaluate the effect of epigenetic modulators of the different enzyme classes on renal development. For this, we selected a library of 22 FDA-approved small compounds with demonstrated inhibitory activity [46–56] (Figure 4A). Using Six2.Cre-reporter mice to evaluate nephron development, the renal structures were cultured for 3 days with the inhibitors in the medium. Size increase over time was compared to the littermate control organs, and the morphology was checked for abnormalities in development (Figure 4B). Several inhibitors could be shown to interfere with normal ex vivo renal development. HDAC inhibitor entinostat, a benzamide histone deacetylase inhibitor with high affinity for HDAC

1, 2 and 3 [57], showed consistent growth reduction and lack of differentiation and proliferation after 3 days (Figure 4C). TH39, developed as a selective HDAC8 inhibitor ($IC_{50}$ HDAC8 88 nM, 26-fold selective against HDAC1, 28-fold selective against HDAC6 [56]), showed a similarly severe inhibition of growth compared to littermate control organs. Furthermore, iron chelators and inhibitors of JmJC deferasirox and deferoxamine showed growth reduction analogous to iron-deficient medium. Additionally, SET7/9 inhibitor cyproheptadine [58,59] showed growth reduction and lack of differentiation and proliferation compared to control kidneys (Figure 4D) but also seemed to interfere with Wnt signaling (Supplementary Figure S3). Other HDAC, HAT, HDM and HMT inhibitors and DNMT inhibitor 5-azacytidine did not show growth reduction or developmental anomalies within the measured time frame (Figure 4A).

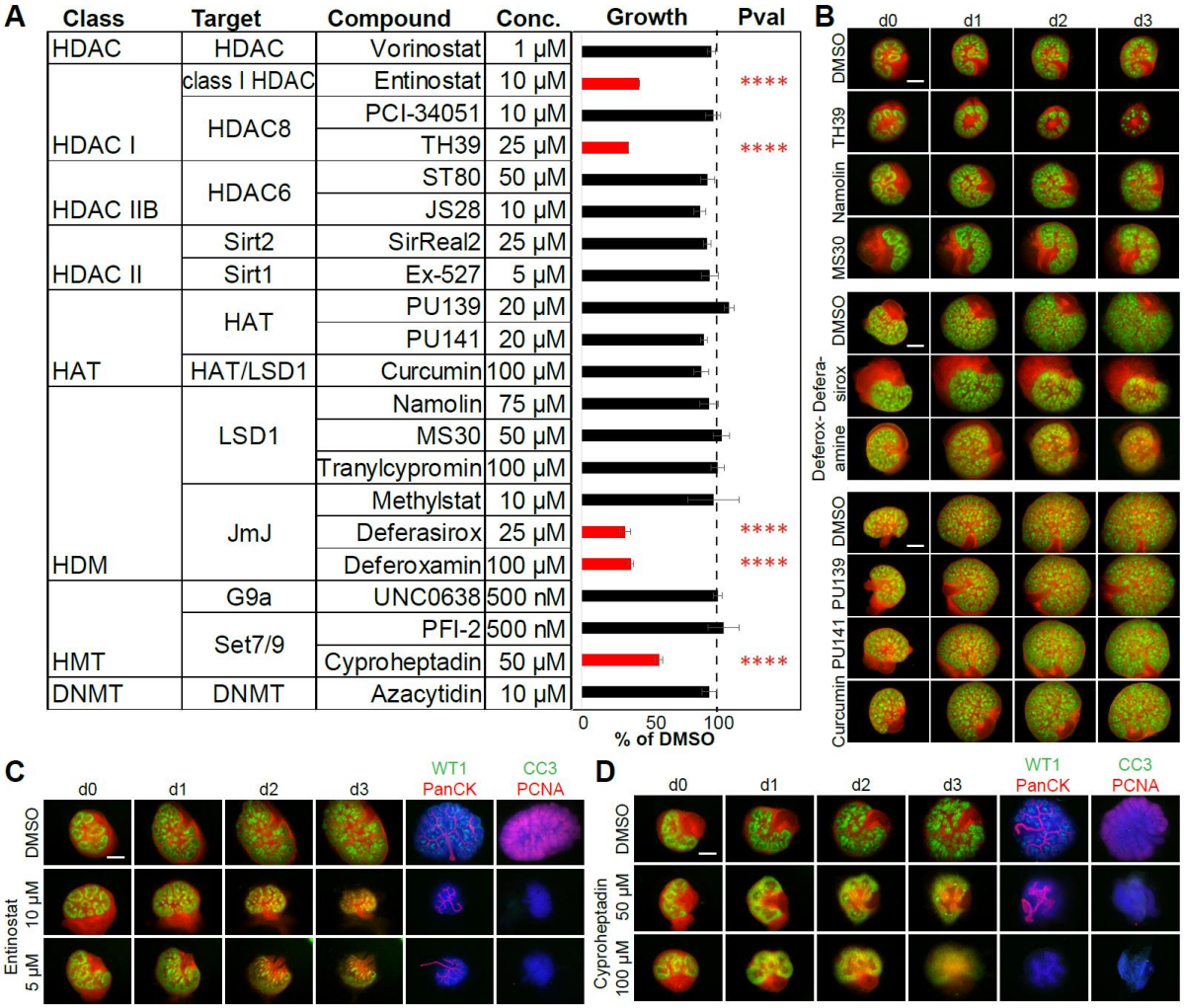


**Figure 4.** Ex vivo small compound screen identifies modulators of renal development. (**A**) List of small compounds, their epigenetic targets and concentration used shows renal growth reduction with entinostat, TH39, deferasirox, deferoxamine and cyproheptadine in ≥3 independent experiments after 3 days in culture. Control cultures were treated with DMSO. ****, *p*-value < 0.0001. (**B**) Examples of two sets of embryonic kidney cultures with pictures taken from day 0 until day 3 showing growth reduction and morphological differences in kidneys treated with TH39, deferasirox and deferoxamine compared to littermate control kidneys. Scale bar: 500 µm. (**C**) Entinostat showed growth reduction at 5 and 10 µM concentration, no nephron differentiation and lack of proliferation after 3 days. (**D**) Cyproheptadine showed growth reduction at 100 and 50 µM concentrations, lack of differentiation, ureter dilation and lack of proliferation after 3 days in culture. Scale bar: 500 µm. PanCK, pan-cytokeratin. CC3, cleaved caspase-3. PCNA, proliferating cell nuclear antigen.

## 3. Discussion

Renal development primarily takes place in utero and is subject to interference from metabolic and environmental influences. Nephron number is determined at birth, and a growing body of evidence suggests low nephron numbers to be a risk factor for the development of hypertension and chronic kidney disease later in life [2–4,60]. However, many factors influencing nephron number and modes of action are still unknown. Here, embryonic kidneys from dual-fluorescent reporter mice cultured on Transwell inserts were used to model maternal metabolic conditions and screen epigenetic inhibitors.

While many studies now involve kidney organoids using human iPS cells [61], kidney cultures are a valuable tool for detailed analysis of phenotypes mediated by metabolic conditions or inhibitory agents. While progenitor cell cultures and kidney organoids are alternatives with significant potential for investigations of teratogenicity, they are subject to limitations, such as high variability in differentiation and growth and lack of a conventional organ structure. This makes metanephric organ culture a valuable alternative to investigate conditions that would not be feasible in vivo.

Thus, hyperthermia and iron deficiency provide two examples of investigating environmental conditions with different outcomes on renal growth and nephron numbers. While data on the effect of hyperthermia on renal growth are scarce, the effect of ex vivo iron restriction is in line with previous reports of maternal iron deficiency in rats [23,24], although the model is limited in replicating the exact in utero state in terms of concentration and iron kinetics. Our results have also shown that mitotic activity is reduced in the iron-restricted condition. Iron plays an essential role in many cellular processes, such as the cell cycle [62]. Our morphological analysis showed an all-proximal nephron differentiation phenotype, possibly as the result of inhibited canonical Wnt signaling. Widespread downregulation of genes associated with Wnt signaling has previously been reported in a microarray analysis of rat offspring exposed to maternal iron deficiency [63]. Mechanistically, intracellular iron depletion by chelating agents has been shown to induce proteasomal degradation of β-catenin, the principal downstream effector protein of the canonical Wnt pathway in cancer and neural progenitor cells [64,65].

As another metabolic condition, modeling high glucose exposure resulted in effects similar to those of in vivo streptozotocin-induced maternal diabetes [10,26,27,66–71]. While our model could not reproduce the effects of 30 mM glucose conditions, likely due to the previously reported influence of mouse background [28,72], 55 mM glucose conditions resulted in growth reduction and decreased nephron numbers. Pronounced changes were visible histologically and ultrastructurally in the glomeruli, with the expansion of the glomerular basement matrix resembling human diabetic nephropathy. The similarities between murine fetal and human adult renal response to high glucose with distinct ECM expansion and downregulation of key podocyte genes was striking and revealed many known diabetes-associated genes, indicating usage of similar mechanisms in the podocytes and tubules. However, whether the same underlying pathways lead to dedifferentiation in diabetic nephropathy and decrease in differentiation during fetal differentiation is so far unknown. Interestingly, nonglucose alterations of the diabetic environment, such as hyperketonemia, have also been shown to mediate teratogenesis but were not replicated in the kidney culture model [73,74]. Long-term effects of hyperglycemia were also reproducible in our model, showing continuous growth retardation after normalization of glycemia similar to previous reports [10]. Additionally, DNA methylation analysis revealed a prolonged DNA hypomethylation at repetitive regions and hypermethylation at the *Ppargc1a* locus after reversal to low glucose medium, indicating the formation of metabolic memory after a period of metabolic stress [30]. Many more of the differentially regulated genes have also previously been shown to be epigenetically regulated in diabetes. For instance, upregulated gene *MEST* is maternally imprinted and hypomethylated in gestational diabetes mellitus [75]. *S100A4* is a differentially methylated marker of insulin resistance in obese children [76]. Of the downregulated genes, *ESM1* and *RASGRP3* are examples of genes differentially methylated in gestational diabetes [77,78], showing the growing emergence

of links between diabetes and epigenetic regulation. Thus, our system highlights epigenetic modification or fetal programming as an important regulatory mechanism.

Several epigenetic regulatory enzymes are known to be involved in both renal morphogenesis and transcriptional regulation in adult organ function and disease [30,40,79–81]. Using kidney cultures as a screening tool, we searched for additional epigenetic modifiers playing a role in renal development and nephron morphogenesis. Entinostat (MS-275) reduced kidney size concordant with previously reported genetic deletion of HDAC1 and HDAC2 in either nephron progenitor cells or ureteric bud cells [44,82,83]. While inhibition of HDAC8 by TH39 also induced a severe growth reduction of the explant and lack of differentiation, the highly specific HDAC8 inhibitor PCI-34051 showed no effect, thus pointing to off-target effects of TH39, such as other HDACs. With a phenotype similar to that of kidneys cultured under iron-deficient conditions, deferasirox and deferoxamine, published inhibitors of the iron-dependent JumonjiC-domain-containing histone demethylases [50], may exhibit off-target effects due to iron chelation. While cyproheptadine, a histamine antagonist and published inhibitor of Set7/9 histone methyltransferase, displayed a unique phenotype by leading to diffusion of the progenitor cell population, additional results pointed to off-target effects involving the Wnt signaling pathway [48]. Altogether, this library of FDA-approved inhibitors shows the potential for fast and effective screening for epigenetic modulators. Due to the limited time frame used, inhibitors requiring prolonged exposure to exert an effect might have been missed in this setup. Thus, azacytidine did not show an effect despite the published phenotype of Dnmt1 knockout [30].

While the kidney culture system offers robust renal development, several aspects limit investigation or interpretation of the results in this reductionist model. First, studies have shown differences in mouse and human development and gene expression, limiting the use of the mouse model. Next, time limitations in this system may not allow for all complex processes to unfold. This may account for some of the environmental conditions and epigenetic inhibitors failing to impact renal development in this study. Moreover, some of the inhibitors show nonspecific effects that can contribute to inhibition of other pathways, such as in the case of cyproheptadine, which appears to exhibit its effect via activation of GSK3-beta, or the case of iron chelation by deferasirox/deferoxamine. Beyond this proof-of-concept study, the epigenetic inhibitor screen could be extended to more (specific) inhibitors; prolonged time periods; additional study criteria, such as nephron number and ureteric bud branching; and transcriptomic and epigenetic studies.

To summarize, kidney cultures enable the characterization of a number of maternal disease models, such as hyperthermia, iron deficiency and maternal diabetes, and the screening of pharmacological compounds, providing a well-suited platform for investigating the crosstalk between environmental influences of the developing kidney and its epigenetic programming.

## 4. Materials and Methods

### *4.1. Animal Handling*

Mice were kept in a specific-pathogen-free environment at the Center for Experimental Models and Transgenic Service (CEMT) in Freiburg, Germany. All mice were raised in a 12/12 h cycle of light and darkness, with access to water and standard chow ad libitum. All experiments were registered with the regional government of Baden-Wuerttemberg under the authorization codes X15/03R and X17/05F.

### *4.2. Timed Harvest of Embryos/Microdissection/Culture of Metanephroi*

Timed-pregnant hNPHS2Cre B6.129(Cg)-Gt(ROSA)26Sortm4(ACTB-tdTomato,-EGFP) Luo/J [5] and Tg(Six2-EGFP/cre)1Amc/J mice [84] were sacrificed at E12.5, and the embryos were harvested. The metanephroi were isolated and cultured on Transwell inserts with culture medium at the medium–air interface. Pairing of metanephroi from the same embryo between control and experimental conditions was maintained throughout the experiments unless mentioned otherwise.

### 4.3. Genotyping

Genotyping of the mice was performed by polymerase chain reaction (PCR) amplification of DNA isolated from tail biopsies and subsequent visualization of the amplified fragments by gel electrophoresis. The following primers were used: Tomato/EGFP forward 5′ CTC TGC TGC CTC CTG GCT TCT 3′ reverse wildtype 5′ CGA GGC GGA TCA CAA GCA ATA 3′ and reverse mutant 5′ TCA ATG GGC CGG GGT CGT T3′, Cre forward 5′ GCA TTA CCG GTC GAT GCA ACG AGT GAT GAG 3′ and reverse 5′ GAG TGA ACG AAC CTG GTC GAA ATC AGT GCG 3′.

### 4.4. Hyperglycemic Conditions

Hyperglycemia medium contained DMEM medium with 10% fetal bovine serum, 100 µg/mL of penicillin, 100 µg of streptomycin and D-glucose for a final concentration of 55 mM D-glucose. For the control medium, an equimolar amount of mannitol was added, for a final concentration of 5 mM of D-glucose and 50 mM mannitol.

### 4.5. Hyperthermic Conditions

For both hyperthermia and control cultures, a serum-free base medium of 1:1 DMEM and Ham's F-12 Medium was supplemented with 100 µg/mL of penicillin, 100 µg/mL of streptomycin, 50 µg/mL of bovine holo-transferrin and 10 mM HEPES for increased buffering capacity. Control cultures were incubated at 37 °C, while hyperthermia cultures were incubated in an identical incubator at a temperature of 40 °C.

### 4.6. Iron-Restriction

Iron-restricted medium consisted of serum-free base medium of 1:1 DMEM and Ham's F-12 medium which was supplemented with 100 µg/mL of penicillin, 100 µg/mL of streptomycin and 50 µg/mL of apo-transferrin. For the iron-sufficient control cultures, 50 µg/mL of holo-transferrin was used instead.

### 4.7. Whole Mount Immunofluorescence Staining of Explants

Cultured explants were either fixed with cold methanol for 20 min or room-temperature 4% paraformaldehyde (PFA) solution for 15 min and subsequently washed three times with room temperature PBST buffer (PBS + 0.1% Tween 20) for 5 min. Blocking solution containing 5% BSA in PBST buffer was added for 3 h at room temperature. After blocking, the cultures were incubated in dilutions of the primary antibodies in blocking solution at 4 °C on an orbital shaker overnight. Cultures were then washed three times with blocking solution for 2 h each and incubated in a 1:300 dilution of secondary antibodies and 1:500 dilution of Hoechst nuclear dye in blocking solution overnight. The cultures were again washed three times for 2 h and mounted with Prolong Gold Antifade mountant using a spacer. The following primary antibodies were used: rabbit anti-active caspase 3 (1:250, AF835; R&D systems Inc., Minneapolis, MN, USA), rabbit anti-JAG-1 (1:100, 260S; Cell Signaling Technology, Denver, MA, USA), sheep anti-Tamm-Horsefall protein (1:250, AB2606308; Thermo Fisher Scientific, Waltham, MA, USA), mouse anti-pan-cytokeratin (1:250, AB11213; Abcam, Cambridge, UK), rabbit anti-SIX2 (1:100, 11562-1-AP; Proteintech Group Inc., Manchester, UK), mouse anti-WT1 (1:100, 05-753; Merck KGaA, Darmstadt, Germany), rat anti-CD326 (1:100; 118202, Biolegend, San Diego, CA), rabbit anti-NKCC2 (1:100, SPC-401D; StressMarq Biosciences, Victoria, BC, Canada), mouse anti-phospho-histone H3 (1:100, 9706S, Cell Signaling Technology, Denver, MA, USA) and mouse anti-E-cadherin (1:200, 4A2C7; Thermo Fisher Scientific, Waltham, MA, USA). The following secondary antibodies were used in 1:300 dilution: Alexa Fluor 488 anti-mouse (R37114) and anti-rabbit (R37118); Alexa Fluor 555 anti-mouse (A-31570), anti-rabbit (A-31572), anti-sheep (A-21436) and anti-rat (A-21434) (all Thermo Fisher). The pairing of explants from the same embryo was not maintained in the stainings against phospho-histone H3 due to the explants detaching from the membrane during PFA fixation.

### 4.8. Imaging

Live imaging of cultured metanephroi from NPHS2-Cre;Tomato/EGFP mice was performed with Zeiss AxioObserver after mounting the membrane inserts on a glass-bottom dish containing 200 µL of cold PBS. Live images were taken as z-stacks with a plane distance of 10 µm. For the glomerular counting, the z-stacked GFP channels were orthogonally projected using Zen Blue and analyzed with ImageJ. Stained cultures were imaged using Zeiss AxioObserver inverted microscope or U2 LSM 510 META laser scanning microscope. Mitotic cells were counted using ImageJ.

### 4.9. Histology

Fixation was performed in 4% PFA solution overnight. The explants were dehydrated with ethanol, incubated with xylene and embedded in paraffin. The paraffin blocks were sectioned at 3 µm and mounted onto glass specimen slides. Hematoxylin/eosin staining (H&E) was performed.

### 4.10. EM

Kidney cultures were fixed in 4% PFA/1% glutardialdehyde in 1x PBS overnight and then embedded in liquid 40 °C agarose. After postfixation with 1% osmium tetroxide in 6.68% sucrose buffer, the samples were washed and stained en bloc with 1% uranyl acetate in 70% alcohol for 1 h, dehydrated in ethanol and propylene oxide and embedded in Durcupan (Plano, Wetzlar, Germany). Ultrathin sections were stained with lead citrate and examined in a Zeiss-Leo 910 transmission electron microscope.

### 4.11. Bisulfite-PCR

DNA from kidney cultures was isolated with DNeasy Blood & Tissue kit (QIAGEN) and bisulfite-converted using EpiTect Bisulfite Kit (QIAGEN) according to the manufacturer's instructions. Converted DNA (20 ng) was used as template in a PCR reaction using AmpliTaq Gold Polymerase (Invitrogen). PCR products were purified using gel electrophoresis and ligated into a pCR4-TOPO vector using the TOPO TA Cloning Kit for sequencing (Invitrogen) and transformed into DH10B *E. Coli* cells. Randomly selected clones were sent for sequencing (GATC, Konstanz). Inspection, alignment, visualization and statistics were performed with QUMA: quantification tool for methylation analysis [85]. The following primers were used: major satellite forward: 5′ GGA ATA TGG TAA GAA AAT TGA AAA TTA TGG 3′, reverse: 5′ CCA TAT TCC AAA TCC TTC AAT ATA CAT TTC 3′, ref. [30] Line-1 forward 5′ TAG GAA ATT AGT TTG AAT AGG TGA GAG GT 3′, Line-1 reverse: TCA AAC ACT ATA TTA CTT TAA CAA TTC CCA 3′, ref. [30] Ppargc1a forward 5′ TGT TAG GGA ATA AGA TTT GTG TTT TTA A 3′, Ppargc1a reverse 5′ CAA ATA CTC CTA TAA ACA ATC CAA ACA A 3′.

### 4.12. RNA Sequencing

The RNA of kidneys grown for 7 days under high or low glucose conditions was isolated using the Qiagen RNeasy Plus Mini Kit. RNA sequencing was performed by GATC Biotech. Quality control was done with FastQC (Barbraham Bioinformatics). Raw reads were trimmed using TrimGalore! (Barbraham Bioinformatics) and mapped with Tophat (v2) [86] to mm10 using Galaxy Freiburg. Read counts were extracted with htseq-count [87]; differential gene expression was analyzed with DESeq2 [88].

### 4.13. Microarray Analysis of Human Kidney Biopsies

Human kidney biopsy specimens and Affymetrix microarray expression data were procured within the framework of the European Renal cDNA Bank–Kröner–Fresenius Biopsy Bank. Biopsies were obtained from patients after informed consent and with the approval of the local ethics committees [89]. Following a renal biopsy, the tissue was transferred to RNase inhibitor and microdissected into glomeruli and tubulointerstitium. Total RNA was isolated from microdissected glomeruli and tubules, reverse transcribed and

linearly amplified according to a protocol previously reported [90]. In this study, we used published microarray expression data from individual patients with diabetic nephropathy, as well as living donors (GSE 99340, LDs: GSE32591, GSE35489, GSE37463). CEL file normalization was performed with the Robust Multichip Average method using RMA-Express (Version 1.0.5) and the human Entrez-Gene custom CDF annotation from Brain Array Version 18, accessed on 23 January 2014 (http://brainarray.mbni.med.umich.edu/Brainarray/Database/CustomCDF/CDF_download.asp). The log-transformed dataset was corrected for batch effect using ComBat from the GenePattern pipeline (version 3.8.0) (http://www.broadinstitute.org/cancer/software/genepattern/). To identify differentially expressed genes, the SAM (Significance Analysis of Microarrays) method was applied using TiGR (MeV, Version 4.8.1) [91].

### 4.14. qPCR

mRNA was reverse transcribed to cDNA using the iScript cDNA synthase kit (Bio-Rad) according to the manufacturer's instructions. qPCR was performed with BioRad CFX Connect Real-Time PCR Detection System in triplicates using SsoAdvanced Universal SYBR Green Supermix. The normalized ΔΔCT values were calculated in the CFX Manager program. The following primers were used: Jag1 forward 5′ TGG TTG GCT GGG AAA TT 3′, Jag1 reverse 5′ TGG ACA CCA GGG CAC ATT C 3′, mHprt forward 5′ GCT TTC CTT GGT CAA GCA GTA CAG 3′, mHprt reverse 5′ GAA GTG CTC ATT ATA GTC AAG GGC ATA TCC 3′ [92].

### 4.15. Statistics

For analysis of paired kidneys, paired *t*-tests were applied using GraphPad Prism 7. For the quantification of unpaired kidneys, pHH3-positive cells and qPCR experiments, unpaired *t*-test was applied.

**Supplementary Materials:** The following are available online at https://www.mdpi.com/article/10.3390/ijms22084157/s1, Figure S1: Ex vivo iron restriction as a model for metanephric development under iron-insufficient conditions, Figure S2: Ex vivo high glucose exposure does not influences long-term memory formation via DNA methylation at 30 mM glucose concentration, Figure S3: Anti-histamine drug Cyproheptadine leads to progenitor cell loss via inhibition of Wnt signaling. Table S1: RNA-seq analysis of high glucose kidney cultures.

**Author Contributions:** Conceptualization, N.W., L.F. and T.B.H.; methodology, L.F., C.H., O.K., S.L. and N.W.; validation, L.F., S.L., C.H., O.K. and N.W.; formal analysis, L.F., S.L., C.H., O.K. and N.W.; resources, A.-T.H., M.J., W.S., M.T.L. and C.D.C.; data curation, N.W.; writing—original draft preparation, L.F. and N.W.; writing—review and editing, L.F., T.B.H., O.K., M.J., W.S. and N.W.; visualization, L.F., S.L., C.H., O.K. and N.W.; supervision, N.W. and T.B.H.; funding acquisition, T.B.H., O.K., M.J., M.T.L. and N.W. All authors have read and agreed to the published version of the manuscript.

**Funding:** This research was funded by the German Research Foundation (Deutsche Forschungsgemeinschaft, DFG): CRC 992 (to M.J. and T.B.H.), CRC 1192 (to T.B.H. and N.W.), Ju295/14-1 (to M.J.) Kr1984/4-1 (to O.K.) and under Germany's Excellence Strategy—EXC-2189—Project ID 390939984. Furthermore, this study was supported by the Heisenberg program (to T.B.H.), the European Research Council grant 616891 (to T.B.H.), the H2020-IMI2 consortium BEAt-DKD (Biomarker Enterprise to Attack Diabetic Kidney Disease) (115974, to T.B.H.), STOP-FSGS (Speed Translation-Oriented Progress to Treat Focal Segmental Glomerulosclerosis) 01GM1901C (to T.B.H.), and the Else-Kröner Fresenius Stiftung (iPRIME (innovative Promotionsförderung im Bereich translationale Entzündungsforschung)). The Galaxy server that was used for some calculations is in part funded by Collaborative Research Centre 992 Medical Epigenetics (Deutsche Forschungsgesellschaft (DFG) grant SFB 992/1 2012) and the German Federal Ministry of Education and Research (Bundesministerium für Bildung und Forschung (BMBF) grants 031 A538A/A538C RBC, 031L0101B/031L0101C de.NBI-epi, 031L0106 de.STAIR(de.NBI)).

**Institutional Review Board Statement:** The study was conducted according to the guidelines of the Declaration of Helsinki and approved by the Institutional Review Board (or Ethics Committee) of Klinikum der Universität München (250-16).

**Informed Consent Statement:** Informed consent was obtained from all subjects involved in the study.

**Data Availability Statement:** Raw and processed RNA-seq data will be made available on GEO upon publication.

**Acknowledgments:** ERCB-KFB was supported by the Else Kröner-Fresenius Foundation. We also thank all participating centers of the European Renal cDNA Bank–Kröner-Fresenius biopsy bank (ERCB-KFB) and their patients for their cooperation. For active members at the time of the study, see N. Shved et al., *Scientific Reports* 7, 8576 (2017).

**Conflicts of Interest:** The authors declare no conflict of interest.

## References

1. Barker, D.J. The fetal and infant origins of adult disease. *BMJ* **1990**, *301*, 1111. [CrossRef]
2. Wang, X.; Garrett, M.R. Nephron number, hypertension, and CKD: Physiological and genetic insight from humans and animal models. *Physiol. Genom.* **2017**, *49*, 180–192. [CrossRef] [PubMed]
3. Hughson, M.D.; Douglas-Denton, R.; Bertram, J.F.; Hoy, W.E. Hypertension, glomerular number, and birth weight in African Americans and white subjects in the southeastern United States. *Kidney Int.* **2006**, *69*, 671–678. [CrossRef] [PubMed]
4. Keller, G.; Zimmer, G.; Mall, G.; Ritz, E.; Amann, K. Nephron number in patients with primary hypertension. *N. Engl. J. Med.* **2003**, *348*, 101–108. [CrossRef] [PubMed]
5. Lelievre-Pegorier, M.; Vilar, J.; Ferrier, M.L.; Moreau, E.; Freund, N.; Gilbert, T.; Merlet-Benichou, C. Mild vitamin A deficiency leads to inborn nephron deficit in the rat. *Kidney Int.* **1998**, *54*, 1455–1462. [CrossRef] [PubMed]
6. Langley-Evans, S.C.; Welham, S.J.; Jackson, A.A. Fetal exposure to a maternal low protein diet impairs nephrogenesis and promotes hypertension in the rat. *Life Sci.* **1999**, *64*, 965–974. [CrossRef]
7. Singh, R.R.; Moritz, K.M.; Bertram, J.F.; Cullen-McEwen, L.A. Effects of dexamethasone exposure on rat metanephric development: In vitro and in vivo studies. *Am. J. Physiol. Renal. Physiol.* **2007**, *293*, F548–F554. [CrossRef]
8. Cain, J.E.; Di Giovanni, V.; Smeeton, J.; Rosenblum, N.D. Genetics of renal hypoplasia: Insights into the mechanisms controlling nephron endowment. *Pediatr. Res.* **2010**, *68*, 91–98. [CrossRef]
9. Lewis, R.M.; Forhead, A.J.; Petry, C.J.; Ozanne, S.E.; Hales, C.N. Long-term programming of blood pressure by maternal dietary iron restriction in the rat. *Br. J. Nutr.* **2002**, *88*, 283–290. [CrossRef]
10. Hokke, S.N.; Armitage, J.A.; Puelles, V.G.; Short, K.M.; Jones, L.; Smyth, I.M.; Bertram, J.F.; Cullen-McEwen, L.A. Altered ureteric branching morphogenesis and nephron endowment in offspring of diabetic and insulin-treated pregnancy. *PLoS ONE* **2013**, *8*, e58243.
11. Hughson, M.; Farris, A.B., 3rd; Douglas-Denton, R.; Hoy, W.E.; Bertram, J.F. Glomerular number and size in autopsy kidneys: The relationship to birth weight. *Kidney Int.* **2003**, *63*, 2113–2122. [CrossRef] [PubMed]
12. Bianchi, G.; Fox, U.; Di Francesco, G.F.; Giovanetti, A.M.; Pagetti, D. Blood pressure changes produced by kidney cross-transplantation between spontaneously hypertensive rats and normotensive rats. *Clin. Sci. Mol. Med.* **1974**, *47*, 435–448. [CrossRef] [PubMed]
13. Trowell, O.A. A modified technique for organ culture in vitro. *Exp. Cell Res.* **1954**, *6*, 246–248. [CrossRef]
14. Saxen, L.; Lehtonen, E. Embryonic kidney in organ culture. *Differentiation* **1987**, *36*, 2–11. [CrossRef]
15. Andersen, A.M.; Vastrup, P.; Wohlfahrt, J.; Andersen, P.K.; Olsen, J.; Melbye, M. Fever in pregnancy and risk of fetal death: A cohort study. *Lancet* **2002**, *360*, 1552–1556. [CrossRef]
16. Edwards, M.J. Hyperthermia as a teratogen: A review of experimental studies and their clinical significance. *Teratog. Carcinog. Mutagen.* **1986**, *6*, 563–582. [CrossRef] [PubMed]
17. Dreier, J.W.; Andersen, A.M.; Berg-Beckhoff, G. Systematic review and meta-analyses: Fever in pregnancy and health impacts in the offspring. *Pediatrics* **2014**, *133*, e674–e688. [CrossRef]
18. Waller, D.K.; Hashmi, S.S.; Hoyt, A.T.; Duong, H.T.; Tinker, S.C.; Gallaway, M.S.; Olney, R.S.; Finnell, R.H.; Hecht, J.T.; Canfield, M.A.; et al. Maternal report of fever from cold or flu during early pregnancy and the risk for noncardiac birth defects, National Birth Defects Prevention Study, 1997-2011. *Birth Defects Res.* **2018**, *110*, 342–351. [CrossRef]
19. Abe, K.; Honein, M.A.; Moore, C.A. Maternal febrile illnesses, medication use, and the risk of congenital renal anomalies. *Birth Defects Res. A Clin. Mol. Teratol.* **2003**, *67*, 911–918. [CrossRef]
20. Edwards, M.J.; Saunders, R.D.; Shiota, K. Effects of heat on embryos and foetuses. *Int. J. Hyperthermia* **2003**, *19*, 295–324. [CrossRef]
21. Edwards, M.J. Congenital defects in guinea pigs: Fetal resorptions, abortions, and malformations following induced hyperthermia during early gestation. *Teratology* **1969**, *2*, 313–328. [CrossRef]
22. Black, R.E.; Victora, C.G.; Walker, S.P.; Bhutta, Z.A.; Christian, P.; de Onis, M.; Ezzati, M.; Grantham-McGregor, S.; Katz, J.; Martorell, R.; et al. Maternal and child undernutrition and overweight in low-income and middle-income countries. *Lancet* **2013**, *382*, 427–451. [CrossRef]

23. Lisle, S.J.; Lewis, R.M.; Petry, C.J.; Ozanne, S.E.; Hales, C.N.; Forhead, A.J. Effect of maternal iron restriction during pregnancy on renal morphology in the adult rat offspring. *Br. J. Nutr.* **2003**, *90*, 33–39. [CrossRef] [PubMed]
24. Sun, M.Y.; Woolley, J.C.; Blohowiak, S.E.; Smith, Z.R.; Siddappa, A.M.; Magness, R.R.; Kling, P.J. Dietary-induced gestational iron deficiency inhibits postnatal tissue iron delivery and postpones the cessation of active nephrogenesis in rats. *Reprod. Fertil. Dev.* **2016**, *29*, 855–866. [CrossRef] [PubMed]
25. Guariguata, L.; Linnenkamp, U.; Beagley, J.; Whiting, D.R.; Cho, N.H. Global estimates of the prevalence of hyperglycaemia in pregnancy. *Diabetes Res. Clin. Pract.* **2014**, *103*, 176–185. [CrossRef] [PubMed]
26. Tran, S.; Chen, Y.W.; Chenier, I.; Chan, J.S.; Quaggin, S.; Hebert, M.J.; Ingelfinger, J.R.; Zhang, S.L. Maternal diabetes modulates renal morphogenesis in offspring. *J. Am. Soc. Nephrol.* **2008**, *19*, 943–952. [CrossRef] [PubMed]
27. Amri, K.; Freund, N.; Vilar, J.; Merlet-Benichou, C.; Lelievre-Pegorier, M. Adverse effects of hyperglycemia on kidney development in rats: In vivo and in vitro studies. *Diabetes* **1999**, *48*, 2240–2245. [CrossRef]
28. Kanwar, Y.S.; Liu, Z.Z.; Kumar, A.; Usman, M.I.; Wada, J.; Wallner, E.I. D-glucose-induced dysmorphogenesis of embryonic kidney. *J. Clin. Investig.* **1996**, *98*, 2478–2488. [CrossRef]
29. Kanwar, Y.S.; Akagi, S.; Nayak, B.; Sun, L.; Wada, J.; Xie, P.; Thakur, A.; Chugh, S.S.; Danesh, F.R. Renal-specific oxidoreductase biphasic expression under high glucose ambience during fetal versus neonatal development. *Kidney Int.* **2005**, *68*, 1670–1683. [CrossRef]
30. Wanner, N.; Vornweg, J.; Combes, A.; Wilson, S.; Plappert, J.; Rafflenbeul, G.; Puelles, V.G.; Rahman, R.U.; Liwinski, T.; Lindner, S.; et al. DNA Methyltransferase 1 Controls Nephron Progenitor Cell Renewal and Differentiation. *J. Am. Soc. Nephrol.* **2019**, *30*, 63–78. [CrossRef]
31. Osterby, R.; Gundersen, H.J. Glomerular size and structure in diabetes mellitus. I. Early abnormalities. *Diabetologia* **1975**, *11*, 225–229. [CrossRef] [PubMed]
32. Mac-Moune Lai, F.; Szeto, C.C.; Choi, P.C.; Ho, K.K.; Tang, N.L.; Chow, K.M.; Li, P.K.; To, K.F. Isolate diffuse thickening of glomerular capillary basement membrane: A renal lesion in prediabetes? *Mod. Pathol.* **2004**, *17*, 1506–1512. [CrossRef] [PubMed]
33. Al Shawaf, E.; Abu-Farha, M.; Devarajan, S.; Alsairafi, Z.; Al-Khairi, I.; Cherian, P.; Ali, H.; Mathur, A.; Al-Mulla, F.; Al Attar, A.; et al. ANGPTL4: A Predictive Marker for Diabetic Nephropathy. *J. Diabetes Res.* **2019**, *2019*, 4943191. [CrossRef] [PubMed]
34. Murakoshi, M.; Tanimoto, M.; Gohda, T.; Hagiwara, S.; Takagi, M.; Horikoshi, S.; Tomino, Y. Mindin: A novel marker for podocyte injury in diabetic nephropathy. *Nephrol. Dial. Transpl.* **2011**, *26*, 2153–2160. [CrossRef] [PubMed]
35. Donegan, D.; Bale, L.K.; Conover, C.A. PAPP-A in normal human mesangial cells: Effect of inflammation and factors related to diabetic nephropathy. *J. Endocrinol.* **2016**, *231*, 71–80. [CrossRef]
36. Huang, C.; Zhang, Y.; Kelly, D.J.; Tan, C.Y.; Gill, A.; Cheng, D.; Braet, F.; Park, J.S.; Sue, C.M.; Pollock, C.A.; et al. Thioredoxin interacting protein (TXNIP) regulates tubular autophagy and mitophagy in diabetic nephropathy through the mTOR signaling pathway. *Sci. Rep.* **2016**, *6*, 29196. [CrossRef] [PubMed]
37. Randhawa, P.K.; Rylova, S.; Heinz, J.Y.; Kiser, S.; Fried, J.H.; Dunworth, W.P.; Anderson, A.L.; Barber, A.T.; Chappell, J.C.; Roberts, D.M.; et al. The Ras activator RasGRP3 mediates diabetes-induced embryonic defects and affects endothelial cell migration. *Circ. Res.* **2011**, *108*, 1199–1208. [CrossRef]
38. Zhang, Y.; Han, D.; Yu, P.; Huang, Q.; Ge, P. Genome-scale transcriptional analysis reveals key genes associated with the development of type II diabetes in mice. *Exp. Ther. Med.* **2017**, *13*, 1044–1150. [CrossRef]
39. Zheng, X.; Soroush, F.; Long, J.; Hall, E.T.; Adishesha, P.K.; Bhattacharya, S.; Kiani, M.F.; Bhalla, V. Murine glomerular transcriptome links endothelial cell-specific molecule-1 deficiency with susceptibility to diabetic nephropathy. *PLoS ONE* **2017**, *12*, e0185250. [CrossRef]
40. Doan, T.N.A.; Briffa, J.F.; Phillips, A.L.; Leemaqz, S.Y.; Burton, R.A.; Romano, T.; Wlodek, M.E.; Bianco-Miotto, T. Epigenetic mechanisms involved in intrauterine growth restriction and aberrant kidney development and function. *J. Dev. Orig. Health Dis.* **2020**, 1–11. [CrossRef]
41. Huang, B.; Liu, Z.; Vonk, A.; Zeng, Z.; Li, Z. Epigenetic regulation of kidney progenitor cells. *Stem Cells Transl. Med.* **2020**, *9*, 655–660. [CrossRef] [PubMed]
42. El-Dahr, S.S.; Saifudeen, Z. Epigenetic regulation of renal development. *Semin. Cell Dev. Biol.* **2019**, *91*, 111–118. [CrossRef]
43. Liu, H.; Hilliard, S.; Kelly, E.; Chen, C.H.; Saifudeen, Z.; El-Dahr, S.S. The polycomb proteins EZH1 and EZH2 co-regulate chromatin accessibility and nephron progenitor cell lifespan in mice. *J. Biol. Chem.* **2020**, *295*, 11542–11558. [CrossRef]
44. Liu, H.; Chen, S.; Yao, X.; Li, Y.; Chen, C.H.; Liu, J.; Saifudeen, Z.; El-Dahr, S.S. Histone deacetylases 1 and 2 regulate the transcriptional programs of nephron progenitors and renal vesicles. *Development* **2018**, *145*. [CrossRef] [PubMed]
45. Zhang, L.; Ettou, S.; Khalid, M.; Taglienti, M.; Jain, D.; Jung, Y.L.; Seager, C.; Liu, Y.; Ng, K.H.; Park, P.J.; et al. EED, a member of the polycomb group, is required for nephron differentiation and the maintenance of nephron progenitor cells. *Development* **2018**, *145*. [CrossRef] [PubMed]
46. Rumpf, T.; Schiedel, M.; Karaman, B.; Roessler, C.; North, B.J.; Lehotzky, A.; Olah, J.; Ladwein, K.I.; Schmidtkunz, K.; Gajer, M.; et al. Selective Sirt2 inhibition by ligand-induced rearrangement of the active site. *Nat. Commun.* **2015**, *6*, 6263. [CrossRef]
47. Senger, J.; Melesina, J.; Marek, M.; Romier, C.; Oehme, I.; Witt, O.; Sippl, W.; Jung, M. Synthesis and Biological Investigation of Oxazole Hydroxamates as Highly Selective Histone Deacetylase 6 (HDAC6) Inhibitors. *J. Med. Chem.* **2016**, *59*, 1545–1555. [CrossRef] [PubMed]

48. Takemoto, Y.; Ito, A.; Niwa, H.; Okamura, M.; Fujiwara, T.; Hirano, T.; Handa, N.; Umehara, T.; Sonoda, T.; Ogawa, K.; et al. Identification of Cyproheptadine as an Inhibitor of SET Domain Containing Lysine Methyltransferase 7/9 (Set7/9) That Regulates Estrogen-Dependent Transcription. *J. Med. Chem.* **2016**, *59*, 3650–3660. [CrossRef] [PubMed]
49. Barsyte-Lovejoy, D.; Li, F.; Oudhoff, M.J.; Tatlock, J.H.; Dong, A.; Zeng, H.; Wu, H.; Freeman, S.A.; Schapira, M.; Senisterra, G.A.; et al. (R)-PFI-2 is a potent and selective inhibitor of SETD7 methyltransferase activity in cells. *Proc. Natl. Acad. Sci. USA* **2014**, *111*, 12853–12858. [CrossRef]
50. Roatsch, M.; Hoffmann, I.; Abboud, M.I.; Hancock, R.L.; Tarhonskaya, H.; Hsu, K.F.; Wilkins, S.E.; Yeh, T.L.; Lippl, K.; Serrer, K.; et al. The Clinically Used Iron Chelator Deferasirox Is an Inhibitor of Epigenetic JumonjiC Domain-Containing Histone Demethylases. *ACS Chem. Biol.* **2019**, *14*, 1737–1750. [CrossRef]
51. Luo, X.; Liu, Y.; Kubicek, S.; Myllyharju, J.; Tumber, A.; Ng, S.; Che, K.H.; Podoll, J.; Heightman, T.D.; Oppermann, U.; et al. A selective inhibitor and probe of the cellular functions of Jumonji C domain-containing histone demethylases. *J. Am. Chem. Soc.* **2011**, *133*, 9451–9456. [CrossRef] [PubMed]
52. Gajer, J.M.; Furdas, S.D.; Grunder, A.; Gothwal, M.; Heinicke, U.; Keller, K.; Colland, F.; Fulda, S.; Pahl, H.L.; Fichtner, I.; et al. Histone acetyltransferase inhibitors block neuroblastoma cell growth in vivo. *Oncogenesis* **2015**, *4*, e137. [CrossRef]
53. Carneiro, V.C.; de Abreu da Silva, I.C.; Torres, E.J.; Caby, S.; Lancelot, J.; Vanderstraete, M.; Furdas, S.D.; Jung, M.; Pierce, R.J.; Fantappie, M.R. Epigenetic changes modulate schistosome egg formation and are a novel target for reducing transmission of schistosomiasis. *PLoS Pathog.* **2014**, *10*, e1004116. [CrossRef] [PubMed]
54. Willmann, D.; Lim, S.; Wetzel, S.; Metzger, E.; Jandausch, A.; Wilk, W.; Jung, M.; Forne, I.; Imhof, A.; Janzer, A.; et al. Impairment of prostate cancer cell growth by a selective and reversible lysine-specific demethylase 1 inhibitor. *Int. J. Cancer* **2012**, *131*, 2704–2709. [CrossRef]
55. Schmitt, M.L.; Hauser, A.T.; Carlino, L.; Pippel, M.; Schulz-Fincke, J.; Metzger, E.; Willmann, D.; Yiu, T.; Barton, M.; Schule, R.; et al. Nonpeptidic propargylamines as inhibitors of lysine specific demethylase 1 (LSD1) with cellular activity. *J. Med. Chem.* **2013**, *56*, 7334–7342. [CrossRef] [PubMed]
56. Heimburg, T.; Chakrabarti, A.; Lancelot, J.; Marek, M.; Melesina, J.; Hauser, A.T.; Shaik, T.B.; Duclaud, S.; Robaa, D.; Erdmann, F.; et al. Structure-Based Design and Synthesis of Novel Inhibitors Targeting HDAC8 from Schistosoma mansoni for the Treatment of Schistosomiasis. *J. Med. Chem.* **2016**, *59*, 2423–2435. [CrossRef]
57. Tatamiya, T.; Saito, A.; Sugawara, T.; Nakanishi, O. *Isozyme-Selective Activity of the HDAC inhibitor MS-275*; AACR: Phila-delphia, PA, USA, 2004.
58. Sharma, N.; Sankrityayan, H.; Kale, A.; Gaikwad, A.B. Role of SET7/9 in the progression of ischemic renal injury in diabetic and non-diabetic rats. *Biochem. Biophys. Res. Commun.* **2020**, *528*, 14–20. [CrossRef] [PubMed]
59. Hirano, T.; Fujiwara, T.; Niwa, H.; Hirano, M.; Ohira, K.; Okazaki, Y.; Sato, S.; Umehara, T.; Maemoto, Y.; Ito, A.; et al. Development of Novel Inhibitors for Histone Methyltransferase SET7/9 based on Cyproheptadine. *ChemMedChem* **2018**, *13*, 1530–1540. [CrossRef]
60. Keijzer-Veen, M.G.; Schrevel, M.; Finken, M.J.; Dekker, F.W.; Nauta, J.; Hille, E.T.; Frolich, M.; van der Heijden, B.J.; Dutch, P.-C.S.G. Microalbuminuria and lower glomerular filtration rate at young adult age in subjects born very premature and after intrauterine growth retardation. *J. Am. Soc. Nephrol.* **2005**, *16*, 2762–2768. [CrossRef]
61. Hurtado Del Pozo, C.; Garreta, E.; Izpisua Belmonte, J.C.; Montserrat, N. Modeling epigenetic modifications in renal development and disease with organoids and genome editing. *Dis. Model Mech.* **2018**, *11*. [CrossRef]
62. Nurtjahja-Tjendraputra, E.; Fu, D.; Phang, J.M.; Richardson, D.R. Iron chelation regulates cyclin D1 expression via the proteasome: A link to iron deficiency-mediated growth suppression. *Blood* **2007**, *109*, 4045–4054. [CrossRef] [PubMed]
63. Swali, A.; McMullen, S.; Hayes, H.; Gambling, L.; McArdle, H.J.; Langley-Evans, S.C. Processes underlying the nutritional programming of embryonic development by iron deficiency in the rat. *PLoS ONE* **2012**, *7*, e48133. [CrossRef] [PubMed]
64. Mandala, A.; Armstrong, A.; Girresch, B.; Zhu, J.; Chilakala, A.; Chavalmane, S.; Chaudhary, K.; Biswas, P.; Ogilvie, J.; Gnana-Prakasam, J.P. Fenofibrate prevents iron induced activation of canonical Wnt/beta-catenin and oxidative stress signaling in the retina. *NPJ Aging Mech. Dis.* **2020**, *6*, 12. [CrossRef] [PubMed]
65. Song, S.; Christova, T.; Perusini, S.; Alizadeh, S.; Bao, R.Y.; Miller, B.W.; Hurren, R.; Jitkova, Y.; Gronda, M.; Isaac, M.; et al. Wnt inhibitor screen reveals iron dependence of beta-catenin signaling in cancers. *Cancer Res.* **2011**, *71*, 7628–7639. [CrossRef]
66. Zhao, X.-P.; Liao, M.-C.; Chang, S.-Y.; Abdo, S.; Aliou, Y.; Chenier, I.; Ingelfinger, J.R.; Zhang, S.-L. Maternal diabetes modulates kidney formation in murine progeny: The role of hedgehog interacting protein (HHIP). *Diabetologia* **2014**, *57*, 1986–1996. [CrossRef] [PubMed]
67. Chang, S.-Y.; Chen, Y.-W.; Zhao, X.-P.; Chenier, I.; Tran, S.; Sauvé, A.; Ingelfinger, J.R.; Zhang, S.-L. Catalase prevents maternal diabetes–induced perinatal programming via the Nrf2–HO-1 defense system. *Diabetes* **2012**, *61*, 2565–2574. [CrossRef] [PubMed]
68. Chen, Y.-W.; Chenier, I.; Tran, S.; Scotcher, M.; Chang, S.-Y.; Zhang, S.-L. Maternal diabetes programs hypertension and kidney injury in offspring. *Pediatric Nephrol.* **2010**, *25*, 1319–1329. [CrossRef]
69. Chen, Y.-W.; Chenier, I.; Chang, S.-Y.; Tran, S.; Ingelfinger, J.R.; Zhang, S.-L. High glucose promotes nascent nephron apoptosis via NF-κB and p53 pathways. *Am. J. Physiol. Ren. Physiol.* **2010**, *300*, F147–F156. [CrossRef]
70. Nehiri, T.; Van Huyen, J.-P.D.; Viltard, M.; Fassot, C.; Heudes, D.; Freund, N.; Deschênes, G.; Houillier, P.; Bruneval, P.; Lelièvre-Pégorier, M. Exposure to maternal diabetes induces salt-sensitive hypertension and impairs renal function in adult rat offspring. *Diabetes* **2008**, *57*, 2167–2175. [CrossRef]

71. França-Silva, N.; Oliveira, N.D.G.; Balbi, A.P.C. Morphofunctional renal alterations in rats induced by intrauterine hyperglycemic environment. *Arch. Med. Sci. AMS* **2016**, *12*, 243. [CrossRef]
72. Pani, L.; Horal, M.; Loeken, M.R. Polymorphic susceptibility to the molecular causes of neural tube defects during diabetic embryopathy. *Diabetes* **2002**, *51*, 2871–2874. [CrossRef] [PubMed]
73. Buchanan, T.A.; Denno, K.M.; Sipos, G.F.; Sadler, T.W. Diabetic teratogenesis. In vitro evidence for a multifactorial etiology with little contribution from glucose per se. *Diabetes* **1994**, *43*, 656–660. [CrossRef] [PubMed]
74. Wentzel, P.; Eriksson, U.J. Insulin treatment fails to abolish the teratogenic potential of serum from diabetic rats. *Eur. J. Endocrinol.* **1996**, *134*, 459–466. [CrossRef]
75. El Hajj, N.; Pliushch, G.; Schneider, E.; Dittrich, M.; Muller, T.; Korenkov, M.; Aretz, M.; Zechner, U.; Lehnen, H.; Haaf, T. Metabolic programming of MEST DNA methylation by intrauterine exposure to gestational diabetes mellitus. *Diabetes* **2013**, *62*, 1320–1328. [CrossRef] [PubMed]
76. Anguita-Ruiz, A.; Mendez-Gutierrez, A.; Ruperez, A.I.; Leis, R.; Bueno, G.; Gil-Campos, M.; Tofe, I.; Gomez-Llorente, C.; Moreno, L.A.; Gil, A.; et al. The protein S100A4 as a novel marker of insulin resistance in prepubertal and pubertal children with obesity. *Metabolism* **2020**, *105*, 154187. [CrossRef] [PubMed]
77. Hjort, L.; Martino, D.; Grunnet, L.G.; Naeem, H.; Maksimovic, J.; Olsson, A.H.; Zhang, C.; Ling, C.; Olsen, S.F.; Saffery, R.; et al. Gestational diabetes and maternal obesity are associated with epigenome-wide methylation changes in children. *JCI Insight* **2018**, *3*. [CrossRef] [PubMed]
78. Quilter, C.R.; Cooper, W.N.; Cliffe, K.M.; Skinner, B.M.; Prentice, P.M.; Nelson, L.; Bauer, J.; Ong, K.K.; Constancia, M.; Lowe, W.L.; et al. Impact on offspring methylation patterns of maternal gestational diabetes mellitus and intrauterine growth restraint suggest common genes and pathways linked to subsequent type 2 diabetes risk. *FASEB J.* **2014**, *28*, 4868–4879. [CrossRef] [PubMed]
79. Hilliard, S.A.; El-Dahr, S.S. Epigenetics mechanisms in renal development. *Pediatric Nephrol.* **2016**, *31*, 1055–1060. [CrossRef]
80. Wanner, N.; Bechtel-Walz, W. Epigenetics of kidney disease. *Cell Tissue Res.* **2017**, *369*, 75–92. [CrossRef]
81. Bechtel, W.; McGoohan, S.; Zeisberg, E.M.; Muller, G.A.; Kalbacher, H.; Salant, D.J.; Muller, C.A.; Kalluri, R.; Zeisberg, M. Methylation determines fibroblast activation and fibrogenesis in the kidney. *Nat. Med.* **2010**, *16*, 544–550. [CrossRef]
82. Chen, S.; Yao, X.; Li, Y.; Saifudeen, Z.; Bachvarov, D.; El-Dahr, S.S. Histone deacetylase 1 and 2 regulate Wnt and p53 pathways in the ureteric bud epithelium. *Development* **2015**, *142*, 1180–1192. [CrossRef]
83. Rosenberg, S.L.; Chen, S.; McLaughlin, N.; El-Dahr, S.S. Regulation of kidney development by histone deacetylases. *Pediatric Nephrol.* **2011**, *26*, 1445–1452. [CrossRef] [PubMed]
84. Kobayashi, A.; Valerius, M.T.; Mugford, J.W.; Carroll, T.J.; Self, M.; Oliver, G.; McMahon, A.P. Six2 defines and regulates a multipotent self-renewing nephron progenitor population throughout mammalian kidney development. *Cell Stem Cell* **2008**, *3*, 169–181. [CrossRef]
85. Kumaki, Y.; Oda, M.; Okano, M. QUMA: Quantification tool for methylation analysis. *Nucleic Acids Res.* **2008**, *36*, W170–W175. [CrossRef] [PubMed]
86. Trapnell, C.; Pachter, L.; Salzberg, S.L. TopHat: Discovering splice junctions with RNA-Seq. *Bioinformatics* **2009**, *25*, 1105–1111. [CrossRef]
87. Anders, S.; Pyl, P.T.; Huber, W. HTSeq–a Python framework to work with high-throughput sequencing data. *Bioinformatics* **2015**, *31*, 166–169. [CrossRef] [PubMed]
88. Love, M.I.; Huber, W.; Anders, S. Moderated estimation of fold change and dispersion for RNA-seq data with DESeq2. *Genome Biol.* **2014**, *15*, 550. [CrossRef]
89. Cohen, C.D.; Frach, K.; Schlondorff, D.; Kretzler, M. Quantitative gene expression analysis in renal biopsies: A novel protocol for a high-throughput multicenter application. *Kidney Int.* **2002**, *61*, 133–140. [CrossRef] [PubMed]
90. Cohen, C.D.; Klingenhoff, A.; Boucherot, A.; Nitsche, A.; Henger, A.; Brunner, B.; Schmid, H.; Merkle, M.; Saleem, M.A.; Koller, K.P.; et al. Comparative promoter analysis allows de novo identification of specialized cell junction-associated proteins. *Proc. Natl. Acad. Sci. USA* **2006**, *103*, 5682–5687. [CrossRef]
91. Tusher, V.G.; Tibshirani, R.; Chu, G. Significance analysis of microarrays applied to the ionizing radiation response. *Proc. Natl. Acad. Sci. USA* **2001**, *98*, 5116–5121. [CrossRef]
92. Mamo, S.; Gal, A.B.; Bodo, S.; Dinnyes, A. Quantitative evaluation and selection of reference genes in mouse oocytes and embryos cultured in vivo and in vitro. *BMC Dev Biol.* **2007**, *7*, 14. [CrossRef] [PubMed]

# 2. Aims and Hypotheses

Low nephron numbers of the kidneys at birth are a risk factor for chronic kidney disease and hypertension later in life. The present thesis aims to evaluate three common conditions affecting pregnant women by modelling them in *ex vivo* cultures of murine metanephroi.

- *Ex vivo* exposure of metanephroi to high glucose as a model of maternal diabetes
- *Ex vivo* exposure of metanephroi to high incubation temperatures as a model of maternal hyperthermia
- *Ex vivo* exposure of metanephroi to iron restriction as a model of reduced iron availability

These experimental conditions are hypothesized to reduce the number of nephrons formed in culture. Each of the three conditions will be analyzed for their potential to influence expla

nt growth and nephron number. Any detected reduction in nephron number is to be investigated further in terms of associated morphological alterations and changes in proliferation or cell death.

# 3. Copyright Notice

# 4. Introduction

## 4.1. The Kidney

Kidneys are paired organs, which are vital for the maintenance of electrolyte and acid-base homeostasis, as well as the production of hormones and the regulation of blood pressure. The basic functional units of kidneys are the nephrons (Figure 1). These consist of a renal corpuscle and a communicated renal tubule. The renal corpuscle itself is composed of the glomerulus, with a tuft of capillaries that is covered by podocytes, and the surrounding Bowman's capsule. Primary urine is formed as the blood pressure forces water and low-molecular components of the blood through the glomerular filtration barrier, which consists of the fenestrated endothelium, the glomerular basement membrane, and the slit diaphragms of the podocytes. This primary urine then flows through the connected tubule, where the functionally and anatomically different tubule segments reabsorb water, glucose, sodium, chloride, amino acids, and other substances. Waste products such as urea or uric acid, as well as hydrogen ions and other electrolytes are excreted into the urine as it passes through the tubules. Lastly, all tubules open into the collecting duct system where further reabsorption of electrolytes and water occurs. All of these processes are closely controlled by endocrine as well as paracrine hormones to maintain the homeostasis of blood contents and blood pressure. The volume of primary urine filtered through the glomerular filtration barrier per unit of time is defined as the glomerular filtration rate (GFR), which is widely considered to be the best indicator of kidney function (Jones and Lim 2003), as it closely relates to the kidneys capability to rid the blood of waste products and fulfil its homeostatic functions.

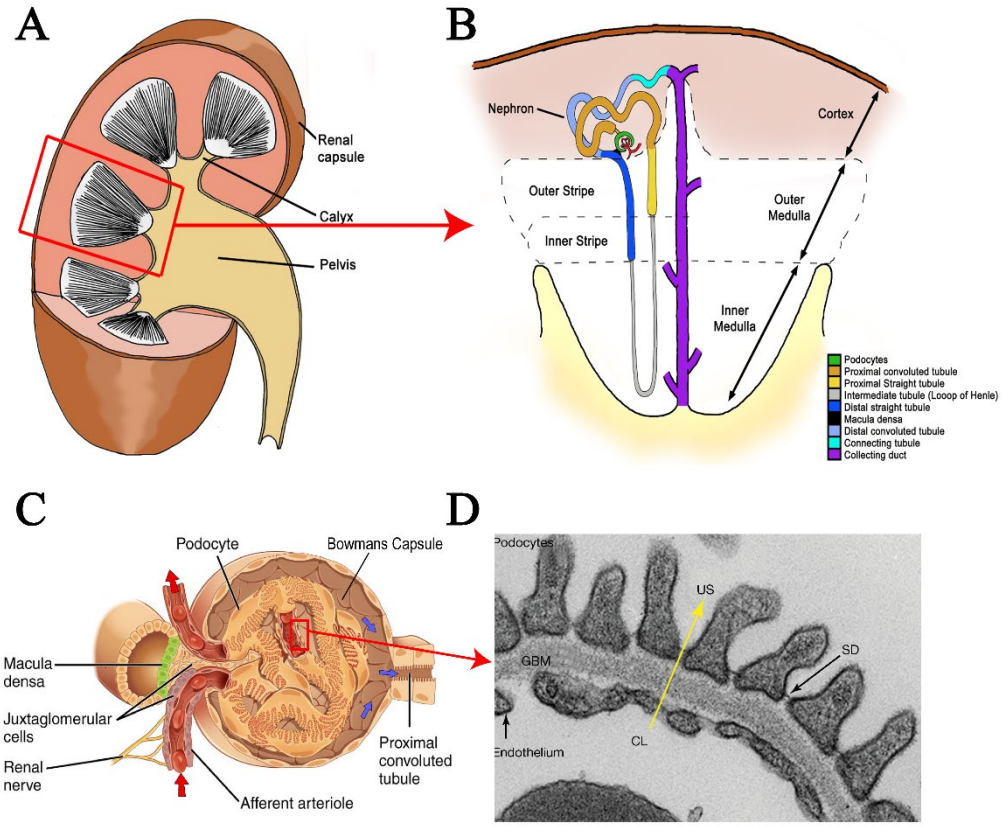


**Figure 1. A,** Schematic of a mature kidney. **B,** Schematic of a nephron, note the indication of multiple nephrons opening into the collecting duct.[I] **C,** Schematic of a single glomerulus, red arrows indicate the flow of blood in the arterioles, blue arrows indicate the flow of primary urine in the Bowman's capsule.[II] **D,** Electron micrograph showing a section through a glomerular arteriole, showing the glomerular filtration barrier consisting of the fenestrated endothelium, glomerular basement membrane (GBM) and slit diaphragm (SD). The yellow arrow indicates the direction of ultrafiltration from the capillary lumen (CL) to the urinary space (US) [III]

## 4.2. Hypertension and Chronic Kidney disease

Hypertension and renal dysfunction are closely interrelated. On the one hand, hypertension is a known risk factor for chronic kidney disease. On the other hand, the kidney plays a central role in the regulation of blood pressure. In "primary" or "essential" hypertension, the most prevalent form hypertension, the immediate cause of the increased blood pressure is, by clinical definition, not known. However, there is good evidence of a pathological contribution of the kidneys, as renal transplantation transmits the disease from donor to recipient in both rats and

---

[I] Reprinted from „*Mouse kidney development*", Alan J. Davidson, StemBook, ed. The Stem Cell Research Community, StemBook, doi/10.3824/stembook.1.34.1. Copyright: ©2008 Alan J. Davidson. Licensed under a Creative Commons Attribution 3.0 Unported License: https://creativecommons.org/licenses/by/3.0/. Alterations: Red square and arrow added for visual clarity.

[II] Reprinted from „*Anatomy and Physiology*", J. Gordon Betts, Kelly A. Young, James A. Wise, Eddie Johnson, Brandon Poe, Dean H. Kruse, Oksana Korol, Jody E. Johnson, Mark Womble, Peter DeSaix ©2013 OpenStax College. Licensed under a Creative Commons Attribution 4.0 License: https://creativecommons.org/licenses/by/4.0/. Alterations: Arrows and Square added for visual clarity.

[III] Reprinted from „*Nefrologia*" Vol. 35. Issue. 2, Page 134, March 2015. Katherine Carranzaa, Dolores Veronb, Alicia Cercadoc, Noemi Bautistac, Wilson Pozod, Alda Tufroe, Delma Veronc, „*Cellular and molecular aspects of diabetic nephropathy; the role of VEGF-A*" © 2015 Katherine Carranza. Licensed under a Creative Commons attribution noncommercial nonderivatives 4.0 international license: https://creativecommons.org/licenses/by-nc-nd/4.0/. No Alterations

humans (Bianchi and Fox *et al.* 1974, Curtis and Luke *et al.* 1983). This form of hypertension is not only a major risk factor for renal, but also for cardiovascular disease. It is considered to be a global public health challenge both medically and economically, and is estimated to affect 1.56 billion people worldwide by 2025 (Kearney and Whelton *et al.* 2005, Lackland and Weber 2015).

In the long run, hypertension can induce renal dysfunction by damaging the renal vasculature, leading to chronic kidney disease (CKD). This condition is defined as a long-term loss of kidney function, typically accompanied by a reduction in GFR. Besides hypertension, it is also commonly caused by diabetes mellitus, glomerulonephritis, or by idiopathic reasons. The global prevalence of CKD is estimated to be 11 %-13 % (Hill and Fatoba *et al.* 2016). While the early stages of kidney dysfunction are not noticeable to the affected, later stages of progression are associated with intense morbidity and may require renal replacement therapy or a kidney transplantation to avoid death. In developed countries, the increased mortality of CKD patients is mainly mediated by an increased risk of cardiovascular events, infections, and malignant conditions, whereas the unavailability of renal replacement therapy in developing countries more commonly results in lethal uraemia or electrolyte disturbances. Overall, CKD is estimated to account for 1.2 million deaths globally each year (Steel 2017). Furthermore it was estimated that the total number of patients receiving renal replacement therapy or a renal transplant will be 5.68 million in 2030, more than double the amount of 2010, making adequate care not only a medical, but also an economic problem of global proportions (Liyanage and Ninomiya *et al.* 2015). These developments necessitate better prevention and detection strategies for both hypertension and chronic kidney disease, which may be enabled by an improved understanding of the underlying causes.

## 4.3. The Barker and Brenner Hypotheses

In 1990, epidemiological observations led David Barker to hypothesise that an adverse intrauterine environment may "program" the foetal physiology and metabolism to be predisposed to diseases such as hypertension and cardiovascular disease later in life (Barker 1990). This was coined the "Foetal Origins of Adult Disease" (FOAD) or Barker hypothesis. Brenner *et al.* expanded on this by hypothesising that the long-term programming of hypertension and renal disease may be mediated by an altered renal microanatomy at birth, more specifically by a reduced number of nephrons. This concept was subsequently referred to as the Brenner hypothesis (Brenner and Garcia *et al.* 1988). The proposed mechanism was that human born with fewer nephrons possess a reduced glomerular filtration surface, which could

impair the sodium excretion and be detrimental to the survival of the glomerulus due to an increased filtering load. The resulting sodium and fluid retention would then contribute to hypertension, further making the nephrons susceptible to glomerulosclerosis. Due to the reduced initial number of nephrons, the kidney's capacity to compensate for a loss of functional nephrons as a consequence of age and disease would also be diminished. It was inferred that individual with low nephron endowment would therefore be predisposed to hypertension and glomerular damage, leading to increased risk of cardiovascular disease and CKD.

In healthy young populations, the number of nephrons per kidney varies widely from individual to individual, variations up to a 13-fold range from 210 thousand to 2.7 million have been reported (Puelles and Hoy *et al.* 2011). This has attracted special attention to possible determinants of the nephron numbers, as humans are not able to form new nephrons after the cessation of nephrogenesis between week 34 and 36 of gestation (Bertram and Douglas-Denton *et al.* 2011, Black and Sutherland *et al.* 2012). Consequentially, the conditions under which the metanephroi mature may have life-long consequences as they may influence the initial endowment and nephrons and thus influence the functional reserves of the kidneys. This has led to a search for intrauterine factors which contribute to greater or smaller nephron endowment. Unfortunately, there is currently no technique available to directly measure the number of nephrons in living humans, which is why rodent studies have been of great relevance to this field. Known risk factors for reduced nephron numbers in rodents include intrauterine growth restriction, maternal low protein diet, medication including corticosteroids or nonsteroidal anti-inflammatory drugs, several monogenetic mutations, low Vitamin A levels as well as maternal diabetes and iron-deficiency (Lelièvre-Pégorier and Vilar *et al.* 1998, Langley-Evans and Welham *et al.* 1999, Lewis and Forhead *et al.* 2002, Singh and Moritz *et al.* 2007, Cain and Di Giovanni *et al.* 2010, Hokke and Armitage *et al.* 2013).

## 4.4. Mammalian Kidney Development

After the formation of the pro- and mesonephroi in the intermediate mesoderm, the development of the kidneys, also referred to as metanephroi, begins as the metanephric mesenchyme induces the ureteric bud to form as an epithelial protuberance of the nephric duct (Figure 2). The newly formed ureteric bud invades in the caudal aspect of the metanephric mesenchyme. In a reciprocal interaction, signals from metanephric mesenchyme induce the ureteric bud to grow and undergo several iterations of dichotomous branching, while signalling molecules from the ureteric bud tips induce the metanephric mesenchyme to condensates and form "caps" surrounding the tips of the ureteric bud. In the direct vicinity of the ureteric bud

tips, the cap mesenchyme cells condense to form pretubular aggregates, the first stage in the development of a nephron. Meanwhile, a population of mesenchymal stem cells must remain in the cap mesenchyme and proliferate without differentiation to replenish the supply of metanephric mesenchyme cells. This is achieved by the expression of Six2 (*Sine oculis*-related homeobox 2) and Osr1 (Odd-skipped-related 1), two transcription factors which prevent differentiation (Xu and Liu *et al.* 2014), among other mechanisms.

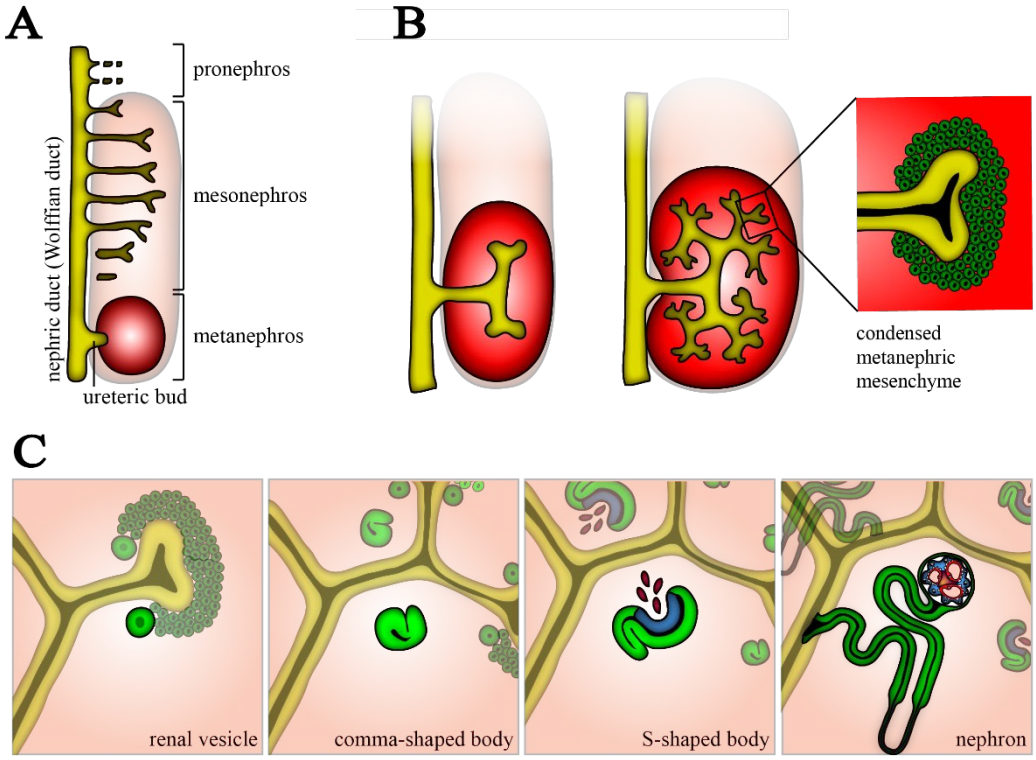


**Figure 2. A,** Schematics of the primitive renal entities. Note that the pronephros is already in the process of degeneration as the ureteric bud invades the metanephric mesenchyme. **B,** The ureteric bud invades the metanephric mesenchyme while it undergoes dichotomic branching. The metanephric mesenchyme cells (green) condense around the in the vicinity of the ureteric bud tips. **C,** Illustration of the consecutive stages of nephron development. Tubule and tubule progenitor cells are shown in green, podocytes and podocyte progenitors are shown in blue and the vascular endothelial cells shown in red.[IV]

The reciprocal interactions between the mesenchyme and the ureteric tips interactions are mediated by a variety of secreted factors. For example, the cells of the metanephric mesenchyme produce GDNF (Glial cell line-derived neurotrophic factor), which provokes Ret-receptor expressing cells of the ureteric bud to proliferate (Costantini and Shakya 2006). Conversely, the ureteric bud induces the cells of the pretubular aggregates to undergo mesenchymal to epithelial transition (MET) via Wnt (Wingless-related integration site) signalling (Carroll and Park *et al.* 2005). During the process of MET, aggregates polarize and

[IV] Reprinted from „*Seminars in Cell & Developmental Biology*“ Vol. 36, December 2014, Page 41, C. Schell, N. Wanner, T. B. Huber, „*Glomerular development – Shaping the multi-cellular filtration unit*“ Copyright © 2014 the Authors, with permission from Elsevier. Licensed under the Attribution-NonCommercial-NoDerivs 3.0 Unported Creative Commons license: https://creativecommons.org/licenses/by-nc-nd/3.0/

form a spherical epithelium with a central lumen, a stage denoted as epithelial renal vesicles. The vesicles then elongate to form comma-shaped bodies. The fate of the epithelial cells is determined by their position along a proximal-distal axis of the nephron via multiple signalling pathways (Kopan and Cheng *et al.* 2007). During this process, this patterning becomes apparent by the differential expression of several genes. The formation of the proximal segment of the comma-shaped body is dependent on Notch2 (Neurogenic locus notch homolog protein 2) signalling. These cells express Wilms tumor protein (Wt1) and later develop to form the podocytes, as well as the cells of the Bowman's capsule (Cheng and Kim *et al.* 2007). The cells of the distal segment, which expresses JAG1, later develop to form the proximal and medial tubule (Heliot and Desgrange *et al.* 2013). As the nephron elongates and folds to form an s-shaped body, a third segment which can be identified by the expression of LGR5 (Leucine-rich repeat-containing G-protein coupled receptor 5), arises at the distal end of the nephron and subsequently forms the distal parts of the tubule (Barker and Rookmaaker *et al.* 2012). As the JAG1-positive segment thus finds itself between the proximal and newly formed distal segment it may also be denoted as the "intermediate" segment. During nephron maturation, the segments are divided into further anatomical and functional subsegments, according to the combined influence of developmental signals. The cells of the different segments show distinct differences in terms of their metabolism and especially the expression of transporter proteins. The cells of the ureteric bud later develop to form the collecting duct system, as well as the calices.

To conceptualize the factors influencing the number of nephrons, three variables which influence this number can be considered. The first variable would be the number of times the ureteric tip branches, as only the tips of the ureteric bud are the primary site of pretubular aggregate formation. A reduction in this variable may explain the reduced nephron numbers in GDNF-heterozygous mice where the ureteric bud is exposed to a reduced dose of this growth factor and thus branches less (Cullen-McEwen and Drago *et al.* 2001). A second variable would be the average number of renal vesicles which each ureteric tip induces to form during its presence, as each vesicle can only mature to form a single nephron. This rate of induction likely depends on the proliferation, arrangement and inducibility of mesenchymal progenitor cells near the tip, as well as the ability of each ureteric bud to expose them to the correct signals. This does not mean that the number of nephrons formed and ureteric tips has to be equal, as it has been shown that the number of nephrons lags the number of ureteric tips in the early phases, while this relationship reverses towards the end of nephrogenesis, when each tip becomes able to induce multiple nephrons (Cebrián and Borodo *et al.* 2004). This increase in inducibility has

been demonstrated to be an intrinsic, age-related process of the pluripotent mesenchymal cell population (Chen and Brunskill *et al.* 2015). The final variable would then be the probability with which each renal vesicle matures to a functional nephron and survives until birth.

Most of what is known about mammalian kidney development has been researched in mice, as will be the case in the experiments in this thesis. Key differences between murine and human nephrogenesis include the longer duration as well as the greater overall nephron number and final kidney size in humans. Furthermore, the formation of nephrons is still rapidly ongoing at birth in mice and terminates in the postnatal period, whereas it cedes before birth in humans (Hartman and Lai *et al.* 2007).

## 4.5. Low Nephron Numbers in Humans.

The greatest obstacle in the investigation of determinants of nephron number in humans has been the lack of a reliable non-invasive technique for nephron counting. It is also known that nephrons are lost throughout life due to aging and disease. Consequentially, post mortem nephron counting is not a valid method for estimating the nephron endowment at birth if the autopsied humans have died at an advanced age or after renal disease. Several studies from autopsies after accidents and neonatal deaths have shown the number of nephrons per kidney to correlate positively with the total birth weight (Mañalich and Reyes *et al.* 2000, Hughson and Farris *et al.* 2003, Hughson and Douglas-Denton *et al.* 2006). A low birth weight can be caused by many adverse circumstances of gestation including premature delivery, maternal hypertension, malnutrition, as well as placental factors such as placental abruption, infarction or insufficiency. It therefore appears that the connection between adverse gestational circumstances and nephron endowment may hold true in humans.

To study the consequences of nephron numbers epidemiologically, reduced birth weight has been used as a surrogate marker for the population for which low nephron numbers can be assumed. Studies linking low birth weight to markers of kidney dysfunction (decreased GFR or increased albumin excretion) first emerged from smaller studies in at-risk populations such as very prematurely born children (Keijzer-Veen and Schrevel *et al.* 2005), or Australian aborigines (Hoy and Rees *et al.* 1999). More recently, a meta-analysis including more than 2 million individuals has estimated that a birth weight <2,500 gram increases the risk of CKD by 70 % (White and Perkovic *et al.* 2009). A connection between adverse intrauterine conditions and kidney disease risk exists thus appears plausible in humans, where reduced nephron numbers are thought of as a mediating factor.

Another line of evidence has linked reduced nephron numbers to primary hypertension, as Brenner *et al.* had initially proposed. A study of the kidneys of accident victims has shown the median number of nephrons in subjects suffering from primary hypertension to be approximately half of the median number in normotensive subjects (~702,000 vs. ~1,429,000) (Keller and Zimmer *et al.* 2003).

In conclusion, low nephron numbers appear to be a relevant risk factor for hypertension and CKD in humans. In order to develop preventative strategies to ensure adequate nephron endowment at birth and to detect pregnancies where kidney development is at risk, a mechanistic understanding of the factors supporting or impeding the development of nephron-rich kidneys is necessary.

## 4.6. *In vivo* and *ex vivo* Experimental Methods of Renal Development

To identify causes of reduced nephron numbers, many *in vivo* animal experiments have been performed. In these studies, conditions such as malnutrition or diabetes mellitus were induced in female animals (usually mice or rats), and the nephron number and blood pressure of the offspring was measured. While this is undoubtedly the closest model to a human pregnancy, it does suffer from a few drawbacks. These include that the conditions surround in the developing kidneys cannot directly controlled, as any change to the maternal organism will entail complex reactions in the maternal, placental and foetal physiology which may themselves alter the kidney development. As a consequence, it may be very difficult to establish the direct cause of any alteration observed in the kidney development. *Ex vivo* modelling techniques circumvent this by the enabling the investigation of kidney development completely separated from the influence of the mother animal, the placenta, as well as the other organs of the fetus. This is achieved by the microsurgical isolation of the metaneproi at an early stage of their development and subsequent *in vitro* culturing of the metanephroi in a more directly controlled environment. Such techniques were pioneered by Oswald Trowell in 1950, who first performed a culture of metanephroi on a medium-air interface (Trowell 1954). The methods of *ex vivo* organ cultures have subsequently been improved, notablyby Saxen *et al.* in 1987, who pioneered the culturing of kidneys on filter membranes (Saxen and Lehtonen 1987).

## 4.7. Renal Development and Maternal Diabetes

Gestational diabetes mellitus (GDM), where the mother develops a diabetic state during pregnancy, is more prevalent than pre-gestational type 1 or 2 diabetes mellitus (PGDM), where the disease precedes the pregnancy. Both conditions are associated with hyperglycemia, which

can disturb both maternal organ function and the gestation. A global review estimated the prevalence in low and middle income countries to range from 0.4–24.3 % for GDM and 0.0-0.7 % for PGDM (Kanguru and Bezawada *et al.* 2014). Recent decades have produced strong increases in the prevalence of both GDM and PGDM in developed countries. A cohort study in the United Kingdom has reported the prevalence of PGDM to be increased from 0.39 to 1.47 % between 1995 and 2012 (Coton and Nazareth *et al.* 2016). Estimations range as high as 2.2 % in the United States of America (Peterson and Grosse *et al.* 2015). If these trends continue in high-income countries, and developing countries follow their example, the consequences of embryonic and fetal development in a diabetic environment appear likely to gain even greater importance in the future.

There is a well-documented teratogenic effect of maternal diabetes during the first trimester in terms of clinically apparent defects such as neural tube, cardiovascular and skeletal defects (Ramos-Arroyo and Rodriguez-Pinilla *et al.* 1992). Considering the growing prevalence in PGDM in recent decades, it has been of interest to investigate whether this condition may also cause sub-clinical alterations of kidney development, such as a reduced nephron number. Along the lines of the Brenner hypothesis, such changes may become apparent by an increased risk of kidney disease or hypertension later in life. Clinical evidence for such "programmed" complications in offspring of pre-gestationally hyperglycemic mothers has first emerged from studies linking pregestational diabetes to albuminuria (Nelson and Morgenstern *et al.* 1998), as well as increased systolic blood pressure in Pima Indian families (Nelson and Morgenstem *et al.* 1998). A meta-analysis has shown *in utero* diabetes exposure (including GDM) to be associated with higher systolic blood pressure (Aceti and Santhakumaran *et al.* 2012). No data from humans has been published concerning the direct effect of PGDM or GDM exposure on the total nephron number due to the before mentioned unavailability of non-invasive measurements for this parameter.

In both mouse and rat models where a diabetic state was induced by streptozotocin (STZ) injection, the offspring was shown to possess smaller kidneys with fewer glomeruli and increased blood pressure (Amri and Freund *et al.* 1999, Nehiri and Van Huyen *et al.* 2008, Tran and Chen *et al.* 2008, Chen and Chenier *et al.* 2010, Chen and Chenier *et al.* 2010, Chang and Chen *et al.* 2012, Hokke and Armitage *et al.* 2013, Zhao and Liao *et al.* 2014, França-Silva and Oliveira *et al.* 2016). Whether this reduced nephron endowment is due to an impairment in initial nephron formation or the destruction of nephrons throughout the gestation is still debated between authors: Tran *et al.* proposed a mechanism primarily by of nephron apoptosis due to oxidative stress (Tran and Chen *et al.* 2008), and have since published data showing a an

amelioration of nephron number and blood pressure by overexpression of catalase (Chang and Chen *et al.* 2012). In contrast, Hokke *et al.* have more recently ascribed the nephron deficit an earlier retardation of metanephric growth, as reduced ureteric branching and kidney size were evident as early as the embryonic day (E) 14.5. In their experiments, insulin replacement after E13.5 did not result in a normalisation in the number of glomeruli in the kidneys, even if the dams were normoglycemic for most of the period of nephron maturation. They concluded that the reduced nephron number at birth would mostly be mediated by an early retardation of growth and branching, which results in fewer nephrons being initially formed, rather than previously formed nephrons being destroyed (Hokke and Armitage *et al.* 2013).

In a transfilter organ culture system, Kanwar *et al.* have reported an increased glucose concentration to lead to a strong (50-30 %) reduction in size, as well as apoptotic dysmorphia of the ureteric bud and a strong reduction in the number of tubules (Kanwar and Liu *et al.* 1996, Kanwar and Akagi *et al.* 2005, Kanwar and Nayak *et al.* 2005).

## 4.8. Renal Development in Hyperthermia and Fever

Fever during pregnancy is a common phenomenon with known teratogenic potential and possible renal complications (Dreier and Andersen *et al.* 2014), yet the question of whether febrile illness during pregnancy or hyperthermia may increase the risk of CKD in the offspring via reduced nephron endowment has not been discussed in the literature. Increased body temperature was first linked to malformations more than 100 years ago, when first evidence emerged of malformations in the offspring of animals which were exposed to external heat during pregnancy (Warkany 1986). It is important to note that such externally induced hyperthermia is mechanistically different from fever, which is defined as an "elevation of body temperature that […] occurs in conjunction with an increase in the hypothalamic set point" (Kasper and Fauci *et al.* 2015). In hyperthermia this set point remains unchanged, and the body temperature is elevated by other factors, exceeding the body's inability to lose heat (Kasper and Fauci *et al.* 2015). Both fever and hyperthermia may share teratogenic effects which are mediated purely by the increased temperature, while differences may occur as a consequence of their different associated causes as well as the organism's compensatory reactions.

Fever during pregnancy is a common phenomenon, as illustrated by 18.5 % of women in the Danish national birth cohort having reported an episode of fever during the first 16 weeks of pregnancy (Andersen and Vastrup *et al.* 2002). However, in most animal studies the increased body temperature is a consequence of external heat application and therefore constitutes hyperthermia, which limits the applicability to human febrile disease.

In humans, the teratogenicity of feverish infections is well-described, a recent meta-review found a 1.5 to 3-fold increase in the risks for heart defects, oral clefts and neural tube defects (Dreier and Andersen *et al.* 2014). Human data on the effect of fever or hyperthermia on the kidney development is scarce, but two case-control studies of infants have shown a significant association between maternal febrile illness during pregnancy and renal malformations, especially renal agenesis (Abe and Honein *et al.* 2003, Waller and Hashmi *et al.* 2018). Both maternal febrile illness and embryonic exposure to extremely warm weather also appear to be associated with decreased birth weight, which as mentioned before is associated with decreased nephron number (Van Zutphen and Lin *et al.* 2012, Philpott and Englund *et al.* 2017).

*In vivo* animal studies have reported similar reductions in the birth weight following maternal hyperthermia (Edwards 1986). This phenomenon has even been used as a method of inducing intrauterine growth restriction in sheep (Galan and Anthony *et al.* 2005). Interestingly, the hyperthermia already induced fetal *in utero* hypertension in these experiments. Unfortunately, no long-term renal outcomes of animal offspring after gestational hyperthermia exposure have been reported. Cases of renal agenesis or hypoplasia have been observed gestational hyperthermia experiments involving guinea pigs and bonnet monkeys (Edwards 1969, Hendrickx and Stone *et al.* 1979), although nephron counting was not performed in any study. Consequently, it is still unknown whether high body temperatures during gestation may induce subclinical reductions in nephron endowment.

## 4.9. Renal Development and Fetal Iron-Deficiency

Iron-deficiency is the most widespread nutrient deficiency worldwide and globally an estimated 19.2 % of pregnant women suffer from iron-deficiency anemia (Black and Victora *et al.* 2013). It has been shown that maternal iron-deficiency results in reduced birth weight (Haider and Olofin *et al.* 2013). It also leads to reduced iron stores of the newborn at birth (Kumar and Rai *et al.* 2008), as measured by cord blood plasma ferritin, which is a commonly accepted as indicator of fetal iron stores (Siddappa and Rao *et al.* 2007). This indicates that the human placental system may not completely compensate for decreased iron availability.

While maternal iron-deficiency anemia is very prevalent, the consequences for the offspring are still unclear. Two cohort studies have found low maternal hemoglobin concentration to be associated with higher offspring blood pressure (Law and Barker *et al.* 1991, Godfrey and Forrester *et al.* 1994), while two others have found an opposite association (Bergel and Haelterman *et al.* 2000, Brion and Leary *et al.* 2008), and three have not found a significant association (Belfort and Rifas-Shiman *et al.* 2008, Alwan and Lawlor *et al.* 2012, Alwan and

Cade *et al.* 2014). However, maternal iron status is not the only determinant of fetal iron stores. Significant reductions in the cord blood ferritin concentrations have also been reported in pregnancies involving maternal obesity (Dosch and Guslits *et al.* 2016), maternal smoking (Sweet and Savage *et al.* 2001) and babies born small for gestational age (McCarthy and Kenny *et al.* 2017), as well as preeclampsia (Chockalingam and Murphy *et al.* 1987) and maternal diabetes (Georgieff and Landon *et al.* 1990), demonstrating that the reduction in ferritin-bound iron may be a common element in conditions involving fetal hypoxia or placental insufficiency. As hypoxic conditions lead to a reactive polyglobulia, the increased iron consumption by the hematopoietic system is thought to decrease the amount of iron available to other organs. This can be hypothesized to cause other organs to undergo a "local" iron-deficiency, although the fetal hemoglobin concentration at birth is normal or even increased. These effects have been well explored in maternal diabetes, which is associated with fetal hypoxia (Taricco and Radaelli *et al.* 2009), most likely due to an increased metabolic rate due to hyperglycemia and hyperinsulinemia. This contributes to increased erythropoietin concentrations (Salvesen and Brudenell *et al.* 1993), which lead to increased fetal hemoglobin concentrations, and an increased hematocrit (Salvesen and Brudenell *et al.* 1992). Newborns of diabetic mothers display drastic shifts in their iron stores, which may, in part, be attributed to the increased erythropoiesis. An autopsy study of newborns of diabetic and nondiabetic mothers revealed the tissue iron concentration to be reduced by 93.4 % in the liver, by 56.1 % in the heart, and 39.4 % in the brain in comparison to newborns from non-diabetic mothers (Petry and Eaton *et al.* 1992). Unfortunately, no data on kidney iron concentration was published, but this indicates that reduced iron availability to fetal organs may occur in conditions other than maternal iron-deficiency.

Animal experiments have demonstrated the impact of iron-deficiency on renal development. Rats born by dams suffering from nutritional iron-deficiency have been shown to suffer from a reduction in the number of glomeruli and increased blood pressure (Lewis and Petry *et al.* 2001, Lewis and Forhead *et al.* 2002, Gambling and Dunford *et al.* 2003, Lisle and Lewis *et al.* 2003, Nehiri and Van Huyen *et al.* 2008), although one study has reported a significant reduction in blood pressure (Sun and Woolley *et al.* 2017). Many detrimental effects of maternal iron-deficiency on the nephrogenesis have been considered, including gestational hypoxia as a consequence of maternal anemia. Only one study has reported the renal iron content at birth, which was reduced by ~50 % in those newborn rats which were exposed to maternal iron-deficiency (Sun and Woolley *et al.* 2017). It thus appears that that the iron uptake by the developing kidney is negatively affected in pregnancies affected by maternal iron-deficiency.

In rats, where nephrogenesis is still ongoing after birth, it was also shown that selective nutritional iron-deficiency after birth still induced a reduced glomerular endowment and kidney iron content (Drake and Sauerbry *et al.* 2009). This indicates that reduced iron availability to the kidneys is not conserved, and may be responsible for a proportion of the nephron deficits, independently of gestational hypoxia caused by maternal iron-deficiency anemia. Little is known about possible alterations of morphogenesis in metanephroi under conditions of reduced iron availability. While the kidney culture model was instrumental in the demonstration of transferrin (Tf) as an iron transporting protein, it has not previously been employed for this purpose

# 5. Materials

## 5.1. Chemicals and Reagents

**Table 1.** Chemicals and Reagents.

| Name | Linear formula | Provider |
|---|---|---|
| **Acetic acid** | $CH_3COOH$ | Carl Roth GmbH, Karlsruhe, Germany |
| **Agarose** | $C_{12}H_{18}O_9$ | Serva Electrophoresis GmbH, Heidelberg, Germany |
| **Aqua ad injectabilia** | $H_20$ | Braun, Melsungen, Germany |
| **BSA (Albumin bovine fraction V)** | - | Serva Electrophoresis GmbH, Heidelberg, Germany |
| **Disodium phosphate** | $Na_2HPO_4$ | Carl Roth GmbH, Karlsruhe, Germany |
| **EDTA (Ethylendiamintetraacidicacid)** | $C_{10}H_{16}N_2O_8$ | Serva Electrophoresis GmbH, Heidelberg, Germany |
| **Ethanol** | $C_2H_6O$ | SAV Liquid Production GmbH, Flintsbach, Germany |
| **Ethidium bromide solution (10 mg/ml)** | $C_{21}H_{20}BrN_3$ | Fiers, Kuurne, Belgium |
| **Glycerol** | $C_3H_8O_3$ | Carl Roth GmbH, Karlsruhe, Germany |
| **Glycine** | $C_2H_5NO_2$ | VWR International GmbH, Darmstadt, Germany |
| **HEPES, 1M (N-2-hydroxyethylpiperazine-N-2-ethane sulfonic acid)** | $C_8H_{18}N_2O_4S$ | Thermo Fisher Scientific, Darmstadt, Germany |
| **Hoechst 33342** | $C_{27}H_{31}Cl_3N_6O$ | Molecular Probes Inc. Eugene, Oregon, USA |
| **Hydrogen chloride** | $HCl$ | Sigma-Aldrich GmbH, Steinheim, Germany |
| **Isopropanol** | $C_3H_8O$ | VWR International GmbH, Darmstadt, Germany |
| **Magnesium chloride (25 mM)** | $MgCl_2$ | Promega, Madison, Wisconsin, USA |
| **Mannitol** | $C_6H_{14}O_6$ | Sigma-Aldrich GmbH, Steinheim, Germany |
| **Methanol** | $CH_3OH$ | Sigma-Aldrich GmbH, Steinheim, Germany |

| | | |
|---|---|---|
| **Monopotassium phosphate** | $KH_2PO_4$ | Carl Roth GmbH, Karlsruhe, Germany |
| **Nucleoside triphosphates (2.5 mM each)** | dATP: $C_{10}H_{16}N_5O_{12}P_3$ | Thermo Fisher Scientific, Darmstadt, Germany |
| | dCTP: $C_9H_{16}N_3O_{13}P_3$ | |
| | dGTP: $C_{10}H_{16}N_5O_{13}P_3$ | |
| | dTTP: $C_{10}H_{17}N_2O_{14}P$ | |
| **Paraformaldehyde** | $OH(CH_2O)_nH_{(n=8-100)}$ | Sigma-Aldrich GmbH, Steinheim, Germany |
| **Penicillin/Streptomycin** | $C_8H_{12}N_2O_5S/C_{21}H_{39}N_7O_{12}$ | Sigma-Aldrich GmbH, Steinheim, Germany |
| **Potassium chloride** | KCl | Carl Roth GmbH, Karlsruhe, Germany |
| **Sodium acetate** | $C_2H_3NaO_2$ | Carl Roth GmbH, Karlsruhe, Germany |
| **Sodium chloride** | NaCl | VWR International GmbH, Darmstadt, Germany |
| **ß-Mercaptoethanol** | $C_2H_6OS$ | Sigma-Aldrich GmbH, Steinheim, Germany |
| **Tris hydrochloride** | $C_4H_{11}NO_3$*HCl | Carl Roth GmbH, Karlsruhe, Germany |
| **Tris(hydroxymethyl) aminomethane** | $C_4H_{11}NO_3$ | Carl Roth GmbH, Karlsruhe, Germany |
| **Tween 20 (Polyoxyethylen-20-sorbitan-monolaurate)** | $C_{58}H_{114}O_{26}$ | AppliChem, Darmstadt, Germany |
| **Water, nuclease-free** | $H_20$ | Thermo Fisher Scientific, Darmstadt, Germany |
| **α-D-glucose** | $C_6H_{12}O_6$ | Sigma-Aldrich GmbH, Steinheim, Germany |

## 5.2. Consumables

**Table 2.** Consumables

| Product | Size | Provider |
|---|---|---|
| **Aluminum foil** | - | Carl Roth GmbH, Karlsruhe, Germany |
| **Cell culture plates, flat bottom** | 12- and 24-well | Sigma-Aldrich GmbH, Steinheim, Germany |
| **Disposable scalpel, Feather™** | #15 | Sigma-Aldrich GmbH, Steinheim, Germany |
| **DNA LoBind™ tubes** | 1.5 ml, 2 ml | Eppendorf, Hamburg, Germany |
| **Falcon™ tubes** | 15 ml, 50 ml | Greiner Bio-One, Frickenhausen, Germany |
| **Gloves, latex** | L | Ansell, Richmond, Australia |
| **Gloves, nitrile** | L | Ansell, Richmond, Australia |
| **Hypodermic needle** | #12 | B. Braun Melsungen AG, Melsungen, Germany |
| **Microscope slides, ground edges** | 25 x 75 x 1 mm | R. Langenbrinck, Emmendingen, Germany |
| **Microscopical cover slips** | 24 x 46 x 0.13 mm | R. Langenbrinck, Emmendingen, Germany |
| **Nail polish** | - | Suhada LIDL Stiftung & Co. KG, Neckarsulm, Germany |
| **Paper wipes, KimTech™** | 11 x 21 cm | Kimberly-Clark Professional, Koblenz, Germany |
| **Parafilm™** | - | Bemis, Neenah, Wisconsin, USA |

| | | |
|---|---|---|
| **Pasteur pipettes** | - | Carl Roth GmbH, Karlsruhe, Germany |
| **PCR single cap 8-piece soft-strips** | 0.2 ml | Biozym, Oldendorf, Germany |
| **PET Cell culture insert, track-etched membrane** | 12 well 0.4 µm pore size | Thermo Fisher Scientific, Darmstadt, Germany |
| **Petri dishes** | 92 x 16 mm, 35 x 10 mm | Sarstedt, Nümbrecht, Germany |
| **Pipette filter tips, sterile** | 0.1 - 10 µl, 1 - 200 µl, 100 - 1000 µl | Biozym, Oldendorf, Germany |
| **Pipette tips** | 0.1 - 10 µl, 1 - 200 µl | Biozym, Oldendorf, Germany |
| **Pipette tips** | 100 - 1000 µl | Sorenson BioScience Inc., Salt Lake City, Utah, USA |
| **Polypropylene reaction tubes** | 1.5 ml, 2 ml | Sarstedt, Nümbrecht, Germany |
| **Precellys lysing kit soft tissue homogenizing tubes with beads** | CK14 | Bertin Technologies, Rockville, Maryland, USA |
| **RNAse away** | - | Thermo Fisher Scientific, Darmstadt, Germany |
| **Sterile pipettes** | 5 ml, 10 ml, 25 ml, 50 ml | Sigma-Aldrich GmbH, Steinheim, Germany |
| **96 well qPCR plate, thin-wall** | | Bio-Rad Laboratories GmbH, Munich, Germany |
| **96 well adhesive seals, Microseal™ 'B'** | | Bio-Rad Laboratories GmbH, Munich, Germany |
| **µ-Dish™, glass bottom, sterile** | 35 mm | ibidi GmbH, Munich, Germany |

## 5.3. Machines and Equipment

**Table 3.** Machines and Equipment.

| Product | Size |
|---|---|
| **Tissue homogenizer, Minilys™** | Bertin Technologies, Rockville, Maryland, USA |
| **12-channel pipette, 0.5 - 10 µl, Discovery comfort™** | Kinesis GmbH, Langenfeld, Germany |
| **Axiocam rev.3 black/white 1388 x 1040** | Zeiss, Oberkochen, Germany |
| **Balance, CPA micro balance CPA26 P** | Sartorius AG, Göttingen, Germany |
| **Beakers, Erlenmeyer flasks, bottles** | Schott, Mainz, Germany |
| **Binokular, S6E** | Leica Mikrosysteme GmbH, Wetzlar, Germany |
| **Centrifuge, 5415 R** | Eppendorf, Hamburg, Germany |
| **Electrophoresis cell , Sub-Cell GT™** | Bio-Rad Laboratories GmbH, Munich, Germany |
| **Forceps, Dumont #5** | Fine Science Tools GmbH, Heidelberg, Germany |
| **Forceps, rounded, Semken** | Fine Science Tools GmbH, Heidelberg, Germany |
| **Freezer, -20 °C** | Liebherr, Bulle, Switzerland |
| **Freezer, HeraFreeze™, -80 °C** | Thermo Fisher Scientific, Darmstadt, Germany |

| | |
|---|---|
| **Gel caster and combs** | Bio-Rad Laboratories GmbH, Munich, Germany |
| **Gel documentation system, Gel iX20 imager™** | Intas Science Imaging Instruments GmbH, Göttingen, Germany |
| **Incubator, HeraCell 240i™, 37 °C, 5 % CO2** | Thermo Fisher Scientific, Darmstadt, Germany |
| **Kühlschrank, 4 °C** | Liebherr, Bulle, Switzerland |
| **Laboratory hood, ZBSA** | Wesemann, Wangen, Germany |
| **Microwave** | Carl Roth GmbH, Karlsruhe, Germany |
| **Mikroscope, inverted, Axiovert 100™** | Zeiss, Oberkochen, Germany |
| **Mikroscope, inverted, AxioObserver™** | Zeiss, Oberkochen, Germany |
| **Mini-centrifuge, Sprout™** | Biozym, Oldendorf, Germany |
| **Mini-Zentrifuge, Rotilabo™** | Carl Roth GmbH, Karlsruhe, Germany |
| **Objective, c-apochromat 63x** | Zeiss, Oberkochen, Germany |
| **Objective, plan-apochromat 20x** | Zeiss, Oberkochen, Germany |
| **Objective, plan-neofluar 5x/0.15** | Zeiss, Oberkochen, Germany |
| **Objektive, EC Plan-Neofluar™ 10x / 0.30 Ph 1** | Zeiss, Oberkochen, Germany |
| **Objektive, Fluar 20x / 0,75** | Zeiss, Oberkochen, Germany |
| **Perforated spoon, Moria™** | Fine Science Tools GmbH, Heidelberg, Germany |
| **pH-indicator strips** | Perth Scientific Pty Ltd, Malaga, Australia |
| **Pipettes** | Gilson, Middleton, Wisconsin, USA |
| **Pipetting aid, Pipetboy™ acu 2** | Integra Biosciences GmbH, Biebertal, Germany |
| **Power supply, PowerPac™** | Bio-Rad Laboratories GmbH, Munich, Germany |
| **Real time PCR detection system, CFX Connect™** | Bio-Rad Laboratories GmbH, Munich, Germany |
| **Spectrophotometer, NanoDrop™ ND-1000** | Thermo Fisher Scientific, Darmstadt, Germany |
| **Sterile bench, HeraSafe™** | Thermo Fisher Scientific, Darmstadt, Germany |
| **Stopwatch** | Carl Roth GmbH, Karlsruhe, Germany |
| **Thermal cycler, Mastercycler™ ep Gradient S** | Eppendorf, Hamburg, Germany |
| **ThermoMixer™ C** | Eppendorf, Hamburg, Germany |
| **U2 LSM 510 META laser scanning microscope** | Zeiss, Oberkochen, Germany |
| **UV Lamp** | CAMAG, Muttenz, Switzerland |
| **Vortex device** | VWR International GmbH, Darmstadt, Germany |

## 5.4. Buffers and Solutions

**Table 4.** Buffers and Solutions

| Name | Composition |
|---|---|
| **Agarose gel, 2 %** | 10 g Agarose<br>500 ml 1x TAE |
| **Antifade reagent, Prolong Gold™** | Thermo Fisher Scientific, Darmstadt, Germany |
| **Blocking buffer for immunofluoresence** | 1x PBST<br>50 mg/ml BSA |
| **DMEM (Dulbecco's Modified Eagle Medium), glucose free** | Thermo Fisher Scientific, Darmstadt, Germany |
| **DNA ladder 100 bp, 1 kb** | Peqlab, Erlangen Germany |
| **DNA loading buffer (6x)** | Peqlab Biotechnologies GmbH, Erlangen, Germany |
| ***Dolichos Biflorus* agglutinin (DBA) FITC-conjugated** | Vectorlabs, Peterborough, UK |
| **Ham's F-12 nutrient solution** | Thermo Fisher Scientific, Darmstadt, Germany |
| **Kidney culture base medium** | 12.5 ml DMEM no glucose<br>12.5 ml Ham's F12<br>250 µl Penicilin/Streptomycin solution, 100x<br>500 µl Holo-Transferrin solution, 1.25mg/ml |
| **Kidney culture high glucose medium** | Kidney culture base medium<br>4.50 mg/ml D-Glucose |
| **Kidney culture hyperthermia/normothermia medium** | Kidney culture base medium<br>10 mM HEPES |
| **Kidney culture iron-deficient medium** | 12.5 ml DMEM no glucose<br>12.5 ml Ham's F12<br>250 µl Penicilin/Streptomycin solution, 100x<br>500 µl Apo-transferrin solution, 1.25mg/ml |
| **Kidney culture low glucose control medium** | Kidney culture base medium<br>4.552 mg/ml mannitol |
| **LysoTracker™ red DND-99** | Thermo Fisher Scientific, Darmstadt, Germany |
| **NaCl solution, 5M** | 14.5 g NaCl<br>50 ml H2O |
| **NaOH solution, 25 mM, pH 12** | 48.75 g NaOH<br>50 ml H2O |
| **Paraformaldehyde (PFA) solution, 4 %** | 20 g PFA<br>500 ml 1x PBS |
| **Phosphate buffered saline solution (PBS), 10x** | 210.4 g NaCl<br>5.3 g KCl<br>30.2 g Na2HPO4 7x H20<br>5.3 g KH2PO4<br>2.5 l ddH20 |
| **PBS, 1x** | 100 ml 10x PBS<br>900 ml H20 |
| **PBST, 1x** | 100 ml 10x PBS<br>900 ml H20 |

| | |
|---|---|
| | 1 ml (0.1 %) Tween20 |
| **PCR master mix, DreamTaq Green™, 2x** | Thermo Fisher Scientific, Darmstadt, Germany |
| **Penicillin/Streptomycin solution, 100x** | 10 ml PBS<br>100 mg Penicillin<br>100 mg Streptomycin |
| **Phosphate buffer, 0.1 M** | Sigma-Aldrich GmbH, Steinheim, Germany |
| **qPCR supermix, SsoAdvanced universal SYBR green™, 2x** | Bio-Rad Laboratories GmbH, Munich, Germany |
| **TAE buffer, (TRIS-acetate-EDTA) 50x** | 242 g TRIS<br>57.1 ml acetic acid<br>18.6 g EDTA<br>H2O ad 1l<br>Adjust pH to 8.8 |
| **TAE, 1x** | 20 ml 50x TAE<br>980 ml H20 |
| **TE-buffer, pH9** | 4.4 g Tris<br>1.62 g EDTA<br>fill to 1 l H2O, adjust pH to 9 |
| **TrisHCl, 10 mM, pH 8** | 0.07 g TrisHCl<br>50 ml H2O<br>adjust pH to 8<br>sterile filtered |
| **TrisHCl, 40 mM , pH 5** | 0.28 g TrisHCl<br>50 ml H2O<br>adjust pH to 12<br>sterile filtered |

## 5.5. Kits

**Table 5.** Kits

| Kit | Provider |
|---|---|
| **iScript Reverse Transcription Supermix for RT-qPCR Kit** | Bio-Rad Laboratories GmbH, München, Deutschland |
| **RNeasy Plus Mini Kit** | Qiagen, Hilden, Deutschland |

## 5.6. Antibodies

**Table 6.** Antibodies.

| Primary Antibody | Raised in | Code | Dilution used | Provider |
|---|---|---|---|---|
| **α-active Caspase 3** | Rabbit | AF835 | 1:250 | R&D Systems, Inc., Minneapolis, Minnesota, Germany |
| **α-JAG1 rabbit** | Rabbit | 2620S | 1:100 | Cell Signaling Technology, Danvas, Massachusetts, USA |
| **Tamm-Horsefall Protein** | Sheep | AB2606308 | 1:250 | Thermo Fisher Scientific, Darmstadt, Germany |
| **α-Pancytokeratin mouse** | Mouse | ab11213 | 1:250 | Abcam, Cambridge, United Kingdom |

| | | | | |
|---|---|---|---|---|
| **α-SIX2 rabbit** | Rabbit | 11562-1-AP | 1:100 | Proteintech Group Inc., Manchester, United Kingdom |
| **α-WT1 mouse** | Mouse | 05-753 | 1:100 | Merck Chemicals GmbH, Darmstadt, Germany |
| **α-CD326 (Ep-CAM)** | Rat | 118202 | 1:100 | BioLegend, San Diego, Kalifornien, USA |
| **α-NKCC2 (Slc12a1)** | Rabbit | SPC-401D | 1:100 | StressMarq Biosciences, Victoria, Kanada |
| **α-Phospho-Histone H3 (pHH3)** | Mouse | 9706S | 1:100 | Cell Signaling Technology, Danvas, Massachusetts, USA |
| **α-E-cadherin** | Mouse | 4A2C7 | 1:200 | Thermo Fisher Scientific, Darmstadt, Germany |
| **Secondary Antibody** | **Raised in** | **Code** | **Dilution used** | **Provider** |
| **Alexa Fluor 488 α-mouse** | donkey | R37114 | 1:300 | Thermo Fisher Scientific, Darmstadt, Germany |
| **Alexa Fluor 488 α-rabbit** | donkey | R37118 | 1:300 | Thermo Fisher Scientific, Darmstadt, Germany |
| **Alexa Fluor 555 donkey α-mouse** | donkey | A-31570 | 1:300 | Thermo Fisher Scientific, Darmstadt, Germany |
| **Alexa Fluor 555 donkey α-rabbit** | donkey | A-31572 | 1:300 | Thermo Fisher Scientific, Darmstadt, Germany |
| **Alexa Fluor 555 donkey α-sheep** | donkey | A-21436 | 1:300 | Thermo Fisher Scientific, Darmstadt, Germany |
| **Alexa Fluor 555 goat α-rat** | donkey | A-21434 | 1:300 | Thermo Fisher Scientific, Darmstadt, Germany |

## 5.7. Primers

**Table 7.** Primers.

| **Genotyping** | **Forward 5'→3'** | **Reverse 5'→3'** |
|---|---|---|
| **O/MR (Tomato)** | CTCTGCTGCCTCCTGGCTTCT | 4350 (WT): CGAGGCGGATCACAAGCAATA<br>4351 (Tomato): TCAATGGGCGGGGGTCGTT |
| **S1xA/B (Cre)** | GCATAACCAGTGAAACAGCATTGCTG | GGACATGTTCAGGGATCGCCAGGCG |
| **qPCR** | | |
| *mHprt* | GCTTTCCTTGGTCAAGCAGTACAG | GAAGTGCTCATTATAGTCAAGGGCATATCC |
| *Jag1* | TGGTTGGCTGGGAAATT | TGGACACCAGGGCACATTC |

## 5.8. Software

**Table 8.** Software

| Product | Version | Provider |
|---|---|---|
| **Adobe Photoshop** | CS5 | Adobe Systems GmbH, München, Germany |
| **Adobe Illustrator** | 15.0.0 | Adobe Systems GmbH, München, Germany |
| **CFX Manager** | 3.01 | Bio-Rad Laboratories GmbH, Munich, Germany |
| **EndNote** | 7.5 | Clarivate Analytics, Philadelphia, Pennsylvania, USA |
| **Fiji (Fiji is just ImageJ)** | 1.51d | National Institutes of Health, Bethesda, Maryland, USA |
| **GrapPad Prism** | 7 | GraphPad Software, La Jolla, California, USA |
| **Micosoft Office** | 2010 | Microsoft, Redmont, Washington, USA |
| **Windows** | 7 | Microsoft, Redmont, Washington, USA |
| **Zen blue and black** | 2012 | Zeiss, Oberkochen, Germany |

# 6. Methods

## 6.1. Animal Handling

Mice were kept in a specific-pathogen-free environment at the Center for Experimental Models and Transgenic Service (CEMT), Stefan-Meier-Straße 17, 7904 Freiburg. All mice were raised in a 12/12 hour cycle of light and darkness, with access to water and standard chow *ad libidum*. Handling, breeding and killing of the animals was performed in cooperation with Dr. Nicola Wanner. All experiments were registered with the regional government of Baden-Wuerttemberg in Freiburg under the authorization codes X15/03R and X17/05F.

## 6.2. Mouse Strain

Transgenic reporter mice were used to distinguish between podocytes and other cells by the expression of different fluorescent reporter proteins. This technique relies on the Cre-loxP transgenic system. The Cre recombinase, which was first found in the genome of bacteriophage P1, specifically recombines DNA between two loxP (locus of X-over P1) sites, which can be used to permanently alter the genome of cells (Sternberg and Hamilton 1981). Transgenic mice which express the Cre recombinase gene under the control of cell type-specific promotors only exert Cre activity in these cells (and their progeny), which enables cell-type specific genetic manipulation (Orban and Chui *et al.* 1992). In the NPHS2.Cre strain used in these experiments, the Cre locus was driven by the NPHS2 promotor, which is podocyte-specific (Moeller and Sanden *et al.* 2003). As a result, all podocytes in these mice exhibit Cre activity, while all other cells do not. The Cre carrying strain was crossed with a dual fluorescent Cre reporter strain (Muzumdar and Tasic *et al.* 2007). This strain carries the genes of two fluorescent proteins behind the same Cytomegalovirus b-actin enhancer-promoter (pCA): the red fluorescent membrane targeted Tomato (mTom) gene immediately downstream of the promotor, and secondly the membrane targeted green fluorescent gene (mGFP) further downstream. Initially, all cells of the embryo transcribe the mTom gene and thus exhibit red fluorescence. The mTom gene is flanked by loxP-sites (floxed). The Cre recombinase, which is expressed specifically in the podocytes mediates the recombination at the loxP sites.

Both the mTomato gene and its polyadenylation sequence are thus excised specifically in the podocytes, whereupon the transcription of the mGFP gene immediately downstream of the second loxP-site takes is initiated in the podocytes (Figure 3). The podocytes cease to express mTom, and begin express mGFP instead. Consequently, they can be distinguished by their green fluorescence in live imaging, while all non-podocyte cells continue to express mTomato and therefore continue to exhibit red fluorescence.

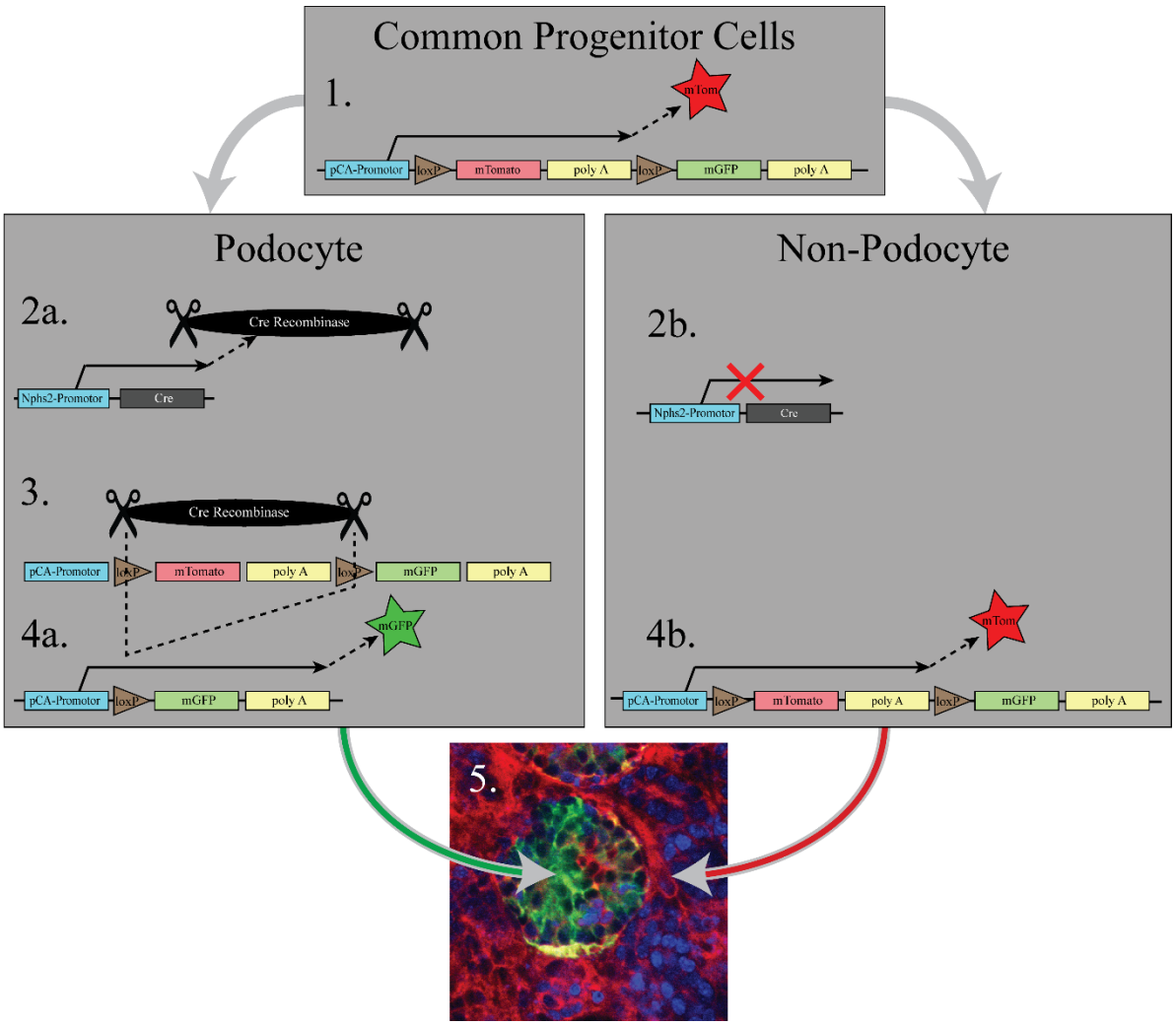


**Figure 3.** NPHS2;mT/mG Reporter Mice Schematic. NPHS2-Cre and pCA (CMV b-actin enhancer-promoter)-mT/mG mice are crossed to combine the presence of their transgenes. **1.** mT with its polyadenlyation sequence was located immediately downstream of the pCA promotor, surrounded by loxP sites, while the mG gene with its own polyadenylation sequence was located immediately downstream. Initially, no Cre activity was present in any of the embryo's cells, only the mT gene is transcribed, and all of the cells exhibit red fluorescence. **2a/b**. During kidney development, only the podocytes begin to produce Cre recombinase, as the transcription at the NPHS2 promotor is activated. **3.** In the podocytes, the Cre excises the mT sequence between the loxP-sites, resulting in the transcription of mG. **4a**. Thereby, the production of mT is stopped, and the expressin of mGFP is initiated at the same time, resulting in a switch from red to green fluorescence (Fig.1.4a). **4b.** All surrounding cells do not exhibit Cre activity and therefore continue to exhibit red fluorescence (Fig.1.4b). **5.** Confocal image of a glomerulus. The podocyte-containing glomeruli can therefore be clearly distinguished from the surrounding tissue by their green fluorescence. Blue channel: nuclear staining by Hoechst dye.

## 6.3. Genotyping

Genotyping of the mice was performed by polymerase chain reaction (PCR) amplification of DNA isolated from tail-biopsies and subsequent visualization of the amplified fragments by gel electrophoresis

### 6.3.1. DNA Isolation

From each animal a small (1-2 mm) tail biopsy was taken and stored in labeled PCR-strips. The biopsies were kept at -20 °C for at least 30 minutes to before further processing. To extract the DNA, 75 µl of 25 mM NaOH (pH 12) solution was added to each biopsy, followed by 30 minutes of incubation at 95 °C in the PCR-cycler. The solution was cooled down to 4 °C and then neutralised by adding further 75 µl of pH 5 40 mM TRIS-HCl solution. Finally, the DNA-solution was either immediately used in a PCR reaction, stored for short term use at 4 °C or frozen at -20 °C.

### 6.3.2. PCR-Reaction

To test for the presence of the relevant transgenes in the mice, the isolated DNA was amplified using primers which produce a fragment of a specific length in the presence of the transgene. When the transgene is not present, the reaction produces no fragment, or a fragment of another length. Table 9 shows the PCR reaction mixes and thermocycling steps for each of the transgenes.

**Table 9.** Genotyping PCR reaction mixes and Thermocycler programs

| **Transgene:** | **Cre** | | |
|---|---|---|---|
| Expected amplicon length | 280 bp (base pairs) | | |
| **Reaction Mix** | | | |
| **Component** | **Volume** | **Concentration** | |
| DNA solution | 2 µl | unknown | |
| $H_2O$ | 3 µl | - | |
| Primers (F/R) | 0.25 µl each | 10 µM | |
| $MgCl_2$ | 1.2 µl | 0.03 µM | |
| DreamTaq™ Green 2x | 7 µl | 1x | |
| **Thermocycler Program** | | | |
| **Step** | **Temperature** | **Duration** | |
| Initial Denaturation | 94 °C | 3 min | |
| Denaturation | 94 °C | 30 s | Repeat x35 |
| Annealing | 57 °C | 30 s | |
| Elongation | 72 °C | 40 s | |
| Final Extension | 72 °C | 5 min | |

| **Transgene:** | **Tomato** | | |
|---|---|---|---|
| Expected amplicon length | 250 bp | | |
| **Reaction Mix** | | | |
| **Component** | **Volume** | **Concentration** | |
| DNA solution | 2.1 µl | unknown | |
| $H_2O$ | 3 µl | - | |
| Primers (F/R) | 0.35 µl each | 10 µM | |
| $MgCl_2$ | 1.2 µl | 0.03 µM | |
| DreamTaq™ Green 2x | 7 µl | 1x | |
| **Thermocycler Program** | | | |
| **Step** | **Temperature** | **Duration** | |
| Initial Denaturation | 94 °C | 3 min | |
| Denaturation | 94 °C | 30 s | Repeat x35 |
| Annealing | 61 °C | 30 s | |
| Elongation | 72 °C | 40 s | |
| Final Extension | 72 °C | 5 min | |

### 6.3.3. Gel Electrophoresis

2 % agarose gels were produced by completely dissolving 2 g of Agarose in 100 ml of TAE buffer by heating the mixture in a microwave. Gels were then supplemented with 5 µl of 10 mg/ml ethidium bromide solution and cast in a tray with slotted combs. After hardening, the gels were immersed in TAE buffer inside the electrophoresis chamber. The samples to be visualized were then mixed with 1/5 of their volume of 6 x loading buffer and applied into the chambers. 6 µl of 100 bp DNA ladder solution were applied to a chamber on the same gel. The electrophoresis was performed at a voltage of 100V for 30 minutes. Finally, the gels were imaged using the gel documentation chamber.

## 6.4. Timed Harvest of Embryos

To harvest mice embryos at the appropriate developmental stages, the time of mating was recorded. Every morning of breeding, a vaginal inspection of the female mice was performed with a pair of rounded-tip forceps. When a vaginal plug was present, midnight of the previous night was designated as the presumed time of conception, also referred to as E0. Therefore, noon on the day of the positive plug-check was referred to as E0.5, and the noon 12 days later was referred to as E12.5.

## 6.5. Microdissection of Metanephroi

At E12.5 the pregnant mice were killed by cervical dislocation. Immediately, the abdomen of the mice was sprayed with 70 % ethanol for disinfection. The abdomen was opened using surgical scissors. The uterus was removed and immersed in ice-cold PBS solution. Under the binocular microscope, the embryos were carefully extracted from the amniotic sack using two pairs of Dumont #5 fine forceps. Before dissection, the embryos were transferred to another dish filled with ice-cold PBS solution using a Moria perforated spoon. Under the binocular microscope, a single embryo at a time was positioned on a small piece of Kimtech® wipe inside a PBS-filled petri dish using the perforated spoon. This process is illustrated in figure 4.

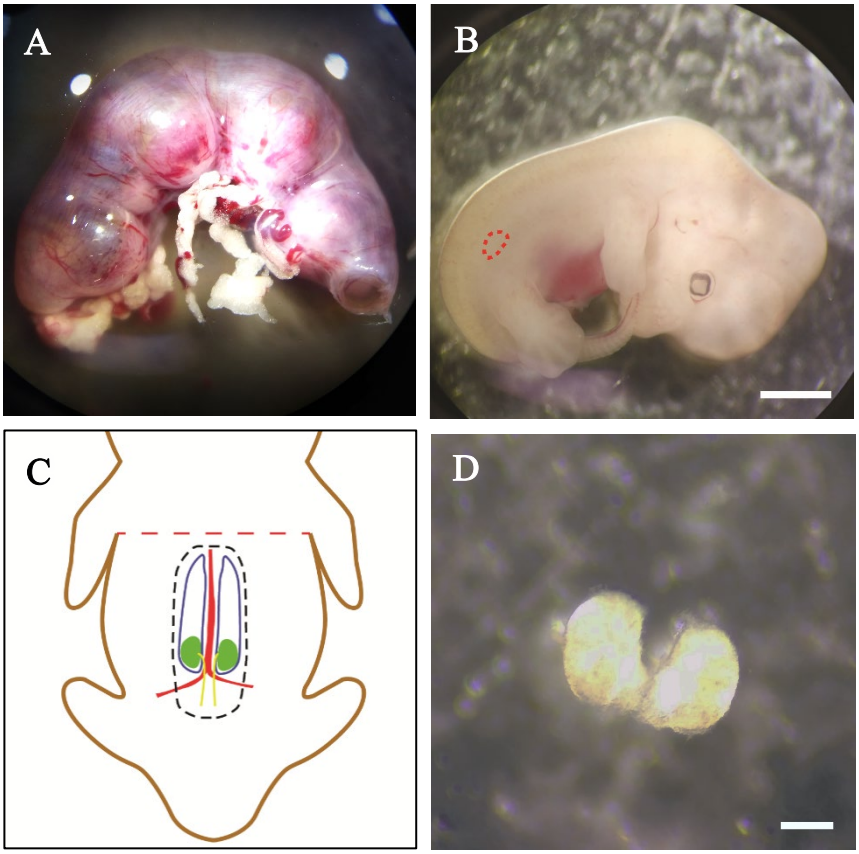


**Figure 4.** Microdissection of metanephroi **A,** Uterus containing four embryos. **B,** Extracted E12.5 embryo. The approximate location of the metanephroi is marked in red. Scale bar: 1000 µm. **C,** Schematic of the retroperitoneal anatomy in frontal view showing the positions of retroperitoneal organs including the aorta (red), urogenital ridge (blue), metanephroi (green) and ureteric duct (yellow). The section being extracted during the dissection process is marked with a dashed black line **D,** Dissected E12.5 kidneys from the same embryo. Scale bar: 500 µm.

Two size 12 Braun Sterican® disposable needles were used to separate the head from the lower body by a shearing motion. Afterwards, one needle was used to affix a hindlimb to the dish while the other needle was used to make an incision just rostrally of the genital tubercle and sever the placental vessels. This step loosens the abdominal wall sufficiently for it to be sheared rostrally, causing an evisceration of the abdominal and thoracic organs. As the organs were held close to the forelimbs with one needle, the other needle was used to cut through the whole embryo just caudally of the forelimbs. This left the back, tail, hindlimbs and retroperioneal organs intact for further dissection. Before proceeding to remove the urogenital ridges, the genital tubercle was split sagittally with a needle. At this stage, the two metanephroi could be seen inside in the urogenital ridges, caudally of the mesonephroi and separated by the developing aorta in the midline. Rostrally of the metanephroi, a pair of tweezers was used to tunnel beneath the urogenital ridges and aorta from laterally. By opening the tweezers, the mesonephroi and aorta were separated from the back and could be gently grabbed. By pulling this section in a caudal direction the complete urogenital ridges, including the metanephroi, could be peeled off. This separated section was moved away from the rest of the embryonic tissue. Using a disposable needle and a sharp pair of tweezers, the tissue surrounding the metanephroi was carefully dissected away. To protect the metanephroi from mechanical damage, this dissection was performed with as little direct contact of the instruments with the metanephroi as possible. Instead, one instrument was used to affix the surrounding tissue to the petri dish, while the other was used to shear between the first instrument and the metanephroi. This way the extrametanephric tissue, except for a small portion of the ureteric bud, was removed. In order to wash off floating debris, the metanephroi were drawn into a 200 µl pipette tip and transferred into the next petri dish, which contained fresh cold PBS solution. Finally, the metanephoi were mounted on the cell culture inserts by drawing them into a fresh pipette tip in as little of surrounding PBS as possible, about 1 µl, and pipetting them onto the membrane. The excess PBS was then drawn off using the pipette.

## 6.6. *Ex vivo* Culture of Metanephroi

To facilitate the controlled alteration of the conditions in which the metanephroi mature, an *ex vivo* culturing system was utilized. The following protocol is a modification based on the technique published by Ekblom *et al.* (Ekblom and Thesleff *et al.* 1981), which is serum-free. Up to six metanephoi were mounted on track-etched PET cell culture membrane inserts, which were then hung into a 12-well plate (Figure 5). Each well contained 500 µl of culture medium, which was sufficient for the media to make contact with the filters. When this volume of

medium is used, the medium adheres to the filter and kidney, but does not flood the insert. This position facilitates the horizontal growth of the kidneys at the air-medium interface on top of the filters. Throughout all experiments, the two kidneys from one embryo were placed on equivalent positions of the two different filters, which would then undergo different conditions during incubation. By this method, each kidney undergoing an experimental condition was paired to its genetically identical partner kidney undergoing the control condition. This pairing also meant that kidney pairs would be identical in age and genetic makeup, as well as being similar in size. The insert rims were marked with permanent marker, so that the two kidneys from the same embryo could be identified throughout all of the following procedures. The base medium consisted of a 1:1 mixture of Ham's F-12 nutrient mixture and glucose-free Dulbecco's Modified Eagle's Medium (DMEM), supplemented with 50 µg/ml bovine holo-transferrin, 100 µg/ml penicillin and 100 µg/ml streptomycin. All media were prepared under sterile conditions under the HeraSafe sterile bench. Unless noted otherwise, cultures were incubated at 37 °C, 100 % humidity and 5 % CO2. Media were replaced every 48 hours in the following manner: 500 µl of new medium was left to acclimatize for at least 15 minutes in another well of the same 12-well plate. Subsequently, the insert containing the kidneys was carefully transferred to the well containing the new medium.

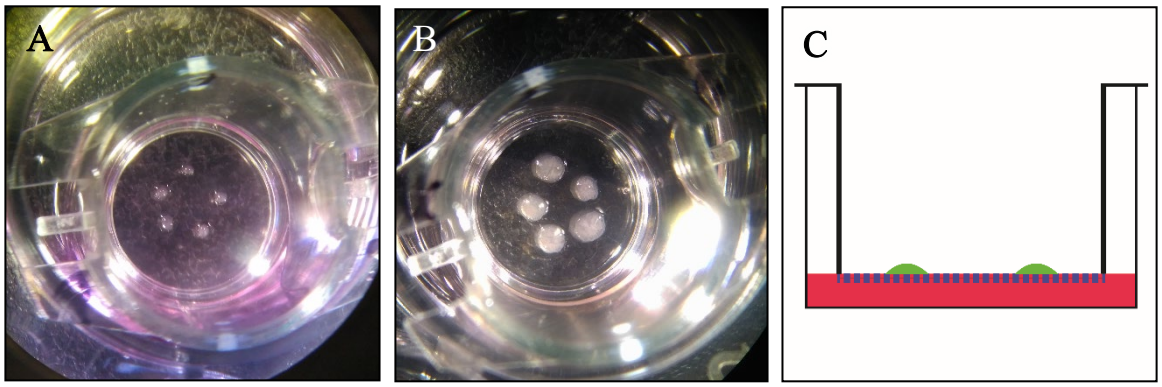


**Figure 5.** Assembly of the kidney culture **A**, *Transwell*® inserts with explants immediately after dissection. ***B****, Transwell*® insert with explants after 7 days of culture. **C**, Schematic of the culture, the metanephroi are shown in green, the membrane is shown as a dashed blue line and the culture medium is shown in red.

### 6.6.1. *Ex vivo* modelling of hyperglycemic conditions

The base medium already contained 5 mM D-glucose. The hyperglycemia medium was prepared by supplementing 25 ml of base medium with 112.6 mg of D-glucose for a final concentration of 30 mM D-glucose. For the control medium, an equimolar amount of mannitol (113.8 mg) was added to 25 ml of base medium for a final concentration of 5 mM of D-glucose and 25 mM mannitol.

### 6.6.2. *Ex vivo* modelling of hyperthermic conditions

Both hyperthermia and control cultures were incubated with the same medium. This medium consisted of the base medium, supplemented with 10 mM HEPES for increased buffering capacity. The hyperthermia cultures were incubated in a second incubator which was set to a temperature of 40 °C, while the control cultures were cultured at the normal 37 °C. All other settings were identical for both conditions.

### 6.6.3. *Ex vivo* modelling of iron-restriction

To model a decreased supply of transferrin-bound iron, the iron-deficient medium was not supplemented with bovine holo-transferrin. Instead, 50 µg/ml apo-transferrin (iron-free) was utilized. For the iron-sufficient control cultures, the base medium with 50 µg/ml holo-transferrin was used.

## 6.7. Live Imaging

To assess the growth of the metanephroi and quantify the development of glomeruli, wide-field live imaging of cultured metanephroi from NPHS2-Cre-Tomato-EGFP mice was performed. After 7 days of culture, the membrane inserts carrying the kidneys were mounted on a glass-bottom dish containing 200 µl of cold PBS. This dish was clamped into the AxioObserver inverted microscope. Tiled Z-Stack fluorescence photographs of the kidneys were produced with the EC Plan-Neofluar 10x objective and AxioCam MR R3 camera under the settings noted in table 10. To produce a z-stack from equivalent z-positions for each kidney, the first plane always chosen just above the membrane, at the lowest position where its pores were not visible. The plane distance of the z-stack was 10 µm. Images were numbered to facilitate the comparison between kidneys from the same embryo.

**Table 10.** Microscope imaging settings of day 7 size and glomerular count imaging

| Fluorescent Protein | Reflector | Excitation Wavelength | Emission Wavelength | Exposure time |
|---|---|---|---|---|
| Tomato | 43 HE Dsred (High Efficiency) | 538-562 | 570-640 | 80 ms |
| GFP | 38 HE GFP | 450-490 | 500-550 | 300 ms |

### 6.7.1. Planar Surface Area Quantification

The area occupied by the kidneys after seven days of culturing was chosen as a surrogate measure of the volume of the kidneys, as these parameters correlate closely (Gupta and Lapointe *et al.* 2003). To quantify this measure, kidney images acquired in 4.7 were processed in the Zen Blue 2: After tracking the outermost border of the kidneys in the lowest z-plane, the area calculated by the program was noted. Ureteric rudiments were not included as part of the kidneys as their dimensions vary with the dissection results. The surface area ratio was calculated separately for each pair of kidneys as follows:

$$surface\ area\ ratio = \frac{surface\ area\ of\ kidney\ cultured\ in\ experimental\ condition}{surface\ area\ of\ kidney\ cultured\ in\ control\ condition}$$

### 6.7.2. Automated counting of Glomeruli

To ensure an unbiased quantification of the number of glomeruli in each kidney, the GFP fluorescence of image files from 4.7 was analyzed by the use of an automated counting macro in ImageJ. For the initial preparation of the files in Zen 2, the Z-Stacks from 4.7. were orthogonally projected through all of their layers. From there on, only the green channel containing the GFP-signal was used for further processing. The pseudocolor of this channel was set to white. Histogram cutoff values were chosen as follows: low=502, high=1997. Images were exported in a 16-bit Tagged Image File Format (TIFF). Finally, these TIFF-files were batch processed in ImageJ using the following macro:

```
run("Gaussian Blur...", "sigma=5");
run("16-bit");
setAutoThreshold("Default");
//run("Threshold...");
setThreshold(50, 255);
run("Convert to Mask");
run("Make Binary");
run("Watershed");
run("3D Objects Counter", "threshold=255 slice=1 min.=600 max.=7967932 objects statistics summary");
```

This macro first reduced the shape complexity by applying a Gaussian blur filter. Next, a threshold filter with a fixed cutoff value of 50 was applied. After converting the file to a binary mask, the watershed tool was executed to separate close glomeruli from each other. Lastly, the 3D object counter counted the remaining glomeruli, while disregarding objects with a pixel size of less than 600. The output and log of the 3D object counter was saved. The process is illustrated in figure 6.

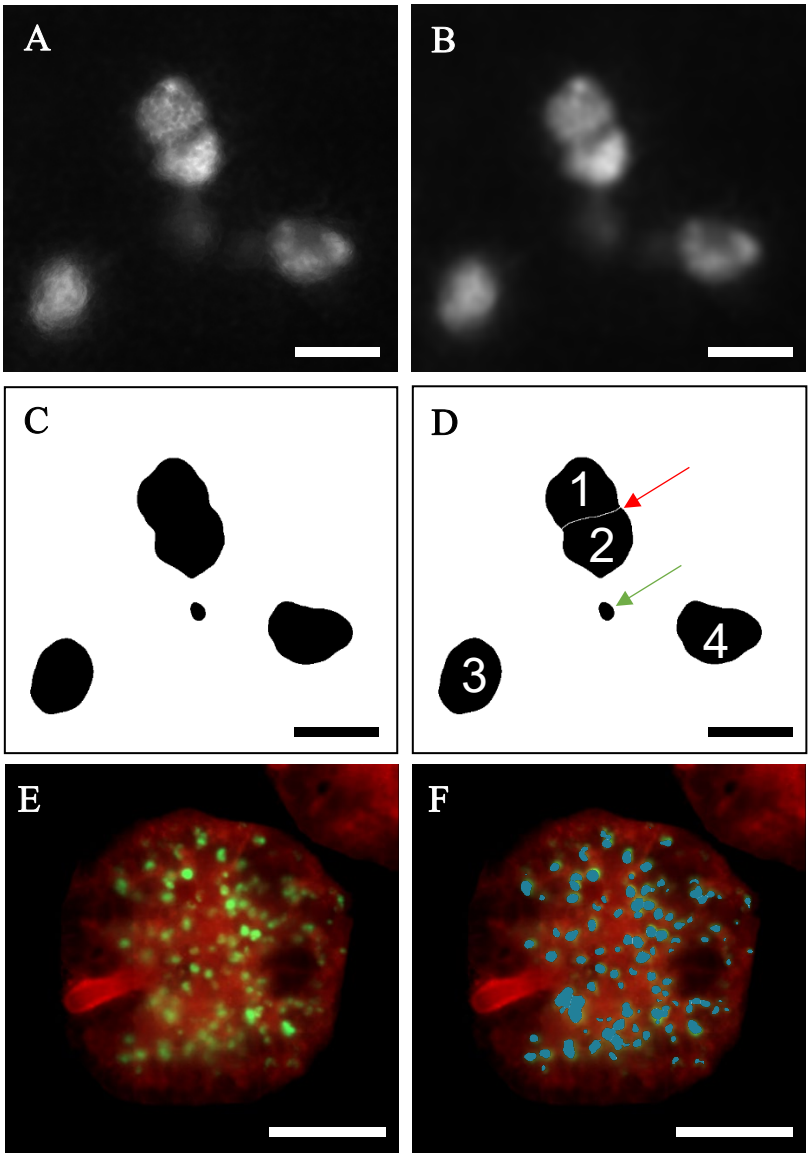


**Figure 6.** Steps of the glomerular counting algorithm. **A,** Cutout of an original GFP channel showing glomeruli. Scale bar: 100 µm **B,** The same picture after the application of Gaussian blur filter **C,** after the application of a threshold and **D,** after the application of the watershed tool, numbers indicating the result of the 3D counting tool. Note the separation between Glomeruli achieved by the use of the watershed algorithm marked in by the red arrow. The area marked with green arrows which was excluded due to its small size. **E,** A stitched example image of an explant showing mTom fluorescence in red and GFP fluorescence in green. Scale bar: 500 µm. **F,** The same image, with the superimposition of areas identified by the macro shown in blue.

## 6.8. Whole Mount Immunofluorescence staining of Explants

To localize the presence of proteins of interest inside the developing metanephroi, a whole mount immunofluorescence protocol was used. In this method the whole kidneys are fixed and permeabilized, after which the primary antibodies are added, which bind to the protein of interest. After washing, the primary antibodies are then bound to by secondary antibodies, which are conjugated to a fluorophore. Using the appropriate wavelength for excitation of the fluorophore, the microscopical detection of the wavelength emitted from the fluorophore serves to localize the protein of interest. In contrast to paraffin sections this technique enables the visualization of sections of interest *in toto* using wide field microscopy, as well as the flexible choice of focal planes in confocal microscopy.

**Day 1 of staining:** After the desired length of culture, the metanephroi were either fixed with cold methanol or room-temperature 4 % paraformaldehye (PFA) solution. For the methanol fixation, the membrane inserts were first transferred to another well containing 500 µl ice-cold methanol in order to attach the metanephroi to the membranes for 10 minutes. This attachment was very reliable, making it possible to maintain the matching of the two kidneys from the same embryo throughout the staining process by marking the relative positions with an incision on in the membrane. Afterwards, the membranes were cut out with a scalpel and transferred to a 24-well plate containing another 500 µl of ice-cold methanol for 10 minutes for the final fixation.

In case of the PFA fixation, the membranes were immediately cut out and transferred to a 24-well plate containing 500 µl of room-temperature 4 % PFA solution, and fixed for 15 minutes. Unfortunately, the PFA-fixed kidneys loosened from the filters, therefore the pairing was not maintained. Both methanol and PFA-fixed metanephroi were washed three times with room temperature PBST buffer (PBS + 0.1 % Tween 20) for five minutes each. Cultures were blocked with the blocking solution containing 5 % BSA in PBST buffer for three hours at room temperature. After blocking, the cultures were incubated in dilutions of the primary antibodies in blocking solution at 4 °C on an orbital shaker overnight. All antibody dilutions can be found in Table 6.

**Day 2 of staining:** Cultures were washed three times with blocking solution for two hours each. Afterwards, the cultures were incubated in a 1:300 dilution of secondary antibodies and 1:500 dilution of Hoechst nuclear dye in blocking solution overnight. All secondary antibodies were conjugated to Alexa$^{TM}$ Fluor fluorescent dyes.

**Day 3 of staining:** The cultures were washed another three times for two hours. Finally, cultures were mounted on microscope slides: To ensure the metanephroi are not deformed, six drops of nail polish were applied to the microscope slides and dried before the kidneys were transferred. These nailpolish spacers ensure that sufficient distance between the microscope slide and the cover slide is maintained. The membranes were then laid on the slides with the metanephroi facing upwards. PFA-fixed kidneys had to be transferred by pipetting with a 1000 µl tip. Finally, excess liquid was removed using a paper wipe and 100 µl of Prolong Gold mounting medium was applied to the kidneys. Lastly, the cover slide was carefully laid on top. The slides were then left at room temperature overnight to support the hardening of the mounting medium. The slides were stored at 4 °C. A finished slide is illustrated in figure 7.

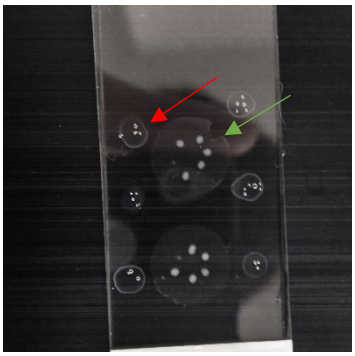

**Figure 7.** Whole mount microscopic slide. The green arrow marks the notch identifies the membrane of the experimental group. The red arrow marks one of the six nail polish spacers.

## 6.9. General Microscopy

Stained cultures were imaged using an AxioObserver inverted microscope, as well as the U2 LSM 510 META laser scanning microscope. Identical settings were used for control and experimental cultures.

### 6.9.1. Counting of Morphological Entities

To quantify the effects of the iron-deficiency condition on the development of the metanephroi some morphological entities were counted. This included the number of branching points of the ureteric bud and the number of Jagged1 (JAG1) -positive segments of early nephrons. For this purpose, kidneys grown in culture for 48 hours were whole mount stained for CD326 (EpCAM), a protein expressed by the ureteric bud, as well as JAG1, a protein expressed by the distal segment of the developing nephron. Subsequently, the kidneys were imaged on a Zeiss Axiovert 200 inverted microscope using the Plan-Neofluar 5x/0.15 Objective and Colibri LED illumination. Table 11 shows the settings used.

**Table 11.** Microscope imaging settings of JAG1 segment and branching point quantification.

| Protein | Wavelength | Filter Set | Excitation Wavelength | Emission Wavelength | Exposure time |
|---|---|---|---|---|---|
| **JAG1 (Alexa 555)** | 555 nm | 63 HE Red Fluoresc. Prot. | 559-585 nm | 600-690 nm | 6.5 ms |
| **CD326 (Alexa 488)** | 470 nm | 44 HE FITC | 455-495 nm | 505-555 nm | 950 ms |

The channels of the images were then split in ImageJ, and the cell counting tool was used to manually mark all branching points and JAG1-positive nephron segments.

### 6.9.2. Quantification of Mitotic Cells.

The density of mitotic cells in iron-sufficient and iron-deficient cultures was determined after 24 hours of culture by whole mount staining against phosphohistone H3 (pHH3). The antibodies against pHH3 only detect histone H3 when it is phosphorylated at serine 10. This phosphorylation occurs as part of the chromosome condensation during mitosis (Hendzel and Wei *et al.* 1997). Therefore, the antibody specifically marks the chromatin of mitotic cells, which could then be counted in a confocal plane.

Kidneys were fixed with 4 % PFA and stained against pHH3 and CD326 and counterstained with Hoechst dye according to 4.8. The staining for CD326 was used to mark the ureteric bud.

Stained cultures were imaged using the U2 LSM 510 META laser scanning microscope with the Plan-Apochromat 20x objective, using a pixel-time of 0.8 µs and 8x averaging using the filter settings as noted in table 12. For all kidneys, the focus was set to include the primary ureteric branches using the green CD326 channel. The Hoechst channel was used to ensure that the complete field of view is occupied by kidney cells. For this, its gain had to be adjusted. Finally, the image was taken using all three channels and saved as a .CZI file using Zen Black.

**Table 12.** Confocal imaging settings for the quantification of mitotic cells.

| Laser Wavelength | Intensity | Filters | Master Gain |
|---|---|---|---|
| **405 (Hoechst)** | 28 % | BP 420-480 (Band Pass) | variable |
| **488 (Epcam)** | 17 % | BP 505-550 | 753 |
| **561 (pHH3)** | 50 % | BP 575-615 IR (Infrared) | 647 |

As the kidneys were only cultured for 24 hours, the cell density was similar, so the number of pHH3-positive cells per field of view could be used as a measure of mitotic activity. The counting was performed by applying the following macro to the .CZI images files using ImageJ.

```
imageTitle=getTitle()
run("Split Channels");
selectWindow("C2-"+imageTitle);
close();
selectWindow("C3-"+imageTitle);
close();
run("Gaussian Blur...", "sigma=2");
run("Threshold...");
setThreshold(78, 255);
run("Make Binary");
run("Watershed");
run("3D Objects Counter", "threshold=128 slice=1 min.=40 max.=1048576 objects statistics summary");
```

This macro counts cells visible in the pHH3-channel using the same method as in 1.7.2., with different brightness and size thresholds.

## 6.10. Lysotracker Staining and Imaging

To assess the impact of iron-deficiency on the lysosomal activity in the ureteric bud, a live-staining with Lysotracker Red DND-99 and fluorescein-conjugated *Dolichos Biflorus* agglutinin (DBA) was performed. Lysotracker is a fluorescent dye which penetrates live cells and only exhibits its full fluorescence in an acidic environment. Its fluorescence is therefore a specific marker for acidic organelles such as lysosomes. However, as the acidity of the organelles is lost upon fixation the staining must take place while the cells are still alive. DBA is a lectin isolated from the seeds of the horse gram plant. It binds N-acetyl-galactosamine, which is part of the glycocalyx on the membrane of the ureteric bud epithelium. When conjugated the green fluorophore fluorescein it can be used to mark the ureteric bud for fluorescence microscopy of live kidney cultures.

The following protocol was performed after wild-type metanephroi had been cultured for 48 h. In a 24-well plate, 250 µl of the medium in which the kidneys had been cultured was supplemented with 1 µl of 2 mg/ml flourescein-conjugated DBA stock solution and pre-warmed to 37 °C for 15 minutes. The filters were then cut out, and placed into the pre-warmed medium with the kidneys facing upwards. The plate was then incubated for 60 minutes at 37 °C and 5 % $CO_2$ atmosphere. Subsequently, 2.5 µl of 1:1 Lysotracker:PBS dilution was added to the wells, and the plate was incubated for another 45 minutes.

After the incubation, the kidneys were washed three times for five minutes with 37 °C PBS. Fixation was achieved by transferral of the kidneys to 4 % PFA solution and incubation at room temperature for 60 minutes. The kidneys were then washed once with cold PBS before being stained with a 1:1000 Hoechst:PBS dilution at 4 °C overnight. To reduce background fluorescence the kidneys were then dehydrated in 50 % and then 100 % ice cold methanol for five minutes each. Finally, the kidneys were mounted on microscope slides with Prolong Gold in the same manner as in the whole mount immunofluorescence experiments. Images of these stainings were taken on the U2-SLM (scanning laser microscope) with the C-apochromat 63x objective, a pixel-time of 1.6 µs and 8x averaging using the filter settings noted in table 13. Identical settings for all pictures were used in the red and green channels. However, due to imperfect Hoechst penetration, the Hoechst channel laser strength and gain had to be adjusted from picture to picture to facilitate the localisation of nuclei.

The process of imaging was performed as follows: Firstly, branching points were visually located through the binoculars using the GFP filter set. The correct z-value to image through the lumen of the branching point was found by live observation of the confocal Hoechst channel while the focus plane was manually changed. The gain in the Hoechst channel was adjusted and the image was taken. Counting of the Lysotracker-positive organelles in the area of the ureteric bud was performed using the cell counter tool in ImageJ. The total area of the ureteric bud in each image was measured using the spline tool in Zen Blue 2. Lastly, for each image, the number of lysotracker-positive organelles inside the ureteric bud was divided by the area occupied by the ureteric bud in the same image.

**Table 13.** Lysotracker confocal imaging settings.

| Laser Wavelength | Intensity | Filters | Master Gain |
|---|---|---|---|
| **405 (Hoechst)** | variable | BP 420-480 | variable |
| **488 (Fluorescein)** | 55 % | BP 505-550 | 888 |
| **561 (Lysotracker)** | 35 % | BP 575-615 IR | 484 |

## 6.11. qPCR

To compare the relative amount of *Jag1* mRNA between kidneys cultured under iron-sufficient and iron-deficient condition the total RNA from each condition was isolated and reverse transcribed to cDNA for subsequent real-time quantitative polymerase chain reaction (qPCR) analysis.

### 6.11.1. RNA isolation

RNA was isolated after 48 hours of culture, either immediately or after freezing the metanephroi at -80 °C. The workplace, including all instruments, was wiped with RnaseAway to reduce the risk of nuclease contamination. The *Transwell*™ filters with the kidneys were transferred to CK14-*PreCellys*™ tubes containing 300 µl of buffer RLT plus from the *RNeasy*™ Plus Mini Kit and 3 µl beta-mercaptoethanol. The tubes were then shaken on the Minilys homogenizer for 40 seconds at 5000 rpm. Afterwards, the lysate was centrifuged for 30 seconds at 10,000 rpm to reduce the amount of foam, and transferred to a microcentrifuge tube. The lysate was centrifuged for another three minutes at 13,800 rpm. The supernatant was processed further according to the instructions included in the *RNeasy*™ Plus Mini Kit. In the final steps the RNA solution was eluted in 30 µl of nuclease-free water. This elution step was repeated once using the eluate. The final eluate was either immediately processed, or frozen at -80 °C.

### 6.11.2. RNA Concentration Measurement

To measure the concentration of nucleotides in the in the RNA solution the *NanoDrop*™ spectrophotometer was used. Initially the machine was calibrated with 1.5 µl of nuclease free water. Subsequently 1.5 µl of sample solution was applied to the pedestal, and the automatic spectrophotometry was started.

### 6.11.3. Reverse Transcription

Before qPCR measurement, the mRNA had to be reverse transcribed to cDNA using the *iScript*™ cDNA synthase kit, because the qPCR Polymerases do not recognize RNA. RNA solution was pipetted into PCR-tubes to a known total amount of RNA. Nuclease free water was added ad 16 µl, and 4 µl of 5x *iScript*™ Reverse Transcription Supermix was added. The samples were mixed well by pipetting before starting the reaction in the thermal cycler using the program denoted in table 14.

**Table 14.** Reverse transcription thermocycler program.

| Phase | Time | Temperature |
|---|---|---|
| **Priming** | 5 min | 25 °C |
| **Reverse transcription** | 30 min | 42 °C |
| **Inactivation** | 5 min | 85 °C |

### 6.11.4. qPCR Conditions

In an ideal PCR-reaction the amount of amplified DNA is doubled with every thermal cycle. By utilizing SYBR-Green, a fluorescent dye which exhibits increased fluorescence when bound to double stranded DNA, the intensity of fluorescence can be measured as a surrogate of DNA concentration. In RT-qPCR fluorescence intensity is measured after every cycle, and the number of cycles needed to reach a threshold above the background noise is termed “cycle threshold” or $C_t$. As every cycle reflects a doubling of amplicon DNA, this value is proportional to $-\log_2$ of the initial template concentration. In order to exclude effects of varying dilutions, the target gene $C_t$ is subtracted by the $C_t$ of a reference gene. These reference genes are assumed to be expressed at a constant level across samples and conditions, which makes them suitable as a baseline to which the “relative” expression of target genes to can be normalized. As the reaction progresses, the amount of DNA stops rising exponentially and reaches a plateau due to the consumption of the necessary components.

The assumption of exponential amplification had to be empirically tested for each pair of primers. This was achieved by measuring a dilution series of cDNA from newborn kidneys in triplicates, with each triplicate containing 50, 10, 2 and 0.4 ng of cDNA, respectively. The Bio-Rad CFX Manager™ Software was used to calculate the doubling efficiency of the reactions, 100 % corresponded to an exact doubling with every cycle. Efficiency values between 90 % and 110 % were deemed acceptable (according to the MIQE quidelines, PMID: 19246619). The $R^2$-value was also calculated with CFX Manager™ for each dilution series. The $R^2$ calculation is based on the proximity of the $C_t$ Values to a logarithmic standard equation, and serves as a combined measure of the inter-replicate and inter-concentration variation. $R^2$-Values between 0.98 and 1 were deemed acceptable. This process is illustrated in figure 8.

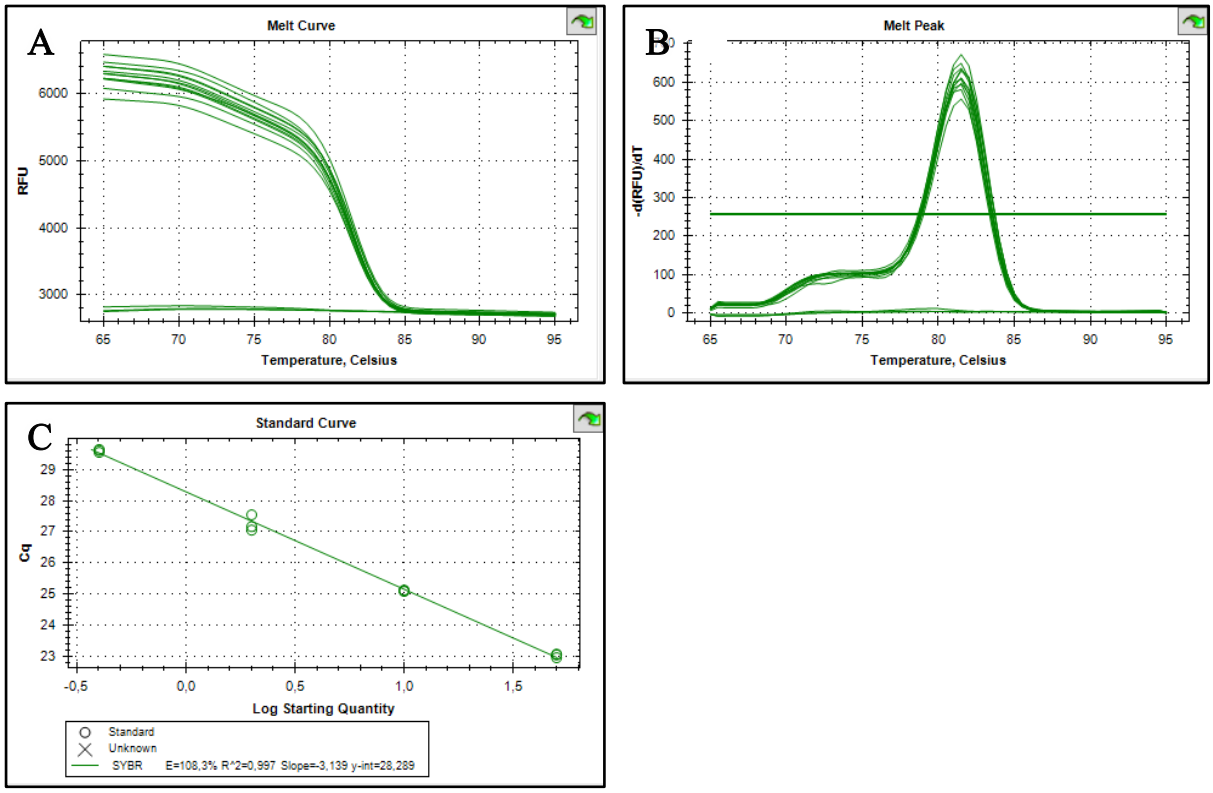


**Figure 8.** Example results of primer testing. **A,** Example melt curve **B,** Example melt peak curves of a primer showing a single peak (negative derivative of melt curve). **C,** Example standard curve from the primer testing

To ensure that only the desired amplicon is produced, a melting curve analysis was performed after the PCR. Stepwise, the temperature is increased and the fluorescence is measured. As the melting point is reached, the DNA strands dissociate from each other, leading to a decrease in fluorescence. The negative first derivative of the fluorescence curve marks the temperatures at which the fluorescence decreased at the greatest rate with a peak. Multiple amplicons or primer-dimers produce peak diagrams with multiple peaks, therefore experiments were discarded if multiple peaks were present.

In all experiments, *Hprt* (hypoxanthine guanine phosphoribosyl transferase), was chosen as the reference gene. The enzyme encoded by this gene is necessary for the purine salvage pathway, and its expression had been shown to be stable in adult metabolic models as well as embryos (Mamo and Gal *et al.* 2007, Gong and Sun *et al.* 2016). For the non-template controls the DNA solution was substituted with DNAse-free water. Reactions were assembled in triplicates according to table 7 in 96-well PCR plates, which were then mounted in the CFX Connect Real Time PCR Detection System before the program was started. The settings are displayed in table 15. The normalized ΔΔCT values were calculated in the CFX Manager program.

**Table 15.** qPCR reaction mix and Thermocycler program.

| **qPCR reaction mix** | | | |
|---|---|---|---|
| **Component** | **Volume** | **Final Concentration** | |
| SsoAdvanced Universal SYBR Green Supermix (2x) | 5 µl | 1x | |
| Forward primer | 0.125 µl | 10 µM | |
| Reverse primer | 0.125 µl | 10 µM | |
| Template cDNA | 0.4 µl | 2 ng/µl | |
| H2O | 4.35 µl | - | |
| Total volume | 10 µl | - | |
| **Thermocycler Program** | | | |
| **Step** | **Temperature** | **Duration** | |
| Initial Denaturation | 95 °C | 3 min | |
| Denaturation | 95 °C | 10 s | Repeat x40 |
| Annealing | 55 °C | 10 s | |
| Elongation | 72 °C | 30 s | |
| Final Extension | 72 °C | 10 s | |
| Melting curve | 65 °C to 95 °C | 0.5 °C increase /5 s | |

## 6.12. Statistics

In all of the size and glomerular quantification experiments, as well as the JAG1-positive early nephron quantification and the branching point quantification, paired t-tests were applied using Graphpad Prism 7. The pairing enabled the direct comparison between the two kidneys from the same embryo. For the quantification of pHH3-positive cells an unpaired t-test was applied, as kidney pair matching was not maintained throughout this staining process. The same test was also applied to the relative expression data from the qPCR experiments.

# 7. Results

## 7.1. *Ex vivo* metanephric development under high glucose conditions

Previous reports have indicated that *ex vivo* high glucose exposure of metanephric explants may replicate aspects of renal development under the influence of maternal diabetes. In order to investigate the morphological alterations associated with a high glucose environment one kidney from each embryo was exposed to a high glucose concentration of 30 mM (540 mg/dl), while the other was exposed to the low glucose control medium containing 5 mM glucose and 25 mM mannitol.

### 7.1.1. High glucose induces a small but significant reduction in explant surface growth

Both kidneys cultured under low and high glucose continually grew throughout the seven days of culture. At d7 glomeruli were plentiful and mostly well-rounded in both conditions as illustrated in figure 9.

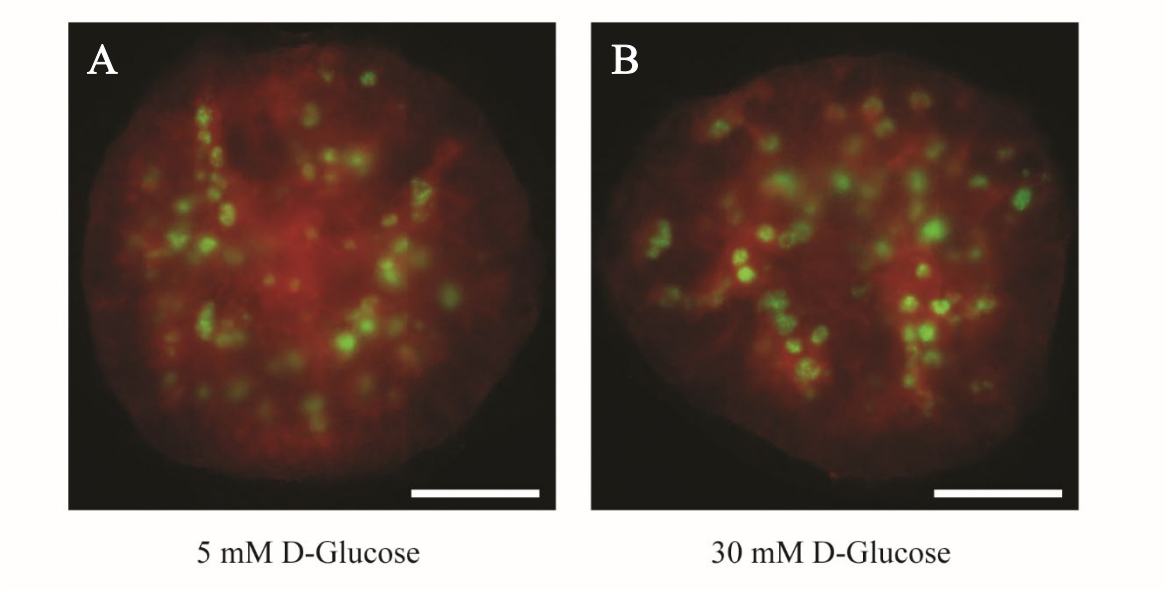


**Figure 9**. Comparison of live wide-field images of a pair of explants from the same embryo. **A,** Image of an explant cultured for 7 days in 5 mM (low) glucose medium. **B,** Image of the partner explant cultured in 30 mM (high) glucose for 7 days. Scale bars: 500 µm. Images shown are representative in size and number of glomeruli.

The paired t-test of the planar surface area showed that high-glucose cultured kidneys were significantly smaller (p=0.0442) than their low-glucose cultured counterparts (Figure 10). By calculation of the surface area ratio for each pair the effect strength could be quantified. The average surface area ratio was 0.9615 (95 % CI: 0.924-0.991), meaning that that the kidneys cultured in 30 mM glucose were, on average, only 3.85 % smaller than their low glucose counterparts. Variances of surface area between high and low glucose groups were not significantly different (F-test: p=0.4329).

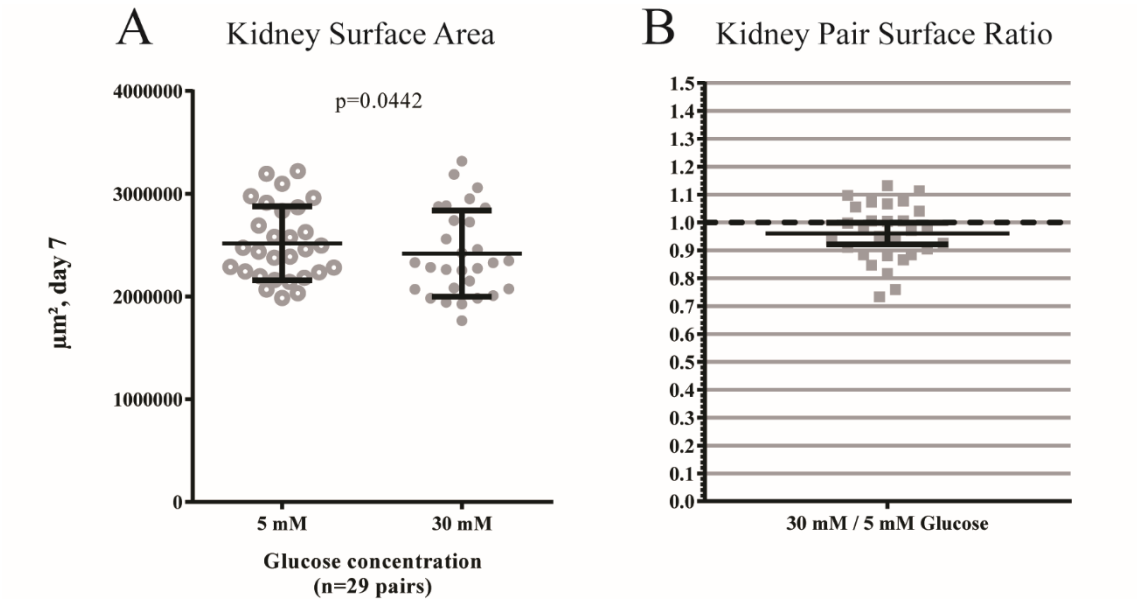


**Figure 10.** Comparison of low and high glucose explant surface areas. **A,** Kidney surface areas of the explant groups. n=29 pairs, paired t-test. Error bars are mean ±SD. **B,** Surface ratios of kidney pairs (high glucose kidney surface/low glucose kidney surface), n=29 pairs, error bars are mean ± 95 % CI.

### 7.1.2. High glucose unexpectedly increased *ex vivo* glomerular formation

In order to quantify the effect of a high glucose environment on the glomerulogenesis, the number of glomeruli formed during the seven days of culture was counted. The green fluorescent glomeruli in all of the images of Cre-carrying kidneys were of automatically counted using an ImageJ macro. This showed that the number of glomeruli formed in the high glucose cohort was significantly greater than that of the respective control kidneys (Figure 11). As the high glucose condition had led to a reduced total surface area this also resulted in higher density of glomeruli as compared to the low glucose kidneys. These results do not support the hypothesis of a reduction in nephron number under high glucose conditions.

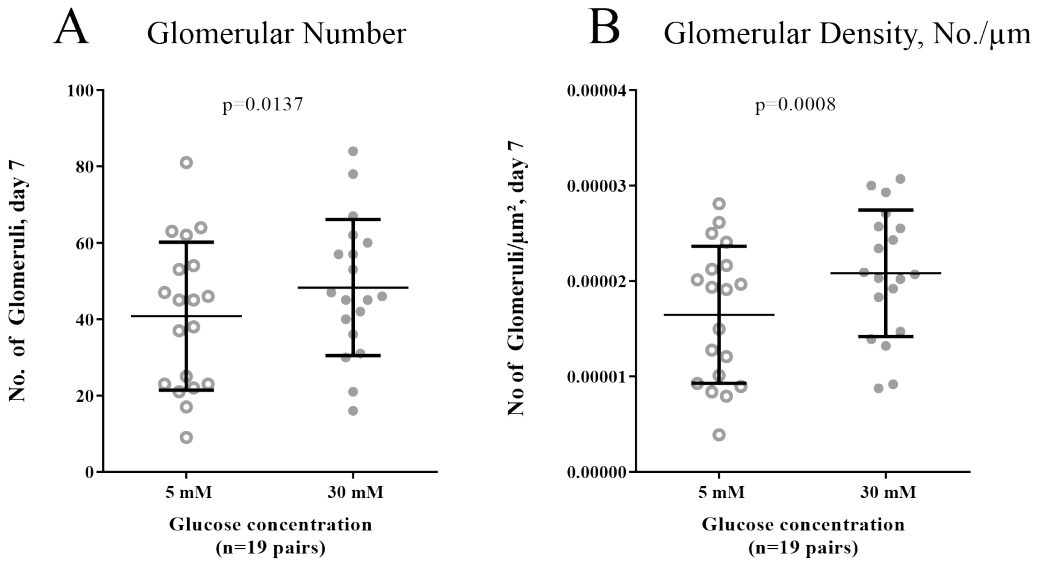


**Figure 11.** Comparison of low and high glucose glomerular formation. **A,** Number of glomeruli in the high and low glucose explant groups. n=19, paired t-test, mean ± SD., **B,** Glomerular density (number of glomeruli in each explant per µm of surface area), n=19, paired t-test, mean ± SD.

### 7.1.3. High glucose does not induce overt ureteric bud dysmorphogenesis or tip blunting

A whole mount staining with a pancytokeratin antibody was performed to assess the ureteric bud morphology, as Kanwar *et al.* had published data suggesting that the tips of the ureteric bud are blunted and heavily dysmorphic when cultured in the presence of 30 mM D-glucose (Kanwar and Liu *et al.* 1996). To visualize the ureteric tree *in toto,* wide-field fluorescence microscopy images of whole kidneys were taken after seven days of culture (Figure 12, A). These showed widespread branching of the ureteric bud in all kidneys of both conditions. Confocal imaging showed that the ureteric tip epithelium was intact and without pyknotic nuclei in both conditions.

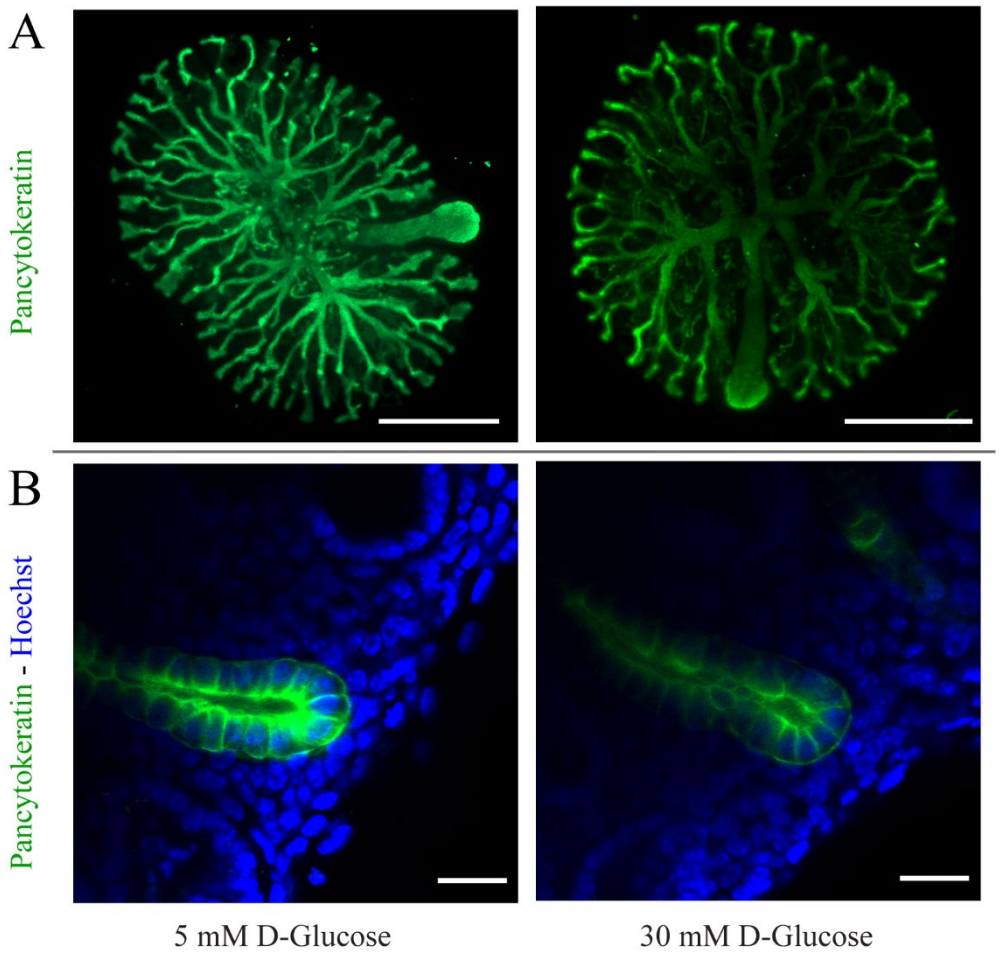


**Figure 12** Visualization of ureteric tree morphology by immunofluorescence. Kidneys were methanol-fixed and whole mount-stained after 7 days of culture **A,** Orthogonal projections of wide-field fluorescence images showing kidneys from the same embryo. Scale bars: 500 µm **B,** Confocal sections of ureteric tips, with Hoechst counterstain. Scale bars: 20 µm

### 7.1.4. High glucose does not induce overt tubular dysmorphogenesis

To assess the tubular development, kidneys were stained against Tamm-Horsefall glycoprotein (THP) after seven days of culture in low glucose or high glucose conditions. THP is expressed in the epithelium of the thick ascending loop of Henle. Wide-field imaging revealed no visually discernible difference in the number or arrangement of stained tubular segments. Kidneys from both conditions even showed some degree of the physiological, centripetal arrangement of tubuli (Figure 13).

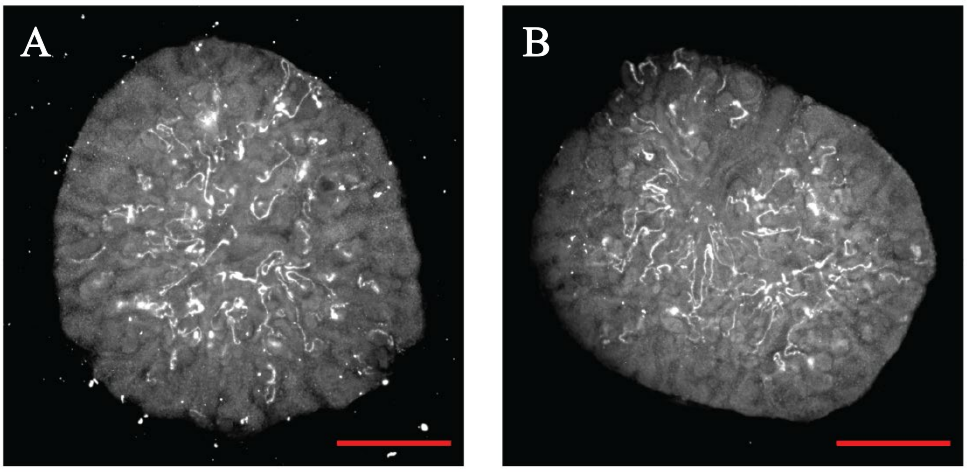


**Figure 13.** Visualization of thick ascending loop of Henle morphology by immunofluorescence. Wide-field images taken after 7d of culture and whole mount staining against THP. **A,** Widefield image of low glucose explant **B,** image of partner high glucose explant. Scale Bars: 500 µm.

## 7.2. *Ex vivo* metanephric development under fever-range hyperthermic conditions

While maternal conditions associated with increased body temperature such as fever or hyperthermia are known teratogens, little is known about their effect on nephrogenesis. To assess the impact of prolonged, fever-range hyperthermic conditions on kidney growth and nephron formation, one kidney of each pair was cultured at 40 °C. Meanwhile in the same medium and otherwise identical conditions, the control kidney was cultured at 37 °C.

### 7.2.1. High incubation temperature induces significant metanephric growth retardation

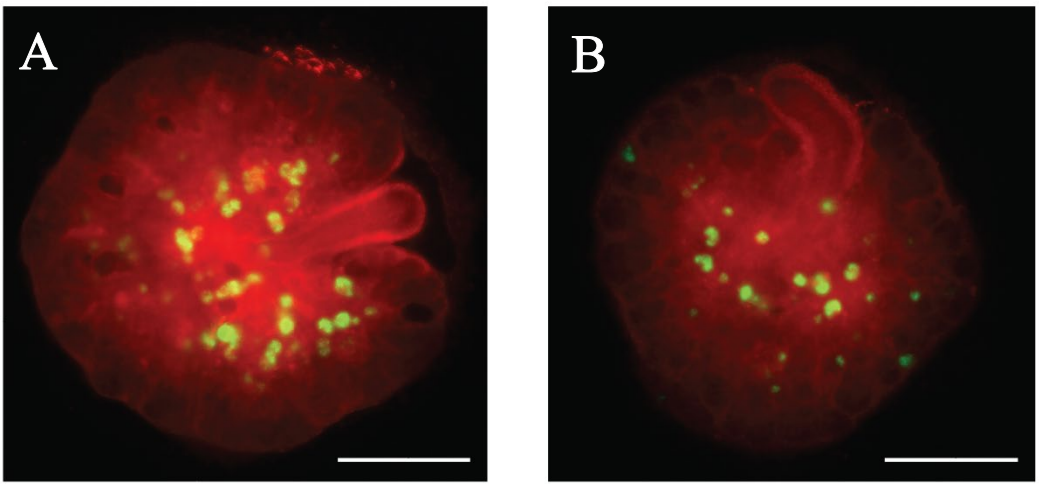


**Figure 14.** Comparison of live wide-field images of a pair of explants from the same embryo. **A,** Image of an explant cultured for 7 days at 37 °C. **B,** Image of the partner explant cultured at 40 °C for 7 days. Scale bars: 500 µm. Images shown are representative in size and number of glomeruli.

After 7 days of culture, images of the metanephroi isolated from embryos were taken in live fluorescence microscopy as before (Figure 14).

The paired t-test of the planar surface area showed that kidneys cultured at 40 °C were significantly smaller ($p=<0.0001$) than their low-glucose cultured counterparts (Figure 15). By calculation of the surface area ratio for each pair the effect strength was quantified: The average surface area ratio was 0.8164 (95 % CI: 0.7454-0.8875), meaning that that the kidneys cultured in 40 °C were, on average, 18.36 % smaller than their 37 °C counterparts. It was also noted that the variance of surface area was increased in the 40 °C condition (F test: $p=0.0002$).

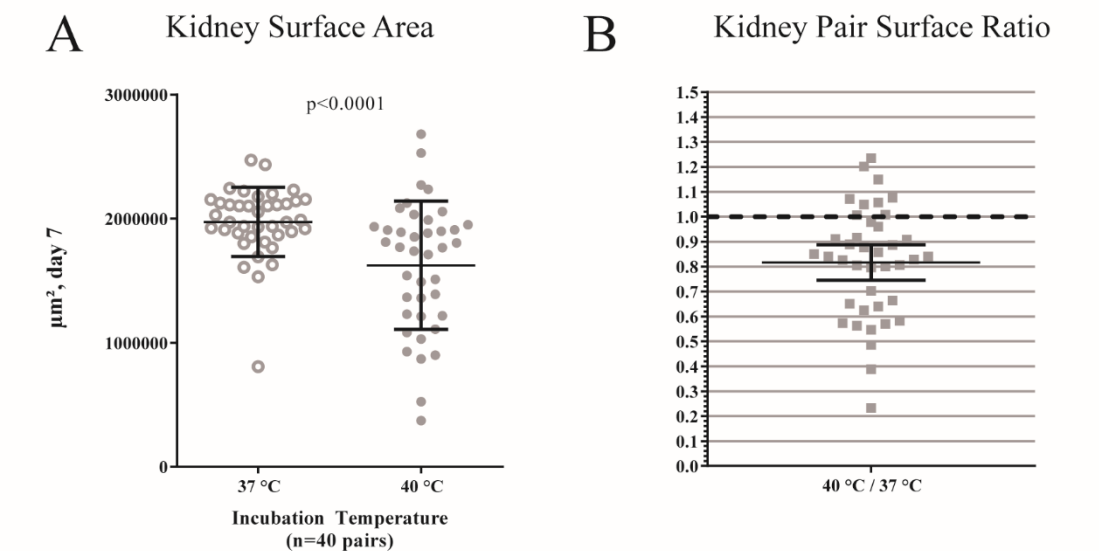


**Figure 15.** Comparison of normal and high temperature cultured explant surface areas. **A,** Surface areas of the explant groups. n=40 pairs, paired t-test. Error bars are mean ± SD. **B,** Surface ratios of kidney pairs (40 °C kidney surface/37 °C kidney surface), n=29 pairs, Error bars are mean ± 95 % CI.

### 7.2.2. High incubation temperature does not alter the quantity of glomeruli formed

The number of glomeruli formed in each explant image after seven days of culture was automatically counted using the before mentioned ImageJ macro. No significant difference of the number of glomeruli per kidney or the glomerular density was found between the groups (Figure 16). Nevertheless, the decreased overall growth of the kidneys shows that increased temperature did have a negative effect on kidney development.

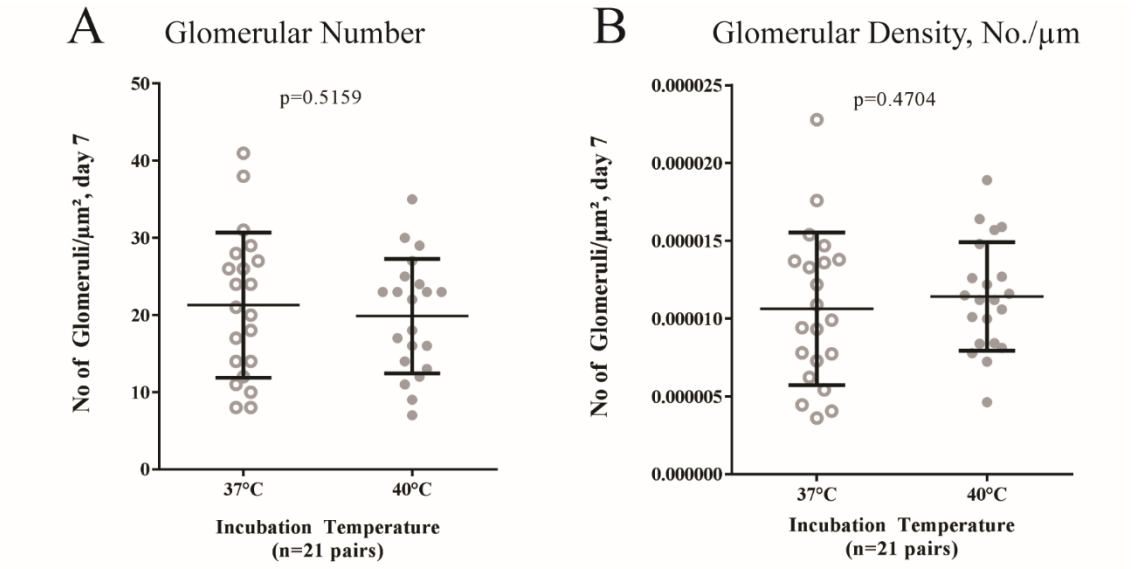


**Figure 16.** Comparison of 37 °C and 40 °C glomerular formation. **A,** Number of glomeruli in the 37 °C and 40 °C temperature explant groups. n=21, paired t-test, mean ± SD., **B,** Glomerular density (number of glomeruli in each explant per µm of surface area), n=21, paired t-test, mean ± SD

## 7.3. *Ex vivo* metanephric development under iron restricted conditions

In order to assess the impact of reduced transferrin-bound iron supply on kidney growth and nephrogenesis, one kidney of each pair was in cultured in the base medium containing the normal 50 µg/ml iron-saturated holo-transferrin. The other kidney was cultured using medium containing 50 µg/ml of iron-depleted apo-transferrin. Subsequently the apo-transferrin cultured kidneys will be referred to as iron-deficient, while the holo-transferrin cultured conditions are referred to as iron-sufficient.

### 7.3.1. *Ex vivo* iron restriction induces significant explant growth retardation

After seven days of culture, a reduced growth of the iron-restricted kidneys in comparison to their iron-sufficient partner kidneys was observed (Figure 17).

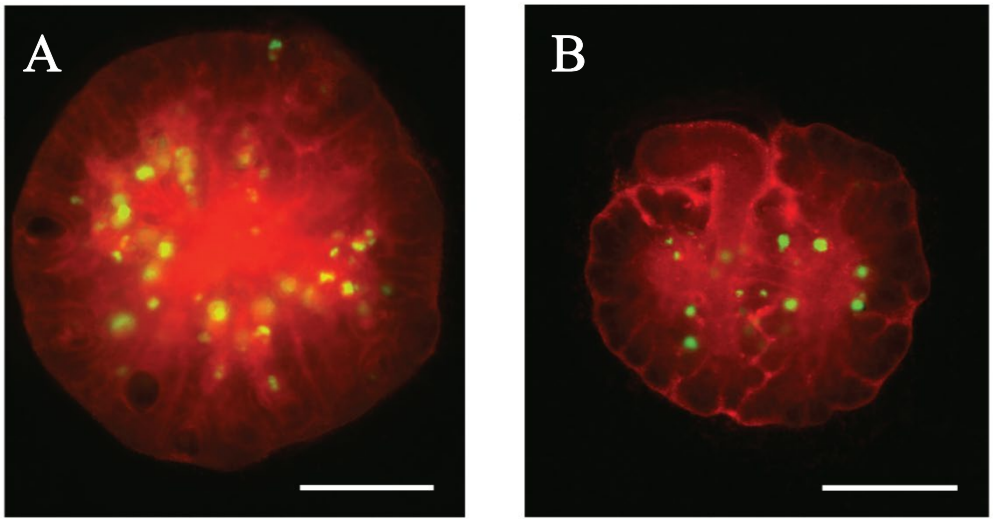


**Figure 17.** Comparison of live wide-field images of a pair of explants from the same embryo. **A,** Image of an explant cultured for 7 days in medium containing iron-saturated holo-transferrin **B,** Image of the partner explant cultured in medium containing iron depleted apo-transferrin for 7 days. Scale bars: 500 µm. Images shown are representative in size and number of glomeruli.

Paired t-test analysis of the kidney surface area revealed this growth reduction to be highly significant ($p<0.0001$) (Figure 18). The iron-deficient kidneys were, on average, only 47.9 % of the size of their holo-transferrin cultured counterparts (95 % CI: 45.1 %-50.7 %).

Morphologically, the apo-transferrin-cultured kidneys showed a demarcation of the mesenchymal caps in the wide-field fluorescence microscopy. Additionally, the ureteric bud and its primary branches were hardly discernible in the iron-sufficient kidneys, they could often be visualized in the iron-deficient kidneys, which may be due to a reduced overall thickness.

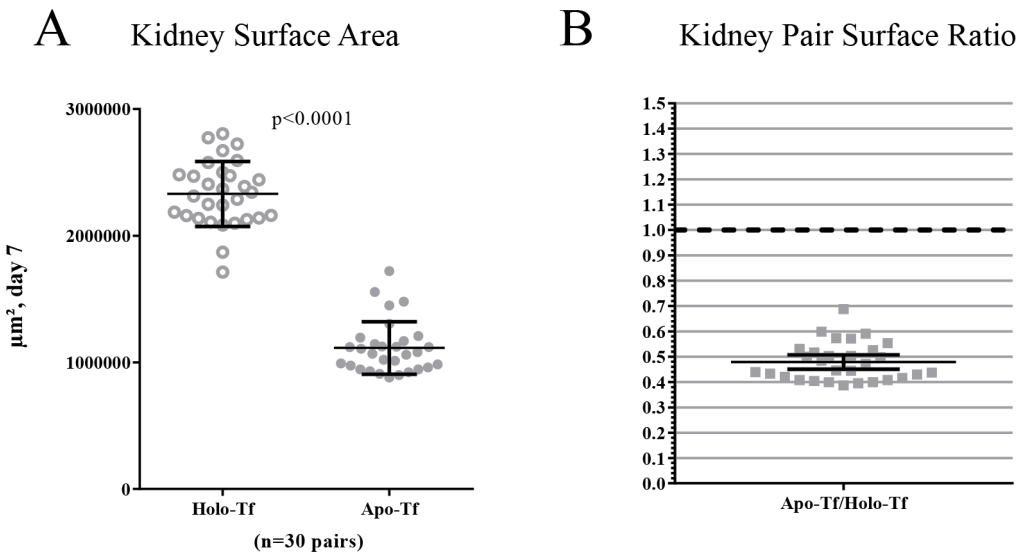


**Figure 18.** Comparison of holo-Tf and apo-Tf cultured explant surface areas. **A,** Kidney surface areas of the explant groups. n=30 pairs, paired t-test. Error bars are mean ±SD. **B,** Surface ratios of kidney pairs (holo-Tf kidney surface/apo-Tf kidney surface), n=30 pairs, Error bars are mean ±95 % CI.

### 7.3.2. *Ex vivo* iron restriction reduces glomerular formation

As before, the green fluorescent glomeruli of each kidney were counted (Figure 19). Iron-deficient kidneys showed a reduction in the overall number of glomeruli per kidney (p>0.0001). None of the iron-deficient kidneys failed to produce any glomeruli, and they produced an average of 9 glomeruli per kidney. The reduction in glomerulogenesis was still significant in terms of the density of glomeruli per unit of planar surface area. This indicates that the lack of transferrin-bound iron impedes, but does not completely abrogate glomerulogenesis.

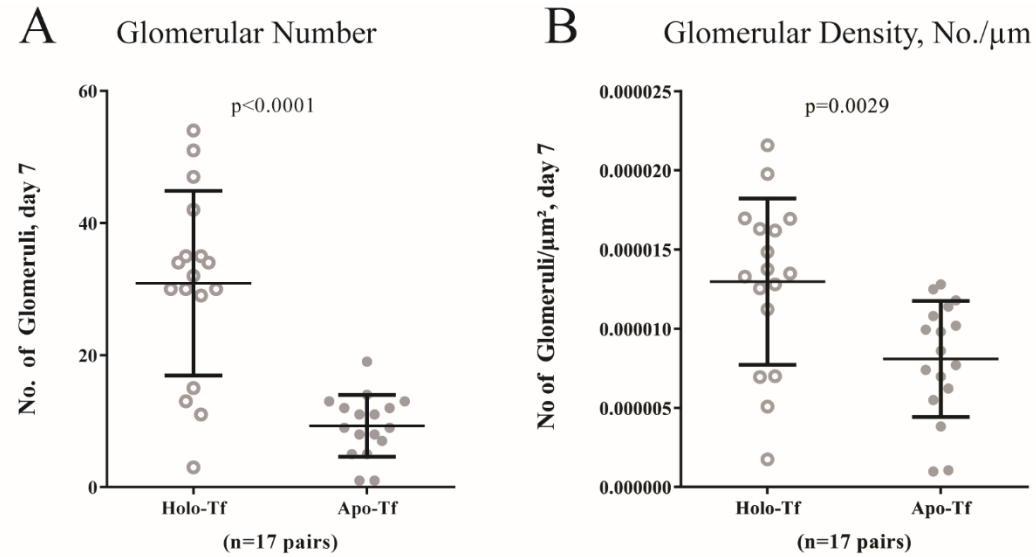


**Figure 19.** Comparison of glomerular formation in holo-tf and apo-tf supplemented media. **A,** Number of glomeruli in the holo-tf and apo-tf temperature explant groups. n=17, paired t-test, mean ±S.D., **B,** Glomerular density (number of glomeruli in each explant per µm of surface area), n=17, paired t-test, mean ± SD

### 7.3.3. *Ex vivo* iron restriction reduces explant mitotic activity

It was hypothesized that the reduced growth in iron-deficient conditions was due to a reduction in cell division. To quantify this, a whole mount staining of iron-sufficient and iron-deficient kidneys with antibodies against the phosphohistone H3 (pHH3) and CD326 (EpCAM) was performed after 24 hours of culture. Anti-pHH3-antibodies only recognize histone 3 when it is phosphorylated, which occurs in mitosis. Stained kidneys were then imaged using a confocal microscope, and the number of pHH3-positive cells per field of view was counted using an ImageJ Macro (Figure 20). This quantification showed that kidneys cultured in iron-deficient medium had significantly fewer pHH3-positive cells per field of view than their iron-sufficient counterparts.

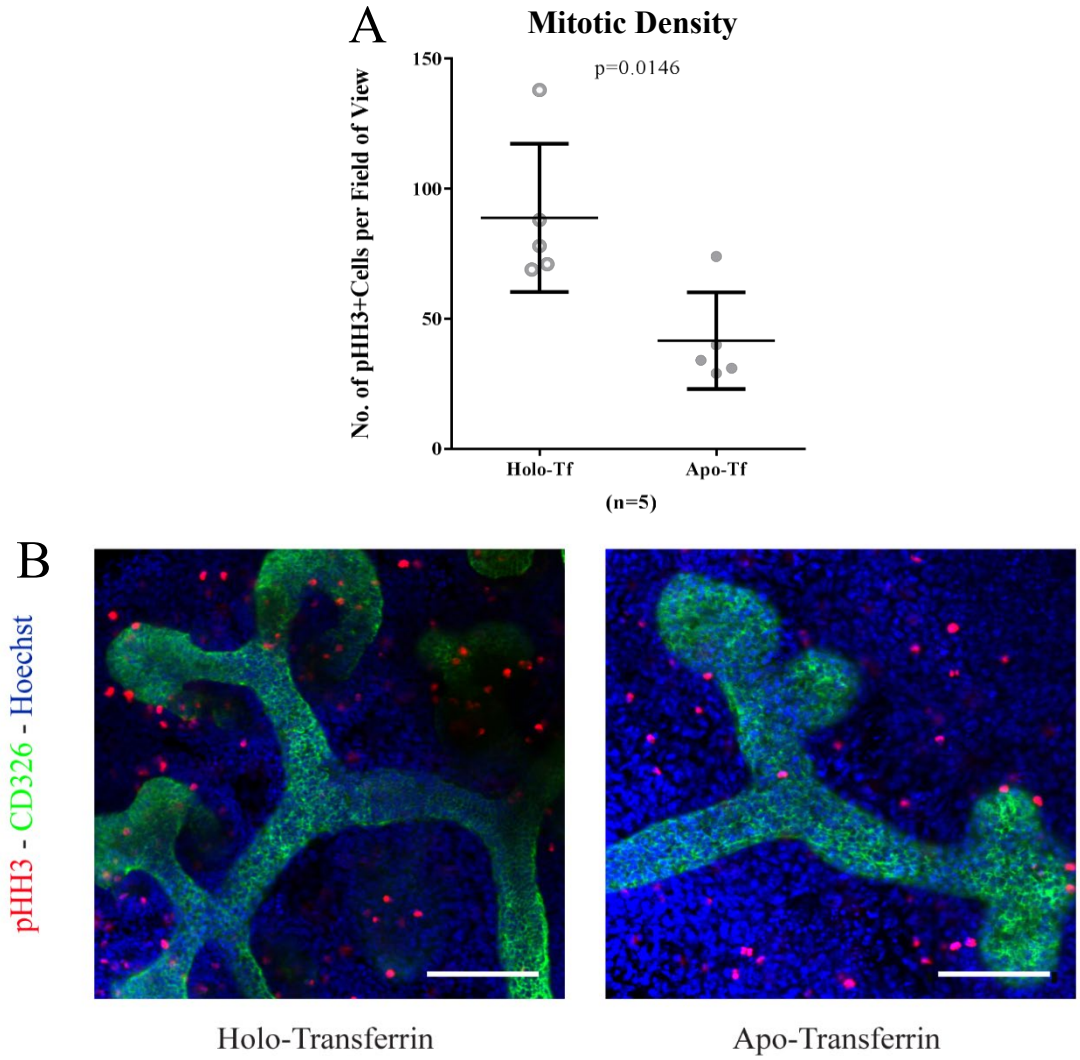


**Figure 20.** Quantification of mitotic activity**. A,** Automatically counted number of mitotic cells per field of view, n=5 kidney pairs, unpaired t-test, n=5 sections from different explants per condition, error bars are mean ± SD. **B,** Representative confocal sections of whole mount stained kidneys after 24 hours of culture. Scale bars: 100 µm

### 7.3.4. *Ex vivo* iron restriction inhibits ureteric branching

The observed reduction in the number of glomeruli was hypothesized to be the consequence of reduced ureteric branching. To test this, the branching sites of 10 kidney pairs were counted after the kidneys pairs were stained against CD326, also known as Ep-CAM or Epithelial cell adhesion molecule after 48 hours of culture. Figure 21 shows that the number of ureteric branching sites is significantly reduced. This indicates the development of the ureteric bud is detrimentally affected by the reduced availability of transferrin-bound iron.

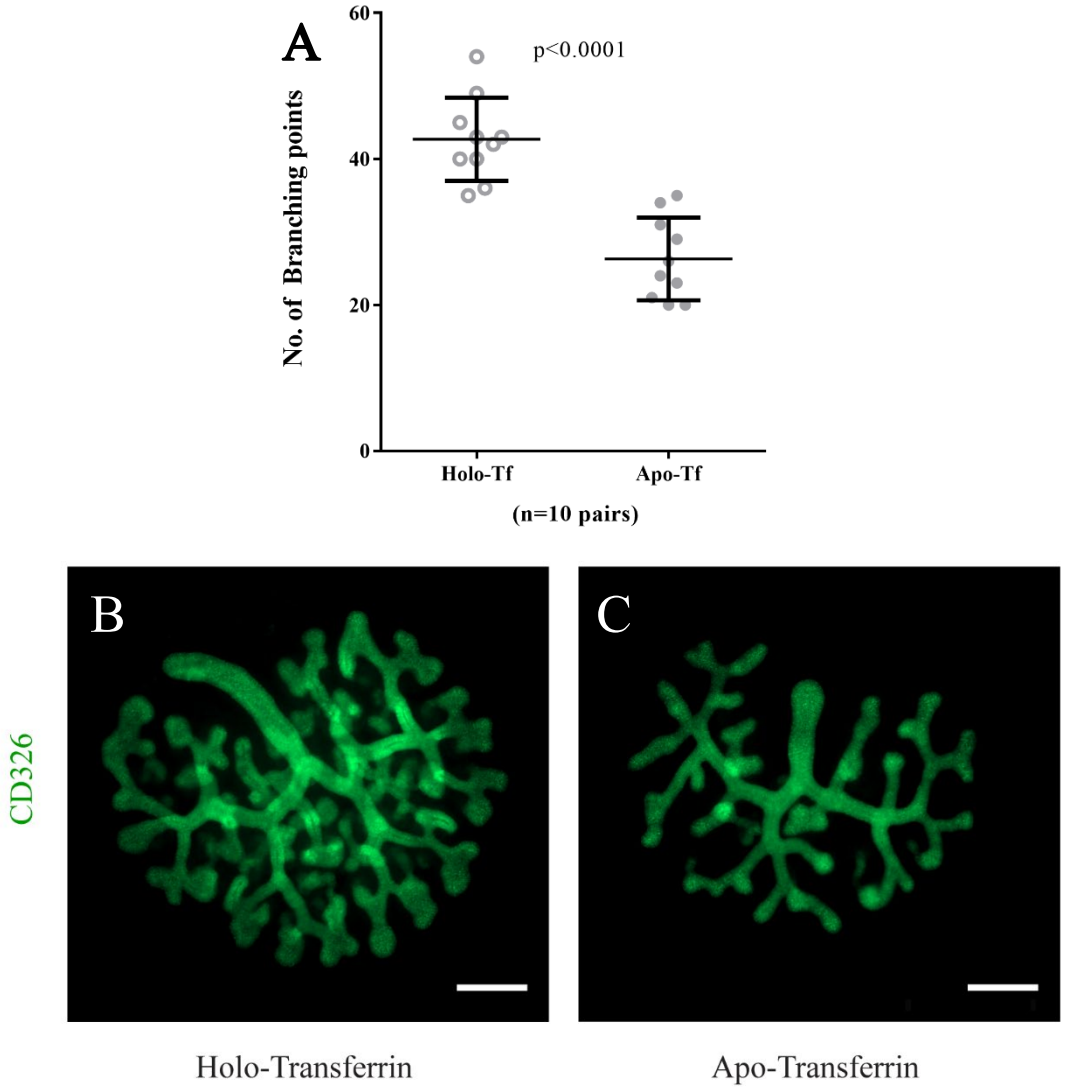


**Figure 21.** Comparison of ureteric bud branching. **A.** Number of branching points per kidney, n= 10 pairs, Mean ± S.D., paired t-test. **B.** Representative example images of explant cultured in medium containing holo-tf for 48h C. Partner explant cultured with Apo-Tf, displaying retarded branching after the same incubation period. Scale bars: 200 µm.

### 7.3.5. *Ex vivo* iron restricted culture does not compromise SIX2-positive mesenchymal progenitor cell arrangement

The growth of metanephroi and the branching of the ureteric bud are dependent on the self-renewal of pluripotent cap mesenchyme cells. These can be distinguished by their production of the SIX2 protein. To assess whether the reduced growth and branching is due to a loss in this cell population by death or premature differentiation, whole mount stainings and wide-field imaging was performed. Paired kidneys were cultured for 48 hours or 7 days, and subsequently stained against SIX2 and epithelial Cadherin (E-Cadherin). In this case, E-Cadherin was used instead of CD362 as it stains epithelial structures in early nephrons as well as the ureteric bud, so that the arrangement of both can be visualized. As shown by Figure 22, A, after 7 days of culture the SIX2-positive mesenchymal caps were present at all the peripheral ureteric tips, indicating that a loss of these caps did not occur by premature differentiation. As expected, stainings after 48 hours of culture similarly showed intact SIX2-positive caps (Figure 22, B). Interestingly, a noticeable reduction in early nephron formation was observed in the iron-deficient kidneys, as fewer epithelialized E-Cadherin expressing comma- and s-shaped bodies were present between the branches of the ureteric bud (Figure 22, C).

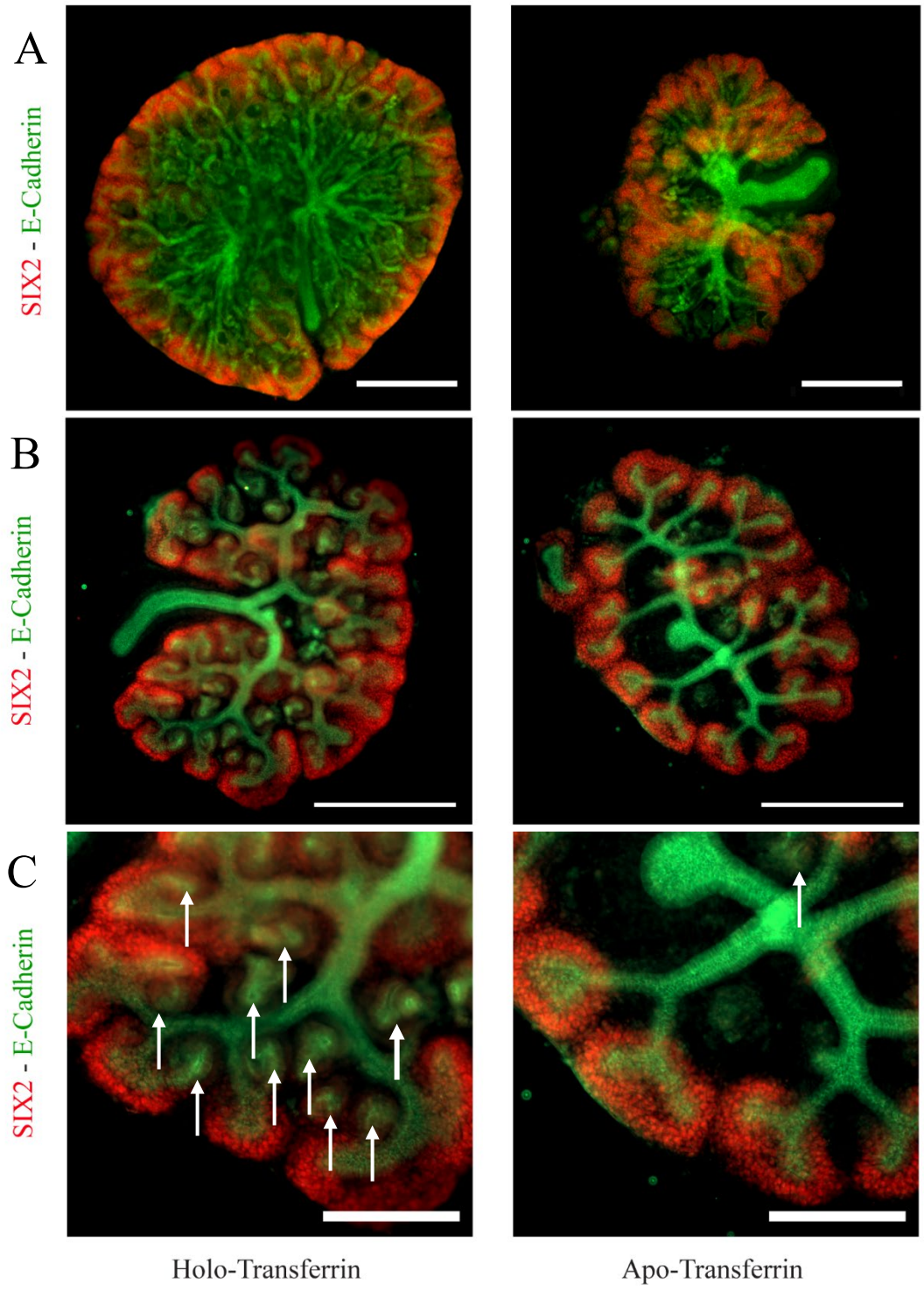


**Figure 22.** Widefield immunofluorescence images showing SIX2 expression in the mesenchymal caps. **A,** whole mount stained kidneys after 7 days of culture showing SIX2-positive mesenchymal caps. **B,** Widefield images of whole mount stained kidneys after 48 hours of culture. Scale bars: 500 µm **C,** Magnification of B, E-cadherin expressing epithelialzed early nephron structures are marked with white arrows. Scale bars: 200 µm

### 7.3.6. *Ex vivo* iron restriction alters number and morphology of early nephrons

In order to visualize the alterations of early nephrogenesis, paired kidneys were cultured for 48 hours, and subsequently a whole mount immunofluorescence staining against WT1 and JAG1 was performed. WT1 is a transcription factor produced by the proximal cell population in early nephrons, while JAG1 is a ligand of the notch pathway which is produced by the more distal cells. This double staining enables the visualization of the early nephron structure. As shown in figure 23, the kidneys cultured in iron-deficient conditions showed an overall reduction in early nephron number as compared to their iron-sufficient counterparts, which indicates that the reduced number of glomeruli which was observed after seven days of culture may have been predetermined by the reduced formation of comma- and s-shaped bodies in the first days of culture.

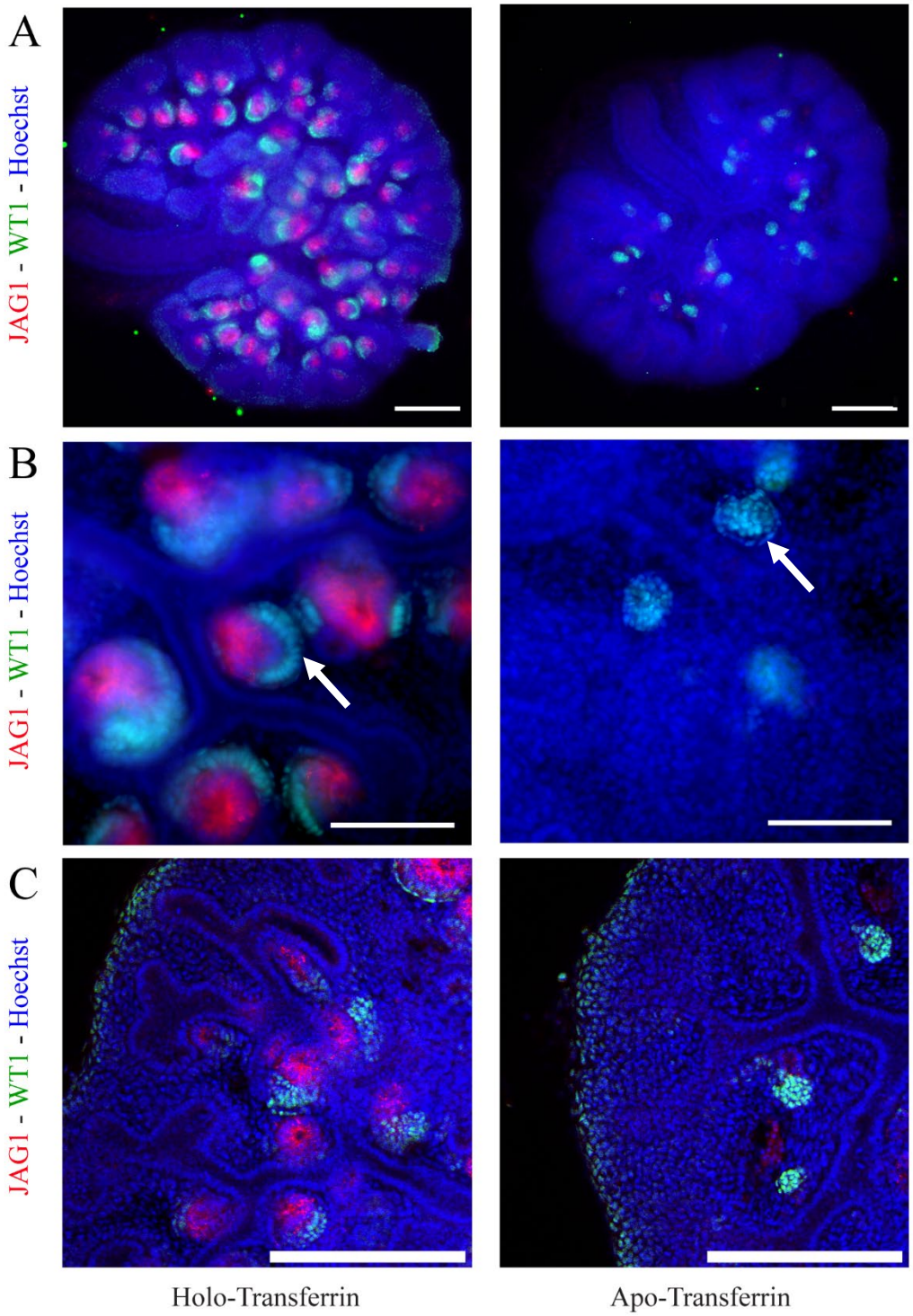


**Figure 23.** Comparison of early nephron morphology **A,** Widefield microscopy after 48 hours of culture shows a marked reduction in JAG1-positive nephron segments. Scale bar: 200 µm **B,** Increased magnification, arrows differing shapes of the WT1-positive segments, which already show a glomerulus-like shape in the iron restricted explants. Scale bar: 100 µm. **C,** Confocal sections from the same stainings. Scale bar: 200 µm

Additionally, the expression of JAG1 and WT1 appeared to be differentially affected. While in the iron-sufficient kidneys the s-shaped bodies always showed the distal JAG1-positive cells at the concave aspect of an arching epithelial arrangement of WT1-positive cells, the same was not observed in iron-deficient explants. Instead, the expression of JAG1 was reduced, with some WT1-positive nephrons not showing any at all. The WT1-positive cells also appeared to be arranged differently, some already having formed conglomerates resembling early glomeruli instead of the physiological arching arrangement seen in the holo-transferrin cultured kidneys.

The number of in JAG1-positive nephrons per kidney was counted, which revealed a highly significant reduction (Figure 24). Furthermore, a significant reduction in *Jag1* mRNA relative expression after 48 hours of culture was found by qPCR. In conclusion, iron-deficient kidneys appeared to form fewer early nephrons, which showed decreased expression of *Jag1*, and an altered arrangement of WT1-positive proximal nephron cells which resembled early glomerular stages.

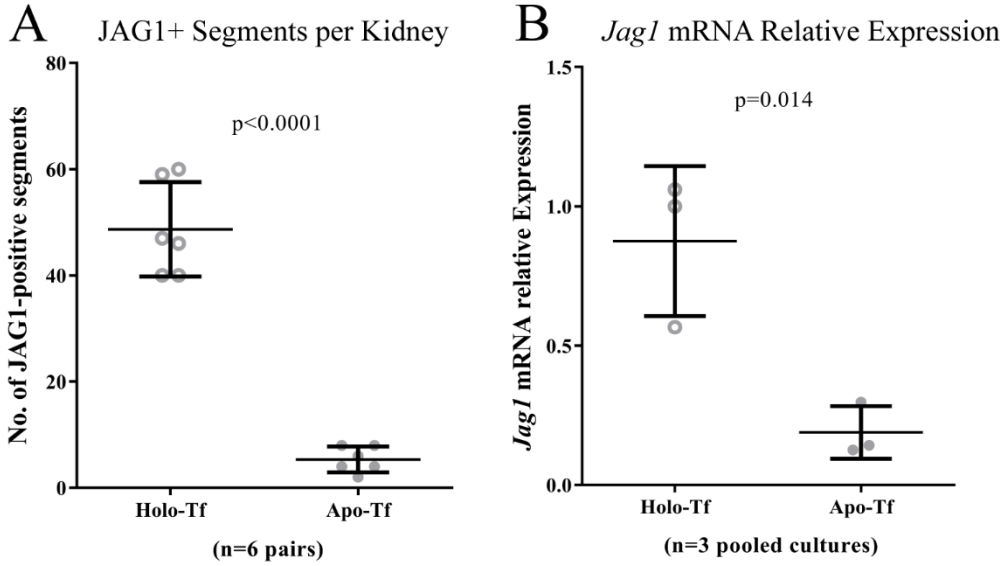


**Figure 24.** Morphometric and transcriptional quantification of JAG1 expression. **A,** Number of JAG1-positive segments in each kidney, n=6, paired t-test, mean ±SD. **B,** *Jag1* mRNA relative to mHprt as evaluated by qPCR, n=3 pooled cultures, paired t-test, mean ±SD.

### 7.3.7. *Ex vivo* iron restriction inhibits distal tubulogenesis

As the cells of the distal JAG1-positive segments of the early nephron develop to form the tubules, the observed reduction of these segments might be an early indicator of disturbed tubulogenesis. To test this hypothesis, kidneys were cultured for 7 days and subsequently stained against Murine Na+ K+ 2Cl- cotransporter protein (NKCC2), a membrane cotransporter of sodium, potassium and chloride which is specifically present at the thick ascending loop of Henle (TAL). The stainings revealed that while TALs were plentiful in iron-sufficient kidneys,

they were markedly reduced in number and length in the metanephroi which were cultured with apo-transferrin (Figure 25). This indicates that in the conditions studied, the development of distal tubular segments was more strongly affected than that of the glomeruli.

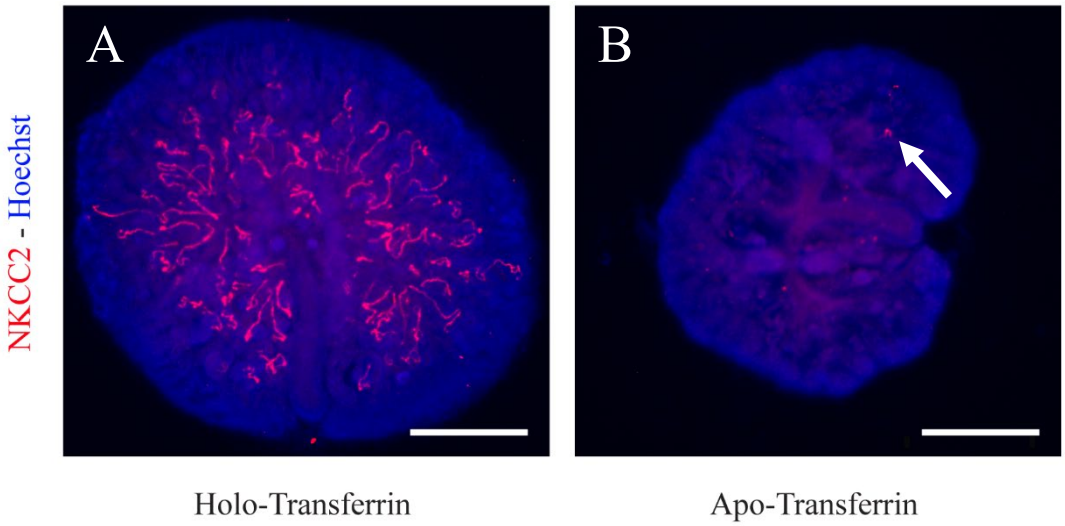


**Figure 25**. Comparison of distal tubule formation. Whole mount immunofluorescence staining against NKCC2 after 7 days of culture. **A,** Plentiful distal tubular segments form the in the iron-sufficient explants. **B,** In iron-deficient kidneys the formation of distal tubule segments was rare, segments were short where they did occur (arrow) Scale bar: 500 µm.

### 7.3.8. *Ex vivo* iron restriction induces ureteric apoptosis

The observed aberration ureteric branching in the iron-deficient condition was hypothesized to be associated with increased apoptotic processes. To test this hypothesis, kidney pairs were again split into iron-sufficient or iron-deficient culture conditions for 48 hours and subsequently whole mount stained with anti-Pancytokeratin and anti-cleaved-Caspase-3 (CC3) primary antibodies. While the subsequent confocal microscopy did not reveal visually noticeable differences in caspase activity in the metanephric mesenchyme, the ureteric bud showed a distinct luminal CC3 staining in the iron-deficient kidneys, but not in the iron-sufficient group (Figure 26). Interestingly, the CC3 staining observed in iron-deficient kidneys was mostly confined to the lumen of the ureter, and CC3 was rarely observed in the ureteric epithelium. When it was observed, the ureteric cells with CC3 staining were at the tips of the ureteric buds. These stainings were repeated with the kidneys of embryos from three different dams, with similar results.

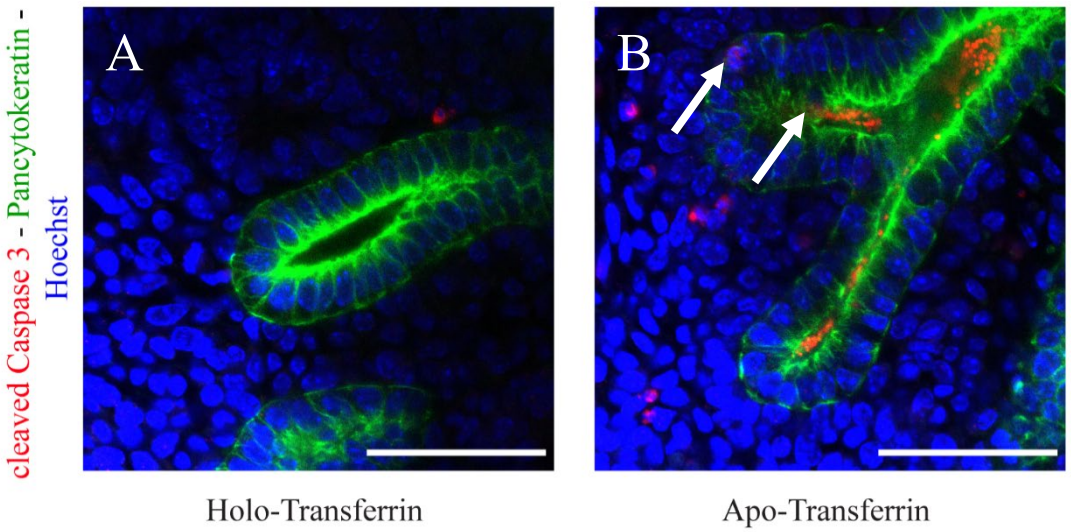


**Figure 26.** Confocal sections of explants stained against cleaved Caspase 3 showing the lumen of the ureteric bud. **A.** Confocal section of whole mount stained holo-transferrin-cultured explant. **B.** Apo-transferrin-cultured partner explants showed luminal Caspase-3 activity in the ureteric bud lumen, indicating increased apoptotic processes. Note the cells with caspase activity marked with an arrow. Scale bars: 20 µm

### 7.3.9. *Ex vivo* iron restriction does not lead to overt alterations of ureteric lysosomal activity

As the activity of Caspase-3 was increased in the ureteric lumen in iron-deficient kidneys, it was hypothesized that this confers an increase in lysosomal activity as the detritus formed apoptotic processes could be lysosomally degraded by the surrounding cells. To test this hypothesis, kidneys were cultured in either iron-sufficient or iron-deficient medium for 48 hours and subsequently stained in live tissue using LysoTracker™ red and fluorescein-conjugated *Dolicholus Biflorus* agglutinin. After fixation and counterstaining using Hoechst nuclear dye, the ureter was confocally imaged at its branching sites, and the number of LysoTracker™-positive organelles per µm of ureteric bud was calculated from 10 non-overlapping images per condition. The unpaired t-test showed that no significant difference was observed between the culture conditions (Figure 27, A). Some images from both conditions did not show any LysoTracker™-positive organelles. The distribution of these organelles was uneven where they did occur, but a tendency of lysosomes to localize to the apical regions of the epithelium as observed. The apoptotic processes induced by a decrease in availability of transferrin bound iron thus do not appear to influence ureteric lysosomal activity.

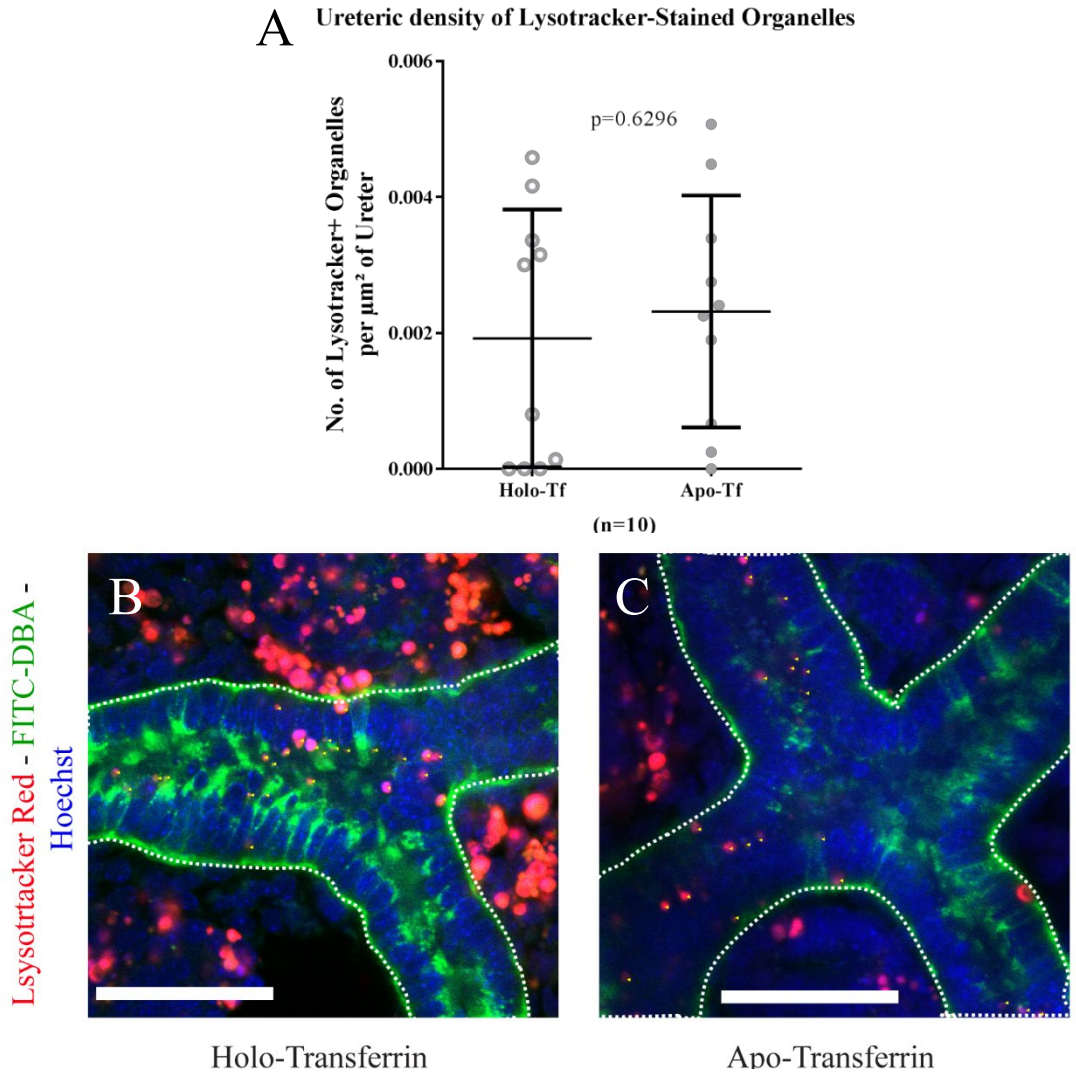


**Figure 27.** Comparison of ureteric lysosomal organelle density. **A.** Density of Lysotracker-positive organelles per µm² of ureteric image surface. Unpaired t-test, mean ±SD. **B.** Example confocal section of live stained explant culture after 48 hours of culture with holo-tf. Ureteric area marked with a dashed white line, counted organelles marked with yellow indicators. **C.** Example confocal section of explant cultured with apo-tf. Scale bars: 20 µm

### 7.3.10. Depletion of intracellular iron reserves repeats similar pattern of ureteric apoptotic activity

In order to compare the previously observed pattern of caspase activity to the one induced by direct depletion of intracellular iron, the iron chelator Deferoxamine (DF) was used. This substance binds free iron in the medium, as well as intracellular iron. In this experiment, both kidneys from each embryo were cultured in holo-transferrin containing media. In the experimental medium, Deferoxamine was present at a concentration of 50 µM. The same staining as in 5.3.8 against cleaved Caspase 3 and cytokeratins were undertaken. Confocal imaging revealed massive apoptosis in the metanephric mesenchyme surrounding the ureteric tips (Figure 28). Luminal CC3 staining inside the ureteric bud was present in the iron-depleted

kidneys as it was in the apo-transferrin-cultured kidneys, but it appeared more widespread. Remarkably, while the surrounding metanephric mesenchyme showed clear signs of apoptosis, namely cytoplasmatic CC3 staining and pyknotic nuclei, the epithelial cells only showed confined CC3 staining, and pyknotic nuclei were only visualized in the ureteric lumen. This indicated that both in conditions of reduced iron availability, as well as direct iron depletion using deferoxamine, the cells of the ureteric epithelium possess mechanisms to defer apoptotic processes caused by a cellular iron-deficiency into the lumen, without an overt loss of epithelial integrity.

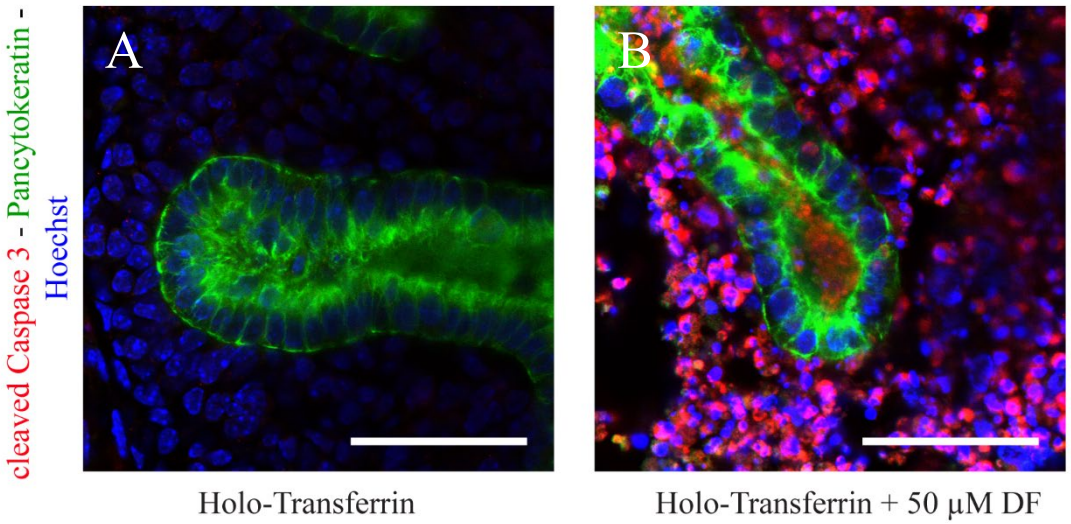


**Figure 28.** Effect of Deferoxamine on ureteric and mesenchymal cell survival. **A,** Confocal sections of whole mount stained kidneys after 48h of culture. **B,** Depletion of cellular iron by Deferoxamine induces widespread mesenchymal caspase-3 activity, but mostly spares the ureteric epithelium. Scale bars: 20 µm

# 8. Discussion

## 8.1. Modelling kidney development *in vitro/ex vivo*

In the present thesis, three common conditions affecting pregnant women were modelled in *ex vivo* cultures of murine metanephroi. Low nephron numbers of the kidneys at birth are a risk factor for chronic kidney disease and hypertension later in life (Bertram and Douglas-Denton *et al.* 2011, Wang and Garrett 2017). This connection was first hypothesized by H.R. Brenner *et al.* in 1988 (Brenner and Garcia *et al.* 1988). Since then, many studies have highlighted the role of disturbances of the kidney development by maternal or environmental factors in the development of adult disease. In rodent studies, several maternal conditions such as diabetes mellitus, low protein alimentation, vitamin A deficiency and iron-deficiency have been shown to induce reduced nephron numbers and hypertension in the offspring (Lelièvre-Pégorier and Vilar *et al.* 1998, Langley-Evans and Welham *et al.* 1999, Lisle and Lewis *et al.* 2003, Chen and Chenier *et al.* 2010). However, the understanding of the underlying mechanisms is still relatively limited which is, in part, due to a lack of robust *ex vivo* models. In this study, key aspects of conditions which commonly affect human gestation were replicated in an *ex vivo* murine kidney culture system in order to evaluate the effects in terms of renal growth and nephron formation, as well as morphological alterations. The diseases chosen to be translated to the culture system were maternal diabetes, elevated body temperature and reduced iron availability to the developing kidneys. The putatively dysmorphogenic aspect of each condition was replicated in the culture system. The experiments revealed a surprising resistance of metanephric tissue to high glucose concentrations, while a moderate growth retardation was induced by fever-range temperatures, and iron-restriction induced severe dysmorphogenic alterations in addition to a reduction of growth and glomerulogenesis.

## 8.2. Advantages and limitations of the *ex vivo* kidney culture system

All experiments in this study were based on a serum-free adaptation of the metanephric *ex vivo* culturing technique developed by Saxen *et al.* (Saxen and Lehtonen 1987). This method involves the microdissection of metanephroi from murine embryos, which are subsequently incubated on top of filter membrane to continue their development *ex vivo* at the medium-air interface. In all experiments, one kidney of each embryo was subject to the control condition, while the other was exposed to the experimental condition. All morphometric comparisons were performed in accordance to this pairing, resulting in the exclusion of any genetic variation, as well as inevitable small variations in gestation length before explantation. This kidney culture

technique represents a middle ground between *in vivo* experiments and cell culture techniques, as it combines the physiological organization of the different types of kidney cells with the controllability of traditional cell cultures. This close controllability can be advantageous compared to *in vivo* experiments, where exposure of the dams to experimental conditions does not only affect the metanephric tissue directly, but also results in complex alterations of the maternal, placental as well as embryonic physiology. Such alterations may then exert secondary effects on the metanephric development which may be confounded with the primary effects of the experimental condition, making it a challenge to delineate the direct causes behind the observed developmental changes. The *ex vivo* organ culture system allows for the immediate reactions of the metanephric tissue to be investigated in isolation from effects mediated by other organ systems. Another advantage of the kidney culture model is that it does not require live animals to be exposed to experimental conditions, and is therefore preferable in terms of animal welfare (Russell and Burch *et al.* 1959). The limitations of the technique lie in the incomplete transferability of the results towards normal gestation, as the explants do not only grow unphysiologically flat and in isolation from the surrounding tissue, but also lack blood vessels and hence blood flow or urine production. Another downside is that under ideal conditions, the explant growth is self-limiting after approximately seven days in the culture system, as increased thickness of the explants limits the diffusion of medium to apically located cells.

A more recently developed alternative to *in vivo* experiments are metanephric mesenchyme progenitor cell cultures. It is known that the balance between self-replication, differentiation and apoptosis of the pluripotent metanephric mesenchyme cells is one of the determinants of the final nephron number. Techniques to isolate and expand these cell populations *in vitro* have enabled the study of factors influencing this balance (Liu and Edgington-Giordano *et al.* 2017). For the aims of this thesis, the culture of whole metanephroi appeared more suitable, as it allows for counting of glomerular numbers, which is more closely related to *in situ* nephron formation than any readout a cell culture could enable. Cell culture models also do not allow for morphological evaluations or conclusions about the various other cell populations present in metanephroi. Their cellular homogeneity may however be advantageous when alterations of the amounts of cellular components are compared. In kidney cultures, any observed alteration of cellular components, such as the amount of a protein of interest, may be influenced by both the level of expression as well as different proportions of the cell types between experimental groups. Ideally, alterations suspected in a specific cell type during *in* or *ex vivo* metanephric development would subsequently be analyzed using a representative cell culture, FACS-sorted cell populations or or using single cell level omics for these methods to complement each other.

In conclusion, the ex vivo culture of metanephroi allows for the immediate control of the conditions in which the process of renal development occurs, while facilitating organ wide morphometric analysis such as the counting of total glomeruli per kidney formed. This combination made the technique suitable for the evaluation for the three putatively harmful alterations to the metanephric environment which were investigated in this thesis.

## 8.3. E*x vivo* high glucose exposure as a model for metanephric development under maternal diabetes

Reduced renal size and nephron endowment as a consequence of artificially induced maternal diabetes mellitus has been reported in several strains of mice and rats (Amri and Freund *et al.* 1999, Tran and Chen *et al.* 2008, Chang and Chen *et al.* 2012, Hokke and Armitage *et al.* 2013). Kanwar *et al.* has previously published two reports about an *ex vivo* a high-glucose metanephric culture model. They reported strong reductions of explant growth and nephrogenesis, as well ureteric bud dysmorphia and an abrogation of tubulogenesis following the culture in medium containing D-glucose at a concentration of 30 mM (540 mg/dl) (Kanwar and Liu *et al.* 1996, Kanwar and Akagi *et al.* 2005). The recognition of low nephron development as a risk factor for human renal dysfunction and hypertension has become more recognized, yet this promising murine *ex vivo* model of glucose induced nephron deficits has not been expanded upon by the other authors. The experiments presented herein sought to reassess the reported alterations using a podocyte-specific fluorescent reporter mouse strain for further characterization by modern microscopic techniques, possible downstream omics analysis and compound screening for substances which may counter the reported dysmorphia. In order for the results to be comparable, the medium composition and glucose content used in the experiments presented herein was a replication of the composition used by Kanwar *et al*. However, no nephron deficit or dysmorphia was detected in the high glucose group of explants, thus no follow-up/screening experiments were performed.

### 8.3.1. Ex *vivo* high glucose exposure does not induce a severe abrogation of metanephric growth or glomerulogenesis

Previous reports had indicated the surface growth of cultured metanephroi to be markedly reduced in a high glucose environment. To quantify this effect, 19 pairs of metanephroi were microscopically measured and showed a small but significant reduction in explant size by 3.85 % as a consequence of glucose exposure. The 1996 report of Kanwar *et al.* described the size reduction as “approximately half” (Kanwar and Liu *et al.* 1996). Their 2005 report included morphometric measures, including the relative sizes of 10 explants cultured at 5 mM and 10

explants cultured at 30 mM D-glucose, which resulted in a 31.9 % smaller surface of the high glucose cultured explants (Kanwar and Akagi *et al.* 2005). The experiments presented in the present thesis resulted in a much smaller effect of the high glucose environment on metanephric growth than what was described before. It thus appears that the isolated exposure of murine metanephroi to high glucose concentrations can result in a much more subtle inhibition of growth than what was previously known.

As a second step, automated counting of the glomeruli revealed their number to be mildly, but significantly higher in those explants cultured in high glucose medium (48.2 vs. 40.1). This was unexpected, as there was no previously published record of near-normal or even increased numbers of glomeruli in high-glucose culture. The 1996 report of Kanwar *et al.* did not include quantification of glomerular numbers, but featured images of paraffin sections showing that in the high glucose-cultured explants, ”very few […] precapillary-stage glomeruli” had formed, which were visibly increased in size (Kanwar and Liu *et al.* 1996). In their 2005 report, the glomeruli of 10 explants per condition were stained by the use of a fluorescent dye-conjugated peanut agglutinin and manually counted. They reported a reduction from an average number of glomeruli from 70.6 to 33.4 due to high glucose exposure. (Kanwar and Akagi *et al.* 2005) The results presented in the present work are thus in disagreement with the previous reports. A reduction as it was reported by Kanwar *et al.* (Kanwar and Akagi *et al.* 2005), instead of an increase, would have been in coherence with the *in vivo* reports of renal development in the offspring of type I diabetic mouse models. Multiple such *in vivo* studies of STZ-induced maternal diabetes have included the counting of nephrons, all of which have reported reductions in the average number of glomeruli (34-40 %) in diabetes-exposed offspring (Tran and Chen *et al.* 2008, Chen and Chenier *et al.* 2010, Chang and Chen *et al.* 2012, Hokke and Armitage *et al.* 2013). The unexpected increase in *ex vivo* glomerular formation appears to show that the *ex vivo* high glucose exposure does not constitute as suitable as a model of metanephric maldevelopment as it is known to occur *in vivo*.

### 8.3.2. *Ex vivo* high glucose exposure did not induce overt alterations of metanephric morphogenesis

To investigate signs of ureteric or tubular dysmorphia which had been reported by Kanwar *et al* (Kanwar and Liu *et al.* 1996), whole mount and confocal microscopy of immunofluorescence-stained explants was performed. Whole mount images of explants stained against cytokeratins revealed the ureteric bud morphology of the explant pairs to be visually indistinguishable, independent of glucose concentration. Higher magnification analysis of the

ureteric tips by confocal imaging further confirmed the typical morphology of the ureteric tips in both high and low-glucose culturing conditions, without any sign of blunting. This was surprising, as the 1996 report of Kanwar *et al.* showed severely abrogated growth of the ureteric bud, which were described as thickened and atrophied with blunted tips (Kanwar and Liu *et al.* 1996). Furthermore, an absence of tertiary branching was described. This was not evident in the images analyzed in the present study, where the ureteric tree showed branching far in excess of three generations with acute tips. In their 2005 study, 10 explants per condition were stained by fluorescein-isothiocyanate (FITC)–conjugated *Dolichos biflorus* lectin, after which the number of ureteric bud tips were counted (Kanwar and Akagi *et al.* 2005). Their number was reported to be reduced from 60.9 to 27.3 as a consequence of high glucose exposure, which again appears to be in disagreement with the results of this thesis.

Hokke *et a*l. have utilized optical projection tomography to parameterize the ureteric trees of E14.5 embryos carried by STZ-induced diabetic dams, which revealed them to possess 46 % fewer ureteric tips than controls (Hokke and Armitage *et al.* 2013). This exceeded the relative deficit found by Zhao *et al.*, who quantified the number of ureteric tips in the kidneys of newborn mice, which showed a reduction by 22.3 % in those exposed to STZ-induced maternal diabetes. The difference between the two *in vivo* studies can most likely be attributed to the later (E13) and lower-dosed STZ injections by Zhao *et al*. A blunting of the tips was described in neither of the *in vivo* experiments. To summarize, a severe retardation of murine ureteric tree branching was reported in the previously mentioned *in vivo* studies, and the high-glucose cultures of Hayreh *et al.* have reflected this, while the experiments presented herein have not. It can nonetheless be concluded that the results presented here are in clear disagreement with the severely dysmorphic ureteric buds presented in Kanwar *et al.*'s first report as well as the quantification of branching in their 2005 report. This suggests that some explants may be much more resistant to glucose-induced ureteric bud dysmorphogenesis than previously thought, especially with regard to a blunting of the ureteric tips or a lack of tertiary branching.

To investigate the effect of high glucose on the formation of tubules, the morphology of the thick ascending loops of Henle were visualized. Immunofluorescence stainings against Tamm-Horsfall protein (THP), a protein expressed by the cells of the thick ascending loop of Henle, revealed widespread tubulogenesis throughout metanephroi of both groups after seven days of culture. This is contrary to the previously of Kanwar *et al.* where '*very few well-developed nephrons* […] *and tubules*' were described (Kanwar and Liu *et al.* 1996). A 2005 review by the same first author includes an image of a paraffin section where the high-glucose cultured explant showed a severe reduction in the number of visible tubules (Kanwar and Nayak *et al.*

2005). The results presented here have shown that glomerulogenesis as well as tubulogenesis are possible in a high glucose environment without major disruption, and thus demonstrate that these previously reported abrogations cannot be generalized.

An explanation for some of the divergence of the results reported here and the observations made by Kanwar *et al.* in their 1996 report may lie in the imaging techniques used. In this study, they compared individual tolouine-blue stained paraffin sections from the cultured explants, but did not describe a matched comparison between explants from the same embryo. In contrast, the experiments and analyses in this thesis maintained the pair-wise matching of metanephroi dissected from the same embryo for all comparisons. Another weakness of section-based morphological analysis arises from the heterogeneity of the metanephric tissue. The cross-sectional area of the explants, as well as the number of visible nephrons and their maturity may all vary depending on the distance between the filter and the sectioning level. This sectioning height is usually not measured or controlled in the process of paraffin microtomy. In contrast, the orthogonally projected wide-field images produced in this thesis serve to display the morphological features through the whole thickness of the explants in a single image, allowing for a comparison independent of sectioning height. In this thesis, the tips were analyzed by confocal imaging, and the imaging plane was manually set to section the ureteric tip centrally through the lumen at their most distal aspect. Nonetheless, no "blunting" was observed at the tips. A possible explanation for the observations made by Kanwar *et al.* could be that they inadvertently described more proximal, obliquely sectioned regions sections of the ureteric bud. (Kanwar and Liu *et al.* 1996*)*

The divergence of the results of the similar experiments presented here indicates that methodological differences which did exist may have had unexpected consequences. There was no difference in composition of the serum-free media. More importantly, the strain of mice used differed from one another. While inbred "Institute of Cancer Research" (ICR) mice had been used by Kanwar *et al.*, mice with a mixed genetic background (C57/B6, ICR, Sv129/S2) were used in this study. Genetically determined differences in the developmental susceptibility towards high glucose concentrations may thus have translated to the observed difference between the results. Some evidence of such genetic factors has been produced by whole embryo culture studies, where the differing degrees of resistance against glucose-induced major malformations correlated with differences in the levels of catalase expression between different rat strains (Cederberg and Erikson 1997). At the moment, ICR mice are still the only mouse strain for which morphometric data concerning the effect of high glucose exposure on cultured explants is available. The results presented here have shown that the effect of high glucose on

the metanephroi of this strain should not be generalized, and that further studies comparing the susceptibility of different mouse strains towards glucose-induced dysmorphogenesis or nephron deficits are necessary. This is especially important for the planning of experiments using genetically modified mice.

Few other studies have sought to investigate the effect of D-glucose on metanephric development in absence of other metabolic or hormonal changes occurring in a diabetic gestation. Tran *et al.* have reported a somewhat counterintuitively increased surface area and nearly a doubling of the number of ureteric tips in murine metanephroi cultured in 25 mM, as opposed to 5 mM D-Glucose after 24 hours of culture (Zhang and Chen *et al.* 2007). This result is surprising as it appears contrary to both the before mentioned reduction in surface area and ureteric blunting reported by Kanwar *et al*,(Kanwar and Liu *et al.* 1996) as well as the small reduction in surface growth observed in the experiments presented in this thesis. This may be explained by differences in culturing techniques, as Tran *et al.* have performed the incubation of the explants directly immersed in the culture medium instead of using the more common filter culturing method. No evidence of nephron formation was demonstrated for their method of culture, and a regression of their surface area back to the initial values levels after 96 hours was reported. This indicates that the submerged culturing technique did not support adequate metanephric growth and may therefore not be an adequate model of diabetic renal dysmorphogenesis. This is especially evident as exposure to STZ-induced maternal diabetes has been demonstrated to incur reduced instead of increased ureteric branching *in vivo* (Hokke and Armitage *et al.* 2013, Zhao and Liao *et al.* 2014).

Other authors have investigated high-glucose kidney culture using metanephroi from rat embryos. These reports include even stronger disturbances of growth and nephrogenesis than those reported in murine offspring: Amri *et al.* reported a (75 %) reduction of nephrons at 13.8 mM compared to 6.9 mM glucose and a complete loss of nephrogenesis at 27.5 mM glucose of cultured rat metanephroi (Amri and Freund *et al.* 1999). Interestingly, the same study showed a smaller reduction in nephron number by just 21 % in the offspring of strongly diabetic dams exposed to an average maternal hyperglycemia of 24.6 mM during pregnancy. This indicates that metanephroi from the Sprague-Dawley rats used in their study may be especially sensitive towards glucose in an *ex vivo* setting. Sprague-Dawley rat metanephroi may therefore be more appropriate for the *ex vivo* induction of glucose induced dysmorphogenesis than the noninbred murine metanephroi used in this thesis.

Important limitations of the experiments presented in this thesis include the lack of morphometric quantification, which would ideally include analysis of three-dimensional reconstruction of the ureteric buds in terms of branching site number and distances. A counting of the stained tubular segments and the investigation into the development of the proximal tubules would also be a further improvement.

### 8.3.3. High glucose exposure: Outlook

As the results revealed that nephrogenesis may not be as sensitive to high glucose exposure as previously thought future studies may also seek to clarify the role of non-glucose factors in the emergence renal dysmorphogenesis in offspring exposed to maternal diabetes. Suspected non-glucose mediators of diabetic maldevelopment include ketonaemia, reduced vitamin A availability, increased somatomedin inhibitor concentrations as well as hypoxia or the before mentioned maldistribution of fetal iron (Basu and Tze *et al.* 1989, Styrud and Thunberg *et al.* 1995, Goldberg 2001). The glucose-independent teratogenic effect of serum from diabetic dams has previously been shown in whole rat embryo culture experiments (Buchanan and Denno *et al.* 1994). This effect has partly been ascribed to increased concentration of low-molecular somatomedin inhibitors in the diabetic serum (Sadler and Phillips *et al.* 1986). Unfortunately, there is little data on the degree to which the non-glucose alterations in the maternal circulation are passed on to metanephric tissues, which hinders an adequate transfer into organ culture systems. It should also be noted that while hyperglycemia is common to all human forms of diabetes mellitus, such non-glucose alterations of the maternal metabolism vary considerably between type-1 or type-2 diabetes. As a starting point, future experiments could utilize glucose-normalized serum from diabetic rodents to investigate its effect on cultured metanephroi in order to explore the possibility of non-glucose mediated metanephric dysmorphogenesis. This way, putative glucose-independent teratogenicity of maternal diabetes could be examined with regard to the developing kidney.

## 8.4. *Ex vivo* high temperature exposure as a model for metanephric development under increased maternal body temperature

The teratogenic effect of increased body temperatures during gestation has been experimentally demonstrated across many mammals (Edwards 1986). Renal aplasia or hypoplasia has been reported as a consequence of the heat exposure of guinea pigs as well as bonnet monkeys (Edwards 1969, Hendrickx and Stone *et al.* 1979). In humans, fever during the first trimester is considered a risk factor for malformations, which is well-supported for neural tube and heart defects (Dreier and Andersen *et al.* 2014). Concerning the kidneys, case-control studies have

indicated increased rates of renal aplasia in human offspring exposed to maternal fever during pregnancy (Abe and Honein *et al.* 2003, Waller and Hashmi *et al.* 2018). However, none of the previous animal or human studies have attempted to detect mild disturbances of kidney development such as reduced nephron numbers, which may potentially compromise kidney function later in life. This study aimed to utilize the *ex vivo* culturing technique to quantify the degree to which metanephric growth and glomerulogenesis are affected by fever-range temperatures. The performed experiments showed that 3 °C increase in incubation temperature significantly reduced explant surface growth, but did not significantly affect the number of glomeruli formed during culture.

The body temperature of mice lies at approximately 37 °C, with some variation depending on the strain, body weight and age as well as other factors (McLaren 1961). A temperature of 40 °C was been chosen for the hyperthermia group of explants, and was sustained for the whole seven days of the incubation in order to simulate prolonged, high-grade fever. Previous studies of hyperthermic teratogenesis in mice used external heat application to raise the core body temperature of pregnant mice, usually to 42 °C or 43 °C. When such an intense exposure is maintained for just 10-15 minutes, severe malformations are induced in a large portion of deformed fetuses. For example, a 15 minute exposure of pregnant mice to 42 °C was reported to result in 91.7 % of fetuses showing skeletal malformations (Shiota 1988). It was decided that such a "heat shock" treatment would be of little relevance to human gestation affected by fever, as evidenced by the excessively high rates of malformations far exceeding those reported in human observational studies. The limit for a dangerous exposure during human gestation has been suggested to lie at a 2 °C elevation when exposed for longer than 24 h (Chambers and Johnson *et al.* 1998). As an elevation of 3 °C is above this limit and is yet realistic in the case of fever, 40 °C was considered an adequate temperature for the relatively long seven-day exposure of the explants. No previous morphometric study of kidney development under elevated temperatures was found in the literature. This study aimed to provide the first of such an evaluation in an *ex vivo* setting.

## 8.5. *Ex vivo* hyperthermia reduces explant growth without significantly affecting glomerulogenesis

The explants exposed to 40 °C showed significantly smaller surface area than their 37 °C counterparts after seven days of culture. This reduction by 18.36 % percent supports the notion that fever range temperatures may reduce kidney growth. Preceding reports have not included measures of renal size, and usually only reported renal agenesis, which generally considered to

be the result of a severe renal malformation. Malformations must occur during the initial formation of the organ, while developmental disruptions can also describe disturbances occurring later during organ growth and maturation (Stevenson 2015). It follows that the experiments presented in this thesis have only regarded the possibility of heat-induced developmental disruption, as the kidney culture systems relies on pre-formed metanephroi. The kidney culture system does not allow for the study of malformations arising during the initial formation of the organ. A complete collapse of nephrogenesis mirroring renal agenesis was not observed, which was expected, as this is unlikely to occur after the initial formation of the organ. Nonetheless, the decreased surface growth shows that metanephroi are sensitive to heat-mediated developmental disruption. Notably, the variability in size was significantly increased, indicating that the developmental disturbance induced by the increased temperature may interact with variations between the explants. Such variations may include minute trauma experienced during dissection or the precise age of the explants at the point of harvesting. As targeted timing of dissection of E12.5 relies on an estimation of the time of conception, a small variation in the duration of gestation is to be expected. It could also be considered be that hyperthermia-induced tissue damage may increase the sensitivity of the explants for further retardation thereby amplifying the effects of any early disruption.

While the surface growth was reduced, no significant difference in the number of glomeruli per explant were found. This suggests that the nephron maturation to be less intensely affected than the processes more closely connected to overall metanephric growth such as mesenchymal cap and ureteric bud proliferation. As an expansion of the performed experiments, a quantification of the shares of ureteric bud cells or SIX2-positive mesenchymal cap cells undergoing mitosis and apoptosis could indicate how intensely these compartments of the metanephroi are affected by heat exposure. If such a decrease in explant size were to be mediated by a reduction in mesenchymal cap progenitor cells, then this may entail a reduction in nephron number after further maturation, as the progenitor cell pools may be depleted sooner. However, such maturation may not be achievable in an *ex vivo* setting and require *in vivo* experiments.

The results should be interpreted with considerations of the limitations of the kidney culture system. Little is known about the precise alterations which the metanephroi are exposed to under maternal hyperthermia or feverish infections. Realistically, a simple increase of the temperature must be regarded as a simplification of these conditions, which may involve a plethora of changes in the maternal circulation and placental physiology. For example, increased cortisol levels have been detected both in feverish infections as well as hyperthermia. Glucocorticoids have previously been demonstrated to reduce the nephron endowment and

could therefore be suspected to mediate between maternal fever and metanephric maldevelopment (Dickinson and Walker *et al.* 2007, Singh and Moritz *et al.* 2007). Experimental hyperthermia has also been shown to induce a thickening of the placental barrier in rats and even been used to induce placental insufficiency and fetal growth retardation in sheep (Morrison 2008). Thus, it must be considered that disturbances of the placental function may also mediate to be detrimental to the kidney maturation, which would not be mirrored in the culture system. In addition, the kidney culture model is limited in the choice of time points of dissection and the start of the culture. The timing between the start of gestation and the episode of hyperthermia has been demonstrated to be closely related to the nature and extend of its teratogenic effects (Edwards 1986). Due to the relatively fixed observable period of the kidney culture model, the period of the highest renal sensitivity to hyperthermia would likely have to be determined in *in vivo* experiments. The limited duration of the kidney culture also limits the possibilities for follow-up investigations. It cannot be predicted whether affected kidney could compensate for heat-induced damage by catch-up growth, or whether the tissue would continue to deteriorate. It should also be noted that all metanephroi were initially exposed to unphysiologically low temperatures before the target temperatures were reached. This occurred when the embryos and explants were kept in ice-cooled phosphate buffered salt solution between the dissection and the start of the culture. The consequence of hypothermia on metanephric developments are not well characterized, but the transient cooling is usually well-tolerated and is even employed for metanephric conservation before experimental transplantation (Hammerman 2002). Nonetheless, a rapid change in temperature occured when the culture was started. This may have exacerbated the effects of the 40 °C exposure, as such a temperature would be approached more slowly in maternal fever or hyperthermia

To summarize, a three-degree increase in the temperature of murine metanephric kidney culture resulted in reduced growth as a sign of developmental disruption, but did not translate to a significant reduction in the number of nephrons formed. This adds to the body of evidence of renal sensitivity towards increased temperatures, although further research into the affected cellular compartments is warranted. As the results suggest that metanephroi may be affected by excessively high temperatures in a subclinical fashion, future animal studies of heat stress during gestation could expand on this by including measures of renal volume and nephron counting. Finally, the question as to whether fever-induced subclinical nephron deficits are a risk to humans themselves will require observational studies with renal endpoints such as renal volume or functional renal assessments of the offspring.

### 8.5.1. High temperature exposure: Outlook

Future studies may seek to clarify the extent to which high temperatures may induce renal malformations, which was not possible using the metanephric culture system. Previous reports of heat treatment of pregnant guinea pigs showed renal agenesis in 37.5 % of fetuses which were exposed to hyperthermia from day 18 to day 25 (Edwards 1969). This time window of hyperthermia therefore coincided with the relatively late initial formation of guinea pig metanephroi on the 23rd day of gestation. For comparison, mice and rats already form the first metanephric rudiments on the 11$^{th}$ or 12$^{th}$ day of gestation (Zoetis and Hurtt 2003). This timing therefore aligns well with the possibility of hyperthermia inducing renal malformation in its strict sense in guinea pigs. The study of such early malformations may be of greater relevance to human renal agenesis following first-trimester fever than the heat-induced developmental disruption reported in the kidney culture model. At the same time, it could be hypothesized that hyperthermic renal malformations may not be a binary phenomenon where only complete agenesis or no malformation are possible outcomes. Milder malformations could result in kidneys with reduced nephron numbers, the equivalent of which would not be clinically detected in humans but may nonetheless mediate debilitating sequelae later in life. Regardless, further *in vivo* rodent studies involving heat exposure surrounding the initial formation of metanephroi may be needed to more closely examine the spectrum of heat induced malformations. As a complement, whole rat embryo cultures encompassing the time of the initial metanephric formation could serve as a closely controllable *in vitro* setting. Rat embryo culture experiments have reported near-normal development for 44 hours after explantation at E11.5 and could therefore encompass the presumably critical period of the rat metanephric rudiment formation at E12.5 (New and Coppola *et al.* 1973). This would enable the study of renal formation in a setting which allows including precise control of the incubation temperature and other factors without necessitating the highly distressing heat exposure of dams.

## 8.6. E*x vivo* iron restriction as a model for metanephric development under iron insufficient conditions

As a third *ex vivo* model, the present thesis evaluates the use of an iron-restricted kidney culture as a model for maternally induced oligonephronia. It has previously been reported that maternal nutritional iron restriction leads to hypertension in rat offspring (Lewis and Petry *et al.* 2001, Lewis and Forhead *et al.* 2002, Gambling and Dunford *et al.* 2003, Lisle and Lewis *et al.* 2003, Nehiri and Van Huyen *et al.* 2008). This hypertension has been shown to coincide with a

reduction in offspring nephron endowment, which has been proposed to contribute to the hypertension (Lisle and Lewis *et al.* 2003, Drake and Sauerbry *et al.* 2009, Sun and Woolley *et al.* 2017). Little is known about how this reduction arises, proposed mechanisms include fetal hypoxia, increased maternal stress and reduced iron supply to the fetus (Drake and Sauerbry *et al.* 2009). While the placental iron transport system may compensate for some reduction in iron availability, several studies indicate that this compensation is incomplete in both rodents and humans, meaning that maternal iron-deficiency during gestation compromises the iron status of newborns (Kumar and Rai *et al.* 2008, Sun and Woolley *et al.* 2017, Swetha and Tarakeswararao *et al.* 2017). Nutritional iron-deficiency of pregnant rats was reported to result in a reduction of offspring renal iron content by approximately 50 %, demonstrating that the iron uptake of the kidneys is not maintained under maternal iron-deficiency (Sun and Woolley *et al.* 2017). Interestingly, human infants exposed to maternal diabetes also show a severe maldistribution of iron towards the hematopoietic system, at the cost of other organs: an average 93 % reduction in liver and 40 % reduction in brain iron content has been reported, indicating that organ-specific developmental iron deprivation may occur even in conditions where total fetal iron uptake is conserved (Petry and Eaton *et al.* 1992). In the present thesis, the effect of reduced iron availability to metanephroi was investigated in a controlled, *ex vivo* setting. For this purpose, explants from the same fetus were cultured in medium which was either supplemented with iron-saturated holo-transferrin or iron-depleted apo-transferrin.

No data on the transferrin concentration or saturation in the environment of the developing metanephros *in situ* is available. The total concentration of transferrin of 50 µg/ml was chosen for these experiments, as it is commonly used in kidney culture and is known to support adequate nephrogenesis. The complete replacement of holo-transferrin with apo-transferrin in the iron-restricted medium likely exceeds the reduction in saturation which occurs even in the most extreme cases of maternal iron-deficiency. However, as all metanephroi initially matured in an iron-sufficient *in situ* environment before the explantation, the intracellular reserves were assumed to exceed those of embryos exposed to maternal iron-deficiency from the beginning of the gestation, necessitating a more intense *ex vivo* iron deprivation. Preliminary testing had revealed the apo-transferrin containing medium to support reduced, but not completely abrogated growth and nephrogenesis within the observable timeframe. This was deemed adequate for the investigation of further morphological alterations associated with this condition. Such alterations may be present but more difficult to detect under less extreme settings, which would be adequate for further confirmation of the relevance of the observations for normal gestations.

### 8.6.1. *Ex vivo* iron restriction reduces metanephric growth and induces oligonephronia

In the present thesis, the metanephroi grown on medium containing depleted transferrin grew to a significantly smaller size, which is in line with previously reported experiments demonstrating the function of transferrin as an iron-transporting protein (Landschulz and Thesleff *et al.* 1984). Iron is an essential co-factor of many cellular processes including DNA replication (Zhang 2014). While smaller kidney size at birth relative to body weight has been reported in *in vivo* studies, the effect was much less extreme (Gambling and Dunford *et al.* 2003). This indicates that the iron deprivation experienced by the explants likely exceeds the degree of iron deprivation induced by maternal iron-deficiency *in vivo.*

A previous *in vivo* study of rats indicated a 23 % reduction in the number of nephrons formed per kidney (Lisle and Lewis *et al.* 2003). In the experiments presented in this thesis, the average number of glomeruli per explant was reduced by 69 %, which again indicates the relative severity of the tested conditions. This reduction is unlikely to be mediated purely by reduced explant size, as the density of nephrons per μm² surface area was reduced by 37.6 %. The glomerulogenesis thus appeared to be reduced in absolute terms as well as being reduced relative to the explant surface area. This served as a first indication that both the growth of the explants, as well as the processes of nephron induction or maturation may be disturbed. As some degree of glomerulogenesis occurred in all iron-deprived explants, it can be concluded that the experimental condition did not prevent the differentiation of metanephric mesenchyme all the way to mature epithelial cells of the nephron, such as podocytes. The *ex vivo* iron deprivation resulted in the replication of reduced nephron endowment without complete abrogation of nephrogenesis. This indicated that the chosen conditions were adequate for further morphological investigation of the developmental processes preceding the reduction in glomerular number.

A retardation of cell cycle was suspected as the cause of the surface growth retardation. Confocal analysis of explants stained against phosphohistone H3 after 48 hours of culture revealed a significantly reduced density of cells undergoing mitosis in the iron-deprived group. This effect is to be expected as intracellular iron reserves are diminished following cell divisions under iron-restricted conditions. Adequate intracellular iron reserves are indispensable for cell tissue proliferation, as key enzymes required for DNA replication and cell cycle progression depend on ferric ions as a cofactor (Zhang 2014). Several other mechanisms by which reduced intracellular iron concentrations promotes a cell cycle arrest in the S or $G_1$ stages are known, which include the increased degradation of cyclin D and P21 protein, as well as reduced

ribonuclease activity (Hershko 2007, Nurtjahja-Tjendraputra and Fu *et al.* 2007). It can be concluded that a reduction in mitotic density induced by the iron deprivation contributes to the reduced growth, although a limitation of these measurements lies in the comparison of spatial density of mitotic cells. Ideally, the number of mitotic cells would be expressed as a proportion of the total number of cells included in the measurement, as this approach is not sensitive to differences in average cell volume. A repetition of these experiments would ideally differentiate between the mitotic rates of specific cell types such as the ureteric bud epithelial cells or *Six2*-expressing pluripotent cap mesenchyme cells to determine the relative degree to which their proliferation is affected.

The number of branching sites formed is known as one of the factors determining the number of nephrons formed (Michos 2009). It was hypothesized that the reduced number of glomeruli after seven days of culture may have been a consequence of a preceding reduction in ureteric tree branching. The quantification of the branching of the ureteric tree revealed a significant reduction of the number of branching points by 38 %. It therefore appears plausible for the reduced number of nephrons observed towards the end of the culture to be a consequence of the reduced branching activity of the ureteric bud. However, this does not, by itself, lead to the conclusion that a primary disturbance must have arisen in the ureteric epithelial cells themselves. There is a close reciprocal induction of the ureteric bud and the metanephric mesenchyme, and the ureteric growth is dependent on the in the release of paracrine growth signals such as glial cell line-derived neurotrophic factor (GNDF) by the metanephric mesenchyme (Sariola and Saarma 2003). Consequently, a disturbance of the induction of the ureteric bud by the metanephric mesenchyme caused by the iron restriction could also serve as an explanation of the reduced ureteric growth.

A depletion of mesenchymal progenitor cells is considered as a possible cause of the reduction in branching activity. The stainings revealed the continued cap-like arrangement of SIX2-positive pluripotent mesenchymal cells surrounding the ureteric bud tips after 7 days of iron-deprived culture. As the expression of SIX*2* would be lost upon cell death or differentiation, (Xu and Liu *et al.* 2014) the continued presence of this protein indicates that neither of these irreversible processes has depleted this pluripotent population. As a consequence, premature differentiation or widespread apoptosis of the mesenchymal cap cells can be excluded as the causes of the reduced overall growth or the retarded ureteric branching. Despite the growth retardation, both ureteric morphology as well as cap architecture appeared intact and similar to earlier stages of metanephric development. This observation is in coherence with the notion that the growth retardation by iron restriction may be partly reversible. One rat study reported

a normalization of the perinatally reduced glomerular numbers within thirty days when maternal dietary iron was restored after birth (Sun and Woolley *et al.* 2017). Unfortunately, a postnatal normalization of nephron numbers cannot be expected in humans even under ideal postnatal iron supplementation, as human nephrogenesis terminates before birth. Hence, a similar catch-up in nephrogenesis would necessitate a normalization of metanephric iron uptake at an earlier point in time.

### 8.6.2. *Ex vivo* iron restriction alters nephron formation and maturation

In addition to the effects on ureteric tree branching, it was suspected that the reduced number of glomeruli formed may be due to disturbed nephron induction and maturation. Epithelialized early nephrons express E-cadherin, which allowed for the evaluation of their development after 48 hours of culture. The iron-restricted explants showed drastically fewer E-cadherin-stained renal vesicles or comma-shaped bodies, while these were present on nearly all branches of the ureteric tree in the iron-sufficient explants. This deficit of nephron formation despite the presence of many architecturally adequate loci near the ureteric tips indicates that the observed reduction in the number of glomeruli was not only due to the reduction in ureteric branching but also in a disturbance of nephron induction where ureteric tips had successfully formed. In the iron restricted kidneys, the mesenchymal caps appeared to lay in the correct position, but the mesenchymal to epithelial transition (MET) to E-cadherin-expressing early nephron entities did not occur. This is consistent with previous reports which have demonstrated the necessity of transferrin-mediated iron intake for the epithelialization of early nephron structures (Thesleff and Ekblom 1984). It is nonetheless a new observation that an environment where the initial epithelialization of renal vesicles is inhibited can nonetheless facilitate the maturation of glomeruli where the MET was successful. The development of glomeruli necessitates several iterations of mitosis after the initial formation of renal vesicles, which contain markedly fewer cells. It thus appears unlikely that the lack of epithelialization near some ureteric tips is due to a critical insufficiency of iron preventing the cytoskeletal reorganization necessary for the formation of renal vesicles. If that was the case, the renal vesicles which successfully formed would be unlikely to possess sufficient intracellular iron reserves for the continued development of entire glomeruli. Instead, it could be hypothesized that the reduced availability of iron may interfere with the inter- and intracellular signaling which induce the mesenchymal to epithelial transition (MET). While there are several paracrine signaling pathways which control the interaction between the ureteric bud and the metanephric mesenchyme, the canonical Wnt/beta catenin signalling pathway has been reported to be central to for the formation of epithelialized

structures in the metanephric mesenchyme under normal conditions (Park and Valerius *et al.* 2007, Schmidt-Ott and Barasch 2008). A widespread downregulation of genes associated with Wnt-signalling has previously been reported in a microarray analysis of rat offspring exposed to maternal iron-deficiency, supporting the notion that an inhibition of this pathway may occur *in vivo* due to this maternal condition (Swali and McMullen *et al.* 2012). Mechanistically, this may be plausible, as intracellular iron depletion by chelating agents has been shown to induce the proteosomal degradation of beta-catenin, the principal down-stream effector protein of the canonical Wnt-pathway, although this effect has only been shown in cancer and neural progenitor cells (Song and Christova *et al.* 2011, Ziaei and Ardakani *et al.* 2015). Future investigations into the relationship between iron metabolisms developmental Wnt-signalling are warranted. An interaction of this nature would not only be relevant to kidney development, but is also in other Wnt-associated developmental processes which are known to be negatively affected by iron-deficiency such as neuron maturation (Greminger and Lee *et al.* 2014). It can be concluded that mesenchymal cap progenitor cells maintain the expression of *SIX2* and a cap-like architecture for several days during iron restricted culture, which would be necessary for continued growth when the supply of iron is restored. A limitation of the performed experiments is the lack of quantification of renal vesicle formation, which would ideally be performed on several time points. Nonetheless, a notable reduction in early nephron formation was found, even where successful branching of the ureteric bud had occurred. This indicates that the reduction in glomerular number can partly be attributed to a reduced formation of epithelialized nephron precursors in addition to the before mentioned reduction in ureteric branching.

Next to MET, the restriction of iron availability may also affect nephron maturation. Stainings against WT1 and JAG1 after 48 hours of culture again demonstrated a reduction in the number of early comma-shaped and S-shaped nephrons. The widespread presence of WT1 positive pre-glomerular early nephron segments without attached JAG1-positive pre-tubular segments indicated a disturbance of tubular development. Meanwhile, the Wt1 expressing pre-glomerular segments were prematurely folded into rounded glomerular shape. This served as an indication that the iron deprivation may have differentially affected glomerulogenesis and tubulogenesis. Unfortunately, no data on the quantitative iron requirements of tubular and glomerular progenitors is available. Nevertheless, it appears plausible that tubular development may be more sensitive to iron restriction than glomerular development due to the greater dimensions of the tubular compartment in terms of cell number and organelle content, which may require greater intake of iron during development. The premature folding of WT1-positive pre-glomerular segments cannot be explained by a simple retardation of overall nephron maturation,

as such a process would have rather led to shortened and less folded WT1-positive segments. Instead, the prematurely folded WT1-positive segments are evidence of dysmorphogenesis as a consequence of iron restriction. While the differing structural iron requirements between glomerulogenesis and nephrogenesis mentioned before are a plausible explanation for the relative retardation of the JAG1-positive segments, differences in the cellular signaling could again be considered. As mentioned above, disturbances in canonical Wnt-activity were suspected to contribute to the observed deficit in nephron induction. A report on the distribution of beta catenin activity, the primary down-stream effect of canonical Wnt-signaling, during *in situ* nephrogenesis has demonstrated the activity to localize to the distal, pre-tubular segments of the developing nephron, while being absent in the segments which will form the glomeruli (Iglesias and Hueber *et al.* 2007). As with the reduction in mesenchymal MET, the observed alterations due to iron restriction overlap with the expected effect of reduced Wnt-signalling. Together with the before mentioned report of a downregulation of Wnt-regulated genes in the fetuses of iron restricted rat dams, further investigation of crosstalk between developmental iron status and canonical Wnt-signalling seems promising (Swali and McMullen *et al.* 2012).

Due to these signs of tubular dysgenesis, the tubular development with regard to the distal tubular segments was investigated further. Under normal conditions, the flow of blood and urine are integral parts of the physiological renal iron distribution, especially with regard to tubular epithelia. Transferrin passes through the glomerular filtration system to be reabsorbed by endocytosis in the tubular system. It is taken up by tubular cells by both transferrin receptor- and cubilin-mediated endocytosis at the apical membrane (Gatter and Brown *et al.* 1983, Kozyraki and Fyfe *et al.* 2001). Because the avascular glomeruli of cultured metanephroi do not produce urine, the degree to which tubular development was possible in the iron-sufficient culture condition had to be confirmed. Staining against NKCC2, an epithelial channel expressed by the distal tubule revealed that the development of distal tubules was widespread in the iron-sufficient explant group after seven days of culture. In the iron-restricted group, their absence was nearly complete, with the exception occasional, shortened segments. Firstly, this confirmed that tubulogenesis was intact in the iron-sufficient explants, notwithstanding the lack of urine flow. Secondly, this confirmed that the tubulogenesis was indeed strongly abrogated in the iron restricted explants, as it had been suspected by the lack of JAG1-positive segments in some s-shaped nephrons. It can thus be concluded that nephrons formed in the iron-restricted explants were not only reduced in numbers, but also morphologically altered. This may, however, also be the product of overall retardation of nephron growth. In the past, all authors have relied on the number of glomeruli as the principal morphometric indicator of future kidney function,

which would not have included alterations of the tubular organization (Lisle and Lewis *et al.* 2003, Drake and Sauerbry *et al.* 2009). The extreme abrogation of distal tubules may have been a consequence of the rather intense iron restriction, and the aphysiological culture system may have exacerbated the disturbance of tubulogenesis. Nonetheless the possibility of qualitative morphological alterations of nephrogenesis in addition to the quantitative reduction in nephron endowment should be considered in future *in vivo* studies. If the development of the tubules, especially the distal tubules is indeed affected more intensely than the glomerular compartment, a reduction in the ability of the tubular system to reabsorb sodium and water would be a plausible consequence, which may contribute to hypotension due to reduced plasma volume rather than contributing to the hypertensive effects of a reduced nephron number. While rat studies have reported hypertension in the offspring of iron-restricted dams, human data on the blood pressure of children exposed to maternal iron-deficiency *in utero* has been inconclusive, with 2 studies reporting higher and 3 studies reporting lower blood pressure in the affected children as compared to the control groups. (Alwan and Hamamy 2015) While there is no evidence of tubule dysfunction in humans exposed to maternal iron-deficiency at this point, future animal experiments may benefit from the inclusion of tubular parameters in the analysis of renal dysmorphogenesis following iron restriction.

### 8.6.3. *Ex vivo* iron restriction induces apoptotic processes in the ureteric epithelium

Increased apoptosis of the ureteric bud cells had been suspected as a reason for the observed reduction in ureteric bud growth. Confocal imaging showed widespread staining for active Caspase 3 in the lumen of the ureteric bud after just 48 hours of culture. Rarely, active caspase and pyknotic nuclei were observed in cells which were still integrated in the epithelium near the ureteric tips. No apoptotic debris was observed at the basal aspect of the epithelium, which demonstrates the epithelium maintained its impermeability and the integrity of its basal membrane. The apoptosis of ureteric bud cells most likely contributed to the before mentioned retardation of ureteric bud growth and branching, which in turn generally contributes to reduced nephron numbers. Such mechanisms were not previously explored, as earlier experiments of maternal iron deprivation have not focused on the ureteric bud development. Physiologically, the observed apoptotic debris including its iron ions would be carried away by the urine. In contrast to the stromal cells, where iron ions can be recycled by the surrounding cells, this loss of cell material into the urine may thus further exacerbate the local iron-deficit. The ureteric epithelial cells where cleaved Caspase 3 was visualized, as well as the apoptotic debris were predominantly visualized at the tips of the ureteric bud. At these tips, the mitotic activity is particularly high, and mitosis has become known to occur by a mechanism known as “mitotic cell dispersal” relatively recently (Packard and Georgas *et al.* 2013). In this process, the cells undergoing mitosis mostly detach from the basal membrane, to which they preserve a small “tether”. Mitosis results in a basal daughter cell which inherits this tether and reinsert at the original position, while the apical daughter cell becomes “mobile” and reinserts at a nearby position. As each iteration of mitosis will result in daughter cells with reduced iron reserves, the high mitotic activity of ureteric tips likely contributed to the apoptosis. Very few intraepithelial cells containing cleaved Caspase 3 were visualized when compared with the apparent volume of the intraluminal apoptotic debris. This could either be explained by a fast detachment of the cells undergoing apoptosis, or by the apoptosis of apical daughter cells which have already detached during the process of mitosis. The contact to the basement membrane is an important suppressor of apoptosis (Assoian 1997), it could therefore be hypothesized that the loss of basement membrane contact of the unattached cells in the process of luminal mitosis may have contributed to the visualized apoptosis. This is supported by the fact that Deferoxamine treatment of holo-transferrin cultured explants showed that epithelial cells which are anchored to the basement membrane are surprisingly resistant even to chemical depletion

of intracellular iron. Such a hypothesis would, however, have to be examined in a live imaging system which facilitates cell tracking as well as live imaging of apoptosis.

Generally, apoptotic processes of the ureteric bud are not well understood, even though they have been clearly demonstrated to be relevant to human disease. Early kidney culture studies reported strongly abrogated development in the presence of caspase inhibitors and thus concluded the necessity of caspase activity for normal kidney development (Araki and Saruta *et al.* 1999). This was later contradicted by reports that the addition Z-VAD, a commonly used caspase inhibitor, actually increases the number of nephrons formed in kidney culture (Clark and Dziarmaga *et al.* 2004). Most information on the consequences of ureteric apoptosis in humans was gained by the study of a rare genetic condition caused by mutations of the *Pax2* (paired box 2) gene. In 1995, Sanyanusin *et al.* had had first linked a syndrome of optic nerve colobomas and renal hypoplasia to a heterozygous frame shift mutation in the *Pax2* gene (Sanyanusin and McNoe *et al.* 1995). Both *ex vivo* and *in vivo* studies later demonstrated that the renal dysmorphogenesis exhibited by *Pax2*-haploinsufficient mice was primarily mediated by increased apoptosis of the ureteric bud cells, which consequentially led to disturbed ureteric bud branching and the formation of fewer nephrons (Clark and Dziarmaga *et al.* 2004, Dziarmaga and Eccles *et al.* 2006). These results indicated that the same mechanism may be responsible for the renal hypoplasia in *Pax2*-haploinsufficient humans. More recently, Quinlan *et al.* have reported a common polymorphism of the *Pax2* gene which was carried by 18.5 % of the study population to be associated with reduction in the kidney volume by an average of 10 % (Quinlan and Lemire *et al.* 2007). It could be hypothesized that the kidney size of those carrying the polymorphism was limited as a consequence of increased ureteric apoptosis, if the mechanism by which the *Pax2*-polymorphism disturbs the nephrogenesis is similar to that the *Pax2*-haploinsufficiency. As the experiments presented in this thesis have shown that reduced iron availability may trigger ureteric apoptosis as well, it should be considered whether carriers of the before mentioned polymorphism may be especially vulnerable to the pro-apoptotic effects of iron restriction. No single genetic or environmental factor has been found to sufficiently explain the extreme variation of human nephron numbers, which is commonly thought to arise by the interaction of many genetic and environmental factors (Brophy 2017). The common element of ureteric apoptosis provides an opportunity to study the interaction between a prevalent genetic and a widespread environmental factor. Under this hypothesis, a strengthened correlation between iron status at birth and renal volume would be expected in those infants carrying the polymorphism. As a proof of principle, it could also be investigated whether maternal iron restriction disturbs the renal development of *Pax2*-haploinsufficient mice

more intensely than in it does in wildtype animals. Lastly, the results have also inadvertedly shown that iron restriction can be used as an *ex vivo* method to induce ureteric apoptosis without the addition of compounds foreign to the organism, and without complete abrogation of nephrogenesis. This may prove to be a useful tool for future studies investigating the process of ureteric apoptosis, or the maintenance of ureteric epithelial integrity.

In order to elucidate the quantity and localization of ureteric cells undergoing apoptosis, further experiments are necessary. The results have shown qualitative evidence of apoptotic debris in the lumen, which does not allow for conclusions about the number of cells which have undergone apoptosis, or the precise location where they have done so. A share of the apoptotic debris may even have originated from the forming nephrons instead of the ureteric bud. However, this is unlikely because of the lack of urine flow in the kidney culture system. Furthermore, apoptotic debris and occasional apoptotic cells were predominantly found at the distal aspect of the ureteric bud tips where no nephrons are connected. If such apoptotic processes were to be investigated in an *in vivo* setting, the detachment of apoptotic cells may hinder their histological detection as they are flushed into the amniotic fluid by the flow of urine. This may, however, be advantageous as it may remain detectable in the fluid by increased cell-free DNA, activated caspase concentrations or even ureter-specific cell components.

To summarize, metanephric development under iron restricted conditions is not simply retarded in terms of size growth and the number of nephrons formed, but also affected by distinct alterations of nephron morphogenesis. This included a disproportionate inhibition of tubulogenesis relative to the glomerular development, which may have functional consequences going beyond the quantitative reduction in nephron numbers. While a reduction in ureteric branching in iron-deprived explants was partly expected due to their previously reported smaller size, the induction of ureteric apoptosis by iron-deficiency is a new observation.

### 8.6.4. Iron restriction: Outlook

Future studies may attempt to align the degree of iron deprivation seen in the explants with the one found *in vivo*. As an approximation, one might empirically increase the content of iron-saturated transferrin in the medium of the iron-deprived kidneys. The target concentration of holo-transferrin would be the one where the iron mass per gram of kidney tissue at the end of the culture is reduced by the same degree as it is in the kidneys of newborns which experienced maternal iron-deficiency. As mentioned before, reduced iron content of fetal tissues is not a phenomenon which occurs exclusively due to maternal iron-deficiency. Pregestational maternal diabetes has also been shown to induce severe reductions in heart, liver and brain iron content

due to excessive iron uptake by the hematopoietic system. Unfortunately, no data is available on how renal iron content is affected during this maldistribution. It is possible that the redistribution of fetal iron reserves under the influence of maternal diabetes might contribute to reductions in nephron endowment. Future studies of renal development during diabetic conditions with measurements of the renal iron content at birth are necessary to determine if this hypothesis is plausible. The findings presented in this thesis are suggestive of multiple mechanisms by which reduced iron availability to the developing metanephroi may result in fewer functional nephrons at birth. Hopefully, a better understanding of renal maldevelopment due to maternal disease may translate to improved preventative strategies against low nephron endowment in the future.

# 9. Summary

Low nephron numbers at birth are thought to contribute to the development of arterial hypertension and kidney dysfunction, two health challenges of utmost importance to global health. While some specific causes of oligonephronia have been identified, the wide variation of nephron number in humans still largely remains unexplained. This thesis utilized an *ex vivo* organ culture system to model the effect of tree common conditions affecting pregnant women using murine metanephroi. The putatively central aspects of these conditions were translated to the *ex vivo* setting. The experimental conditions thus included the exposure of metanephroi to high glucose as a model of maternal diabetes, the exposure to high incubation temperatures as a model of maternal elevated body temperature and the exposure to an iron restricted environment as a model of reduced iron availability to the fetus.

A surprising resistance of the explant development towards high glucose exposure was revealed, which contradicted previous reports. This finding indicated that a high glucose environment alone may not by itself be a sufficient condition to induce a nephron deficit.

Secondly, this thesis includes the first quantification of nephron formation at elevated temperatures, relating to maternal fever or hyperthermia. However, as even the prolonged exposure to 40 °C only mildly affected metanephric growth and did not induce oligonephronia, the results are not suggestive of a notable sensitivity of the nephron formation towards increased maternal body temperatures.

Finally, the reduction of iron availability to the metanephric tissue, as it is thought to occur in several maternal conditions including maternal iron deficiency or diabetes, resulted in significantly reduced growth of the explants and the formation of fewer nephrons. A specific pattern of nephron malformation was detected, which appeared to abrogate the growth of early tubules more strongly than that of the glomerular progenitor cells. Low iron availability was also shown to induce apoptosis of the ureteric bud, which exhibited reduced branching, and a deficit of nephron induction in the vicinity of the bud. These results suggest that reduced metanephric iron uptake should be considered not only as a quantitative, but also as a qualitative disruptor of metanephric environment. Hopefully, a better understanding of renal maldevelopment due to maternal disease may translate to improved preventative strategies against low nephron endowment in the future.

# 10. Zusammenfassung

Eine angeborene niedrige Anzahl von Nephronen wird als wichtiger Risikofaktor für arterieller Hypertonie und Nierenversagen beim Menschen angesehen. Obwohl bislang einige spezifische Ursachen für Oligonephronie identifiziert wurden, ist die große Variation der menschlichen Nephronanzahl weitgehend unerklärt. In dieser Dissertationsarbeit wurde ein murines *ex vivo* Organkultursystem verwendet, um den Einfluss von drei in der Schwangerschaft häufig auftretende Krankheiten zu modellieren, die sich *in utero* auf reifende Metanephroi auswirken.

Als erste diente die Exposition explantierter Metanephroi gegenüber erhöhten Glukosekonzentrationen als Modell für mütterlichen Diabetes. Zweitens wurde die Exposition gegenüber erhöhten Temperaturen dient als Modell für erhöhte Körpertemperatur wie sie bei Fieber oder Hyperthermie auftritt umgesetzt. Zuletzt wurden Explantate einer Umgebung mit verringerter Eisenverfügbarkeit ausgesetzt, wie sie bei mehreren mütterlichen Krankheiten, einschließlich mütterlichem Eisenmangel oder Diabetes als Krankheitsfolge angenommen wird. Es wurde eine überraschende Resistenz der Nephronenentwicklung gegenüber einer hohen Glukosebelastung festgestellt, die im Widerspruch zu früheren Berichten stand. Dieses Ergebnis deutete darauf hin, dass ein hohes Glukosemilieu allein nicht ausreichen muss, um eine Oligonephrie zu induzieren. Im Zusammenhang mit mütterlichem Fieber oder Hyperthermie beinhaltet diese Arbeit erste Quantifizierung der Nephronbildung unter dem Einfluss erhöhter Temperaturen. Da jedoch selbst die längere Exposition gegenüber 40 °C das metanephrische Wachstum nur geringfügig beeinflusste und keine Oligonephronie hervorrief, deuten die Ergebnisse nicht auf eine deutliche Temperaturempfindlichkeit der Nephronbildung hin. Eine Verringerung der Eisenverfügbarkeit hingegen führte in der Organkultur zu einem deutlich reduzierten Wachstum der Explantate, und zu einer Verminderung der Anzahl der gebildeten Nephrone. Zusätzlich führte es auch zu einer Form der Nephronmissbildung, bei der das Wachstum der frühen Tubuli stärker beeinträchtigt wurde als das der frühen Glomeruli. Eine geringe Eisenverfügbarkeit induzierte darüber hinaus die Apoptose von Epithelzellen der Ureterknospe, eine reduzierte Verzweigung derselben und ein Defizit an Nephroninduktion in der Nähe der Knospenspitzen. Diese Ergebnisse deuten darauf hin, dass eine reduzierte metanephrische Eisenaufnahme nicht nur als quantitativer, und qualitativer Disruptor der Nephrogenese angesehen werden sollte. Es ist zu hoffen, dass zukünftig ein besseres Verständnis von renaler Fehlentwicklung die Entwicklung verbesserter präventativen Strategien gegen eine geringe Nephronausstattung ermöglicht.

# 11. Abbreviations

| Abbreviation | Word or Phrase |
|---|---|
| **bp** | Base pairs |
| **BP** | Band pass |
| **CC3** | Cleaved Caspase 3 |
| **CD326** | see EP-CAM |
| **CEMT** | Center for Experimental Models and Transgenic Service |
| **CKD** | Chronic kidney disease |
| **DBA** | *Dolichos Biflorus* agglutinin |
| **DMEM** | Dulbecco's modified Eagle's medium |
| **DNA** | Deoxyribonucleic acid |
| **E-cadherin** | Epithelial cadherin |
| **Ep-CAM** | Epithelial cell adhesion molecule |
| **FIJI** | FIJI is just ImageJ, an image processing package distribution of ImageJ |
| **FOAD** | Foetal origins of adult disease |
| **GDM** | Gestational diabetes mellitus |
| **GDNF** | Glial cell line-derived neurotrophic factor |
| **GFP** | Green fluorescent protein |
| **GFR** | Glomerular filtration rate |
| **HE** | High efficiency (filter set) |
| **IR** | Infrared |
| **ICR** | Institute of Cancer Research |
| **JAG1** | Jagged1 |
| **Lgr5** | Leucine-rich repeat-containing G-protein coupled receptor 5 |
| **loxP** | Locus of X(cross)-over P1 |
| **MET** | mesenchymal to epithelial transition |
| **mG** | Membrane-targeted green fluorescent protein |
| **mGFP** | Membrane-targeted green fluorescent protein |
| **mHprt** | Murine hypoxanthine guanine phosphoribosyl transferase |
| **mRNA** | Messenger ribonucleic acid |
| **mT** | Membrane-targeted tandem dimer Tomato |
| **mTom** | Membrane-targeted tandem dimer Tomato |
| **NKCC2** | Murine Na+ K+ 2Cl- cotransporter protein |
| **Notch2** | Neurogenic locus notch homolog protein 2 |
| **NPHS2** | Human gene encoding for Podocin |
| **Osr1** | Odd-skipped-related 1 |
| **PBS** | Phosphate buffered saline |

| | |
|---|---|
| **PBST** | Phospate buffered saline solution with Tween 20 (Polyoxyethylen-20-sorbitan-monolaurate) |
| **pCA** | Cytomegalovirus b-actin enhancer-promoter |
| **PCR** | Polymerase chain reaction |
| **PET** | Polyethylene terephthalate |
| **PFA** | Paraformaldehyde |
| **PGDM** | Pre-gestational diabetes mellitus |
| **pHH3** | Phosphohistone H3 |
| **qPCR** | Quantitative polymerase chain reaction |
| **RNA** | Ribonucleic acid |
| **SD** | Standard deviation |
| **Six2** | *Sine oculis*-related homeobox 2 |
| **SLM** | Scanning laser microscope |
| **STZ** | Streptozotocin |
| **TAE** | Tris-acetate-EDTA (Ethylenediaminetetraacetic acid) |
| **TAL** | Thick ascending loop of Henle |
| **TF** | Transferrin |
| **THP** | Tamm-Horsfall protein |
| **TIFF** | Tagged image file format |
| **TRIS** | Tromethamine |
| **UK** | United Kingdom |
| **USA** | United States of America |
| **Wt1** | Wilms tumor protein (murine homolog) |

# 12. Literature


Abe, K., M. A. Honein and C. A. Moore (2003). "Maternal febrile illnesses, medication use, and the risk of congenital renal anomalies." Birth Defects Research Part A: Clinical and Molecular Teratology 67(11): 911-918.

Aceti, A., S. Santhakumaran, K. Logan, L. Philipps, E. Prior, C. Gale, M. Hyde and N. Modi (2012). "The diabetic pregnancy and offspring blood pressure in childhood: a systematic review and meta-analysis." Diabetologia 55(11): 3114-3127.

Alwan, N. A., J. E. Cade, D. C. Greenwood, J. Deanfield and D. A. Lawlor (2014). "Associations of maternal iron intake and hemoglobin in pregnancy with offspring vascular phenotypes and adiposity at age 10: findings from the Avon Longitudinal Study of Parents and Children." PloS one 9(1): e84684.

Alwan, N. A. and H. Hamamy (2015). "Prenatal Exposures and Short and Long Term Developmental Outcomes: Maternal Iron Status in Pregnancy and Long-Term Health Outcomes in the Offspring." Journal of pediatric genetics 4(2): 111.

Alwan, N. A., D. A. Lawlor, H. J. McArdle, D. C. Greenwood and J. E. Cade (2012). "Exploring the relationship between maternal iron status and offspring's blood pressure and adiposity: a Mendelian randomization study." Clinical epidemiology 4: 193.

Amri, K., N. Freund, J. Vilar, C. Merlet-Benichou and M. Lelievre-Pegorier (1999). "Adverse effects of hyperglycemia on kidney development in rats: in vivo and in vitro studies." Diabetes 48(11): 2240-2245.

Andersen, A.-M. N., P. Vastrup, J. Wohlfahrt, P. K. Andersen, J. Olsen and M. Melbye (2002). "Fever in pregnancy and risk of fetal death: a cohort study." The Lancet 360(9345): 1552-1556.

Araki, T., T. Saruta, H. Okano and M. Miura (1999). "Caspase activity is required for nephrogenesis in the developing mouse metanephros." Experimental cell research 248(2): 423-429.

Assoian, R. K. (1997). "Anchorage-dependent cell cycle progression." The Journal of cell biology 136(1): 1-4.

Barker, D. J. (1990). "The fetal and infant origins of adult disease." BMJ: British Medical Journal 301(6761): 1111.

Barker, N., M. B. Rookmaaker, P. Kujala, A. Ng, M. Leushacke, H. Snippert, M. Van De Wetering, S. Tan, J. H. Van Es and M. Huch (2012). "Lgr5+ ve stem/progenitor cells contribute to nephron formation during kidney development." Cell reports 2(3): 540-552.

Basu, T., W. Tze and J. Leichter (1989). "Serum vitamin A and retinol-binding protein in patients with insulin-dependent diabetes mellitus." The American journal of clinical nutrition 50(2): 329-331.

Belfort, M. B., S. L. Rifas-Shiman, J. W. Rich-Edwards, K. P. Kleinman, E. Oken and M. W. Gillman (2008). "Maternal iron intake and iron status during pregnancy and child blood pressure at age 3 years." Int J Epidemiol 37(2): 301-308.

Bergel, E., E. Haelterman, J. Belizan, J. Villar and G. Carroli (2000). "Perinatal factors associated with blood pressure during childhood." American journal of epidemiology 151(6): 594-601.

Bertram, J. F., R. N. Douglas-Denton, B. Diouf, M. D. Hughson and W. E. Hoy (2011). "Human nephron number: implications for health and disease." Pediatric nephrology 26(9): 1529.

Bianchi, G., U. Fox, G. Di Francesco, A. Giovanetti and D. Pagetti (1974). "Blood pressure changes produced by kidney cross-transplantation between spontaneously hypertensive rats and normotensive rats." Clinical Science 47(5): 435-448.

Black, M. J., M. R. Sutherland and L. Gubhaju (2012). Effects of preterm birth on the kidney. Basic Nephrology and Acute Kidney Injury, InTech.

Black, R. E., C. G. Victora, S. P. Walker, Z. A. Bhutta, P. Christian, M. De Onis, M. Ezzati, S. Grantham-McGregor, J. Katz and R. Martorell (2013). "Maternal and child undernutrition and overweight in low-income and middle-income countries." The lancet 382(9890): 427-451.

Brenner, B. M., D. L. Garcia and S. Anderson (1988). "Glomeruli and blood pressure: Less of one, more the other?" American journal of hypertension 1(4_Pt_1): 335-347.

Brion, M. J., S. D. Leary, G. D. Smith, H. J. McArdle and A. R. Ness (2008). "Maternal anemia, iron intake in pregnancy, and offspring blood pressure in the Avon Longitudinal Study of Parents and Children." Am J Clin Nutr 88(4): 1126-1133.

Brophy, P. (2017). Maternal determinants of renal mass and function in the fetus and neonate. Seminars in Fetal and Neonatal Medicine, Elsevier.

Buchanan, T. A., K. M. Denno, G. F. Sipos and T. W. Sadler (1994). "Diabetic teratogenesis: In vitro evidence for a multifactorial etiology with little contribution from glucose per se." Diabetes 43(5): 656-660.

Cain, J. E., V. Di Giovanni, J. Smeeton and N. D. Rosenblum (2010). "Genetics of renal hypoplasia: insights into the mechanisms controlling nephron endowment." Pediatric research 68(2): 91.

Carroll, T. J., J.-S. Park, S. Hayashi, A. Majumdar and A. P. McMahon (2005). "Wnt9b plays a central role in the regulation of mesenchymal to epithelial transitions underlying organogenesis of the mammalian urogenital system." Developmental cell 9(2): 283-292.

Cebrián, C., K. Borodo, N. Charles and D. A. Herzlinger (2004). "Morphometric index of the developing murine kidney." Developmental dynamics 231(3): 601-608.

Cederberg, J. and U. J. Erikson (1997). "Decreased catalase activity in malformation-prone embryos of diabetic rats." Teratology 56(6): 350-357.

Chambers, C. D., K. A. Johnson, L. M. Dick, R. J. Felix and K. L. Jones (1998). "Maternal fever and birth outcome: a prospective study." Teratology 58(6): 251-257.

Chang, S.-Y., Y.-W. Chen, X.-P. Zhao, I. Chenier, S. Tran, A. Sauvé, J. R. Ingelfinger and S.-L. Zhang (2012). "Catalase prevents maternal diabetes–induced perinatal programming via the Nrf2–HO-1 defense system." Diabetes 61(10): 2565-2574.

Chen, S., E. W. Brunskill, S. S. Potter, P. J. Dexheimer, N. Salomonis, B. J. Aronow, C. I. Hong, T. Zhang and R. Kopan (2015). "Intrinsic age-dependent changes and cell-cell contacts regulate nephron progenitor lifespan." Developmental cell 35(1): 49-62.

Chen, Y.-W., I. Chenier, S.-Y. Chang, S. Tran, J. R. Ingelfinger and S.-L. Zhang (2010). "High glucose promotes nascent nephron apoptosis via NF-κB and p53 pathways." American Journal of Physiology-Renal Physiology 300(1): F147-F156.

Chen, Y.-W., I. Chenier, S. Tran, M. Scotcher, S.-Y. Chang and S.-L. Zhang (2010). "Maternal diabetes programs hypertension and kidney injury in offspring." Pediatric Nephrology 25(7): 1319-1329.

Cheng, H.-T., M. Kim, M. T. Valerius, K. Surendran, K. Schuster-Gossler, A. Gossler, A. P. McMahon and R. Kopan (2007). "Notch2, but not Notch1, is required for proximal fate acquisition in the mammalian nephron." Development 134(4): 801-811.

Chockalingam, U. M., E. Murphy, J. C. Ophoven, S. A. Weisdorf and M. K. Georgieff (1987). "Cord transferrin and ferritin values in newborn infants at risk for prenatal uteroplacental insufficiency and chronic hypoxia." The Journal of pediatrics 111(2): 283-286.

Clark, P., A. Dziarmaga, M. Eccles and P. Goodyer (2004). "Rescue of defective branching nephrogenesis in renal-coloboma syndrome by the caspase inhibitor, Z-VAD-fmk." Journal of the American Society of Nephrology 15(2): 299-305.

Costantini, F. and R. Shakya (2006). "GDNF/Ret signaling and the development of the kidney." Bioessays 28(2): 117-127.

Coton, S. J., I. Nazareth and I. Petersen (2016). "A cohort study of trends in the prevalence of pregestational diabetes in pregnancy recorded in UK general practice between 1995 and 2012." BMJ open 6(1): e009494.

Cullen-McEwen, L. A., J. Drago and J. F. Bertram (2001). "Nephron endowment in glial cell line-derived neurotrophic factor (GDNF) heterozygous mice." Kidney international 60(1): 31-36.

Curtis, J. J., R. G. Luke, H. P. Dustan, M. Kashgarian, J. D. Whelchel, P. Jones and A. G. Diethelm (1983). "Remission of essential hypertension after renal transplantation." New England Journal of Medicine 309(17): 1009-1015.

Dickinson, H., D. W. Walker, E. M. Wintour and K. Moritz (2007). "Maternal dexamethasone treatment at midgestation reduces nephron number and alters renal gene expression in the fetal spiny mouse." American Journal of Physiology-Regulatory, Integrative and Comparative Physiology 292(1): R453-R461.

Dosch, N. C., E. F. Guslits, M. B. Weber, S. E. Murray, B. Ha, C. L. Coe, A. P. Auger and P. J. Kling (2016). "Maternal obesity affects inflammatory and iron indices in umbilical cord blood." The Journal of pediatrics 172: 20-28.

Drake, K. A., M. J. Sauerbry, S. E. Blohowiak, K. S. Repyak and P. J. Kling (2009). "Iron deficiency and renal development in the newborn rat." Pediatr Res 66(6): 619-624.

Dreier, J. W., A.-M. N. Andersen and G. Berg-Beckhoff (2014). "Systematic review and meta-analyses: fever in pregnancy and health impacts in the offspring." Pediatrics: peds. 2013-3205.

Dziarmaga, A., M. Eccles and P. Goodyer (2006). "Suppression of ureteric bud apoptosis rescues nephron endowment and adult renal function in Pax2 mutant mice." Journal of the American Society of Nephrology 17(6): 1568-1575.

Edwards, M. (1969). "Congenital defects in guinea pigs: fetal resorptions, abortions, and malformations following induced hyperthermia during early gestation." Teratology 2(4): 313-328.

Edwards, M. (1986). "Hyperthermia as a teratogen: a review of experimental studies and their clinical significance." Teratogenesis, carcinogenesis, and mutagenesis 6(6): 563-582.

Ekblom, P., I. Thesleff, A. Miettinen and L. Saxen (1981). "Organogenesis in a defined medium supplemented with transferrin." Cell Differ 10(5): 281-288.

França-Silva, N., N. D. G. Oliveira and A. P. C. Balbi (2016). "Morphofunctional renal alterations in rats induced by intrauterine hyperglycemic environment." Archives of medical science: AMS 12(2): 243.

Galan, H. L., R. V. Anthony, S. Rigano, T. A. Parker, B. de Vrijer, E. Ferrazzi, R. B. Wilkening and T. R. Regnault (2005). "Fetal hypertension and abnormal Doppler velocimetry in an ovine model of intrauterine growth restriction." American journal of obstetrics and gynecology 192(1): 272-279.

Gambling, L., S. Dunford, D. I. Wallace, G. Zuur, N. Solanky and S. K. S. Srai (2003). "Iron deficiency during pregnancy affects postnatal blood pressure in the rat." The Journal of physiology 552(2): 603-610.

Gatter, K. C., G. Brown, I. Trowbridge, R. Woolston and D. Mason (1983). "Transferrin receptors in human tissues: their distribution and possible clinical relevance." Journal of clinical pathology 36(5): 539-545.

Georgieff, M. K., M. B. Landon, M. M. Mills, B. E. Hedlund, A. E. Faassen, R. L. Schmidt, J. J. Ophoven and J. A. Widness (1990). "Abnormal iron distribution in infants of diabetic mothers: spectrum and maternal antecedents." The Journal of pediatrics 117(3): 455-461.

Godfrey, K. M., T. Forrester, D. Barker, A. A. Jackson, J. Landman, J. S. E. Hall, V. Cox and C. Osmond (1994). "Maternal nutritional status in pregnancy and blood pressure in childhood." BJOG: An International Journal of Obstetrics & Gynaecology 101(5): 398-403.

Goldberg, I. J. (2001). "Diabetic dyslipidemia: causes and consequences." The Journal of Clinical Endocrinology & Metabolism 86(3): 965-971.

Gong, H., L. Sun, B. Chen, Y. Han, J. Pang, W. Wu, R. Qi and T. M. Zhang (2016). "Evaluation of candidate reference genes for RT-qPCR studies in three metabolism related tissues of mice after caloric restriction." Sci Rep 6: 38513.

Greminger, A. R., D. L. Lee, P. Shrager and M. Mayer-Pröschel (2014). "Gestational Iron Deficiency Differentially Alters the Structure and Function of White and Gray Matter Brain Regions of Developing Rats–3." The Journal of nutrition 144(7): 1058-1066.

Gupta, I. R., M. Lapointe and O. H. Yu (2003). "Morphogenesis during mouse embryonic kidney explant culture." Kidney Int 63(1): 365-376.

Haider, B. A., I. Olofin, M. Wang, D. Spiegelman, M. Ezzati and W. W. Fawzi (2013). "Anaemia, prenatal iron use, and risk of adverse pregnancy outcomes: systematic review and meta-analysis." Bmj 346: f3443.

Hammerman, M. (2002). Method of preserving metanephroi in vitro prior to transplantation, Google Patents.

Hartman, H. A., H. L. Lai and L. T. Patterson (2007). "Cessation of renal morphogenesis in mice." Developmental biology 310(2): 379-387.

Heliot, C., A. Desgrange, I. Buisson, R. Prunskaite-Hyyryläinen, J. Shan, S. Vainio, M. Umbhauer and S. Cereghini (2013). "HNF1B controls proximal-intermediate nephron segment identity in vertebrates by regulating Notch signalling components and Irx1/2." Development 140(4): 873-885.

Hendrickx, A. G., G. W. Stone, R. V. Henrickson and K. Matayoshi (1979). "Teratogenic effects of hyperthermia in the bonnet monkey (Macaca radiata)." Teratology 19(2): 177-182.

Hendzel, M. J., Y. Wei, M. A. Mancini, A. Van Hooser, T. Ranalli, B. R. Brinkley, D. P. Bazett-Jones and C. D. Allis (1997). "Mitosis-specific phosphorylation of histone H3 initiates primarily within pericentromeric heterochromatin during G2 and spreads in an ordered fashion coincident with mitotic chromosome condensation." Chromosoma 106(6): 348-360.

Hershko, C. (2007). "Cell-cycle regulation by iron depletion." Blood 110(2): 474-475.

Hill, N. R., S. T. Fatoba, J. L. Oke, J. A. Hirst, C. A. O'Callaghan, D. S. Lasserson and F. R. Hobbs (2016). "Global prevalence of chronic kidney disease–a systematic review and meta-analysis." PLoS One 11(7): e0158765.

Hokke, S. N., J. A. Armitage, V. G. Puelles, K. M. Short, L. Jones, I. M. Smyth, J. F. Bertram and L. A. Cullen-McEwen (2013). "Altered ureteric branching morphogenesis and nephron endowment in offspring of diabetic and insulin-treated pregnancy." PloS one 8(3): e58243.

Hoy, W. E., M. Rees, E. Kile, J. D. Mathews and Z. Wang (1999). "A new dimension to the Barker hypothesis: low birthweight and susceptibility to renal disease." Kidney international 56(3): 1072-1077.

Hughson, M., R. Douglas-Denton, J. Bertram and W. Hoy (2006). "Hypertension, glomerular number, and birth weight in African Americans and white subjects in the southeastern United States." Kidney international 69(4): 671-678.

Hughson, M., A. B. Farris, R. Douglas-Denton, W. E. Hoy and J. F. Bertram (2003). "Glomerular number and size in autopsy kidneys: the relationship to birth weight." Kidney international 63(6): 2113-2122.

Iglesias, D. M., P.-A. Hueber, L. Chu, R. Campbell, A.-M. Patenaude, A. J. Dziarmaga, J. Quinlan, O. Mohamed, D. Dufort and P. R. Goodyer (2007). "Canonical WNT signaling during kidney development." American Journal of Physiology-Renal Physiology 293(2): F494-F500.

Jones, G. R. and E.-M. Lim (2003). "The National Kidney Foundation guideline on estimation of the glomerular filtration rate." The Clinical Biochemist Reviews 24(3): 95.

Kanguru, L., N. Bezawada, J. Hussein and J. Bell (2014). "The burden of diabetes mellitus during pregnancy in low-and middle-income countries: a systematic review." Global health action 7(1): 23987.

Kanwar, Y. S., S. Akagi, B. Nayak, L. Sun, J. Wada, P. Xie, A. Thakur, S. S. Chugh and F. R. Danesh (2005). "Renal-specific oxidoreductase biphasic expression under high glucose ambience during fetal versus neonatal development." Kidney international 68(4): 1670-1683.

Kanwar, Y. S., Z. Z. Liu, A. Kumar, M. I. Usman, J. Wada and E. I. Wallner (1996). "D-glucose-induced dysmorphogenesis of embryonic kidney." Journal of Clinical Investigation 98(11): 2478.

Kanwar, Y. S., B. Nayak, S. Lin, S. Akagi, P. Xie, J. Wada, S. S. Chugh and F. R. Danesh (2005). "Hyperglycemia: its imminent effects on mammalian nephrogenesis." Pediatric nephrology 20(7): 858-866.

Kasper, D., A. Fauci, S. Hauser, D. Longo, J. Jameson and J. Loscalzo (2015). "Harrison's principles of internal medicine, 19e." USA2015.

Kearney, P. M., M. Whelton, K. Reynolds, P. Muntner, P. K. Whelton and J. He (2005). "Global burden of hypertension: analysis of worldwide data." The lancet 365(9455): 217-223.

Keijzer-Veen, M. G., M. Schrevel, M. J. Finken, F. W. Dekker, J. Nauta, E. T. Hille, M. Frölich, B. J. van der Heijden and D. P.-C. S. Group (2005). "Microalbuminuria and lower glomerular filtration rate at young adult age in subjects born very premature and after intrauterine growth retardation." Journal of the American Society of Nephrology 16(9): 2762-2768.

Keller, G., G. Zimmer, G. Mall, E. Ritz and K. Amann (2003). "Nephron number in patients with primary hypertension." New England Journal of Medicine 348(2): 101-108.

Kopan, R., H.-T. Cheng and K. Surendran (2007). "Molecular insights into segmentation along the proximal–distal axis of the nephron." Journal of the American Society of Nephrology 18(7): 2014-2020.

Kozyraki, R., J. Fyfe, P. J. Verroust, C. Jacobsen, A. Dautry-Varsat, J. Gburek, T. E. Willnow, E. I. Christensen and S. K. Moestrup (2001). "Megalin-dependent cubilin-mediated endocytosis is a major pathway for the apical uptake of transferrin in polarized epithelia." Proceedings of the National Academy of Sciences 98(22): 12491-12496.

Kumar, A., A. K. Rai, S. Basu, D. Dash and J. S. Singh (2008). "Cord blood and breast milk iron status in maternal anemia." Pediatrics 121(3): e673-677.

Lackland, D. T. and M. A. Weber (2015). "Global burden of cardiovascular disease and stroke: hypertension at the core." Canadian Journal of Cardiology 31(5): 569-571.

Landschulz, W., I. Thesleff and P. Ekblom (1984). "A lipophilic iron chelator can replace transferrin as a stimulator of cell proliferation and differentiation." The Journal of cell biology 98(2): 596-601.

Langley-Evans, S. C., S. J. Welham and A. A. Jackson (1999). "Fetal exposure to a maternal low protein diet impairs nephrogenesis and promotes hypertension in the rat." Life sciences 64(11): 965-974.

Law, C., D. Barker, A. Bull and C. Osmond (1991). "Maternal and fetal influences on blood pressure." Archives of disease in childhood 66(11): 1291-1295.

Lelièvre-Pégorier, M., J. Vilar, M.-L. Ferrier, E. Moreau, N. Freund, T. Gilbert and C. Merlet-Bénichou (1998). "Mild vitamin A deficiency leads to inborn nephron deficit in the rat." Kidney international 54(5): 1455-1462.

Lewis, R., C. Petry, S. Ozanne and C. Hales (2001). "Effects of maternal iron restriction in the rat on blood pressure, glucose tolerance, and serum lipids in the 3-month-old offspring." Metabolism-Clinical and Experimental 50(5): 562-567.

Lewis, R. M., A. J. Forhead, C. J. Petry, S. E. Ozanne and C. N. Hales (2002). "Long-term programming of blood pressure by maternal dietary iron restriction in the rat." Br J Nutr 88(3): 283-290.

Lisle, S. J., R. M. Lewis, C. J. Petry, S. E. Ozanne, C. N. Hales and A. J. Forhead (2003). "Effect of maternal iron restriction during pregnancy on renal morphology in the adult rat offspring." Br J Nutr 90(1): 33-39.

Liu, J., F. Edgington-Giordano, C. Dugas, A. Abrams, P. Katakam, R. Satou and Z. Saifudeen (2017). "Regulation of nephron progenitor cell self-renewal by intermediary metabolism." Journal of the American Society of Nephrology 28(11): 3323-3335.

Liyanage, T., T. Ninomiya, V. Jha, B. Neal, H. M. Patrice, I. Okpechi, M.-h. Zhao, J. Lv, A. X. Garg and J. Knight (2015). "Worldwide access to treatment for end-stage kidney disease: a systematic review." The Lancet 385(9981): 1975-1982.

Mamo, S., A. B. Gal, S. Bodo and A. Dinnyes (2007). "Quantitative evaluation and selection of reference genes in mouse oocytes and embryos cultured in vivo and in vitro." BMC Dev Biol 7: 14.

Mañalich, R., L. Reyes, M. Herrera, C. Melendi and I. Fundora (2000). "Relationship between weight at birth and the number and size of renal glomeruli in humans: a histomorphometric study." Kidney international 58(2): 770-773.

McCarthy, E., L. Kenny, J. O. B. Hourihane, A. Irvine, D. Murray and M. Kiely (2017). "Impact of maternal, antenatal and birth-associated factors on iron stores at birth: data from a prospective maternal–infant birth cohort." European journal of clinical nutrition 71(6): 782.

McLaren, A. (1961). "Some causes of variation of body temperature in mice." Experimental Physiology 46(1): 38-45.

Michos, O. (2009). "Kidney development: from ureteric bud formation to branching morphogenesis." Current opinion in genetics & development 19(5): 484-490.

Moeller, M. J., S. K. Sanden, A. Soofi, R. C. Wiggins and L. B. Holzman (2003). "Podocyte-specific expression of cre recombinase in transgenic mice." genesis 35(1): 39-42.

Morrison, J. L. (2008). "Sheep models of intrauterine growth restriction: fetal adaptations and consequences." Clinical and Experimental Pharmacology and Physiology 35(7): 730-743.

Muzumdar, M. D., B. Tasic, K. Miyamichi, L. Li and L. Luo (2007). "A global double-fluorescent Cre reporter mouse." genesis 45(9): 593-605.

Nehiri, T., J.-P. D. Van Huyen, M. Viltard, C. Fassot, D. Heudes, N. Freund, G. Deschênes, P. Houillier, P. Bruneval and M. Lelièvre-Pégorier (2008). "Exposure to maternal diabetes induces salt-sensitive hypertension and impairs renal function in adult rat offspring." Diabetes 57(8): 2167-2175.

Nelson, R. G., H. Morgenstem and P. H. Bennett (1998). "Birth weight and renal disease in Pima Indians with type 2 diabetes mellitus." American journal of epidemiology 148(7): 650-656.

Nelson, R. G., H. Morgenstern and P. H. Bennett (1998). "Intrauterine diabetes exposure and the risk of renal disease in diabetic Pima Indians." Diabetes 47(9): 1489-1493.

New, D., P. Coppola and S. Terry (1973). "Culture of explanted rat embryos in rotating tubes." Journal of reproduction and fertility 35(1): 135-138.

Nurtjahja-Tjendraputra, E., D. Fu, J. M. Phang and D. R. Richardson (2007). "Iron chelation regulates cyclin D1 expression via the proteasome: a link to iron deficiency–mediated growth suppression." Blood 109(9): 4045-4054.

Orban, P. C., D. Chui and J. D. Marth (1992). "Tissue-and site-specific DNA recombination in transgenic mice." Proceedings of the National Academy of Sciences 89(15): 6861-6865.

Packard, A., K. Georgas, O. Michos, P. Riccio, C. Cebrian, A. N. Combes, A. Ju, A. Ferrer-Vaquer, A.-K. Hadjantonakis and H. Zong (2013). "Luminal mitosis drives epithelial cell dispersal within the branching ureteric bud." Developmental cell 27(3): 319-330.

Park, J.-S., M. T. Valerius and A. P. McMahon (2007). "Wnt/β-catenin signaling regulates nephron induction during mouse kidney development." Development 134(13): 2533-2539.

Peterson, C., S. D. Grosse, R. Li, A. J. Sharma, H. Razzaghi, W. H. Herman and S. M. Gilboa (2015). "Preventable health and cost burden of adverse birth outcomes associated with pregestational diabetes in the United States." American journal of obstetrics and gynecology 212(1): 74. e71-74. e79.

Petry, C. D., M. A. Eaton, J. D. Wobken, M. M. Mills, D. E. Johnson and M. K. Georgieff (1992). "Iron deficiency of liver, heart, and brain in newborn infants of diabetic mothers." The Journal of pediatrics 121(1): 109-114.

Philpott, E. K., J. A. Englund, J. Katz, J. Tielsch, S. Khatry, S. C. LeClerq, L. Shrestha, J. Kuypers, A. S. Magaret and M. C. Steinhoff (2017). Febrile Rhinovirus Illness During Pregnancy Is Associated With Low Birth Weight in Nepal. Open forum infectious diseases, Oxford University Press.

Puelles, V. G., W. E. Hoy, M. D. Hughson, B. Diouf, R. N. Douglas-Denton and J. F. Bertram (2011). "Glomerular number and size variability and risk for kidney disease." Current opinion in nephrology and hypertension 20(1): 7-15.

Quinlan, J., M. Lemire, T. Hudson, H. Qu, A. Benjamin, A. Roy, E. Pascuet, M. Goodyer, C. Raju and Z. Zhang (2007). "A common variant of the PAX2 gene is associated with reduced newborn kidney size." Journal of the American Society of Nephrology 18(6): 1915-1921.

Ramos-Arroyo, M., E. Rodriguez-Pinilla and J. Cordero (1992). "Maternal diabetes: the risk for specific birth defects." European journal of epidemiology 8(4): 503-508.

Russell, W. M. S., R. L. Burch and C. W. Hume (1959). "The principles of humane experimental technique."

Sadler, T., L. Phillips, W. Balkan and S. Goldstein (1986). "Somatomedin inhibitors from diabetic rat serum alter growth and development of mouse embryos in culture." Diabetes 35(8): 861-865.

Salvesen, D. R., J. M. Brudenell, R. J. Snijders, R. M. Ireland and K. H. Nicolaides (1993). "Fetal plasma erythropoietin in pregnancies complicated by maternal diabetes mellitus." American journal of obstetrics and gynecology 168(1): 88-94.

Salvesen, D. R., M. J. Brudenell and K. H. Nicolaides (1992). "Fetal polycythemia and thrombocytopenia in pregnancies complicated by maternal diabetes mellitus." American journal of obstetrics and gynecology 166(4): 1287-1293.

Sanyanusin, P., L. A. McNoe, M. J. Sullivan, R. G. Weaver and M. R. Eccles (1995). "Mutation of PAX2 in two siblings with renal-coloboma syndrome." Human molecular genetics 4(11): 2183-2184.

Sariola, H. and M. Saarma (2003). "GDNF and its receptors in the regulation of the ureteric branching." International Journal of Developmental Biology 43(5): 413-418.

Saxen, L. and E. Lehtonen (1987). "Embryonic kidney in organ culture." Differentiation 36(1): 2-11.

Schmidt-Ott, K. M. and J. Barasch (2008). "WNT/β-catenin signaling in nephron progenitors and their epithelial progeny." Kidney international 74(8): 1004-1008.

Shiota, K. (1988). "Induction of neural tube defects and skeletal malformations in mice following brief hyperthermia in utero." Neonatology 53(2): 86-97.

Siddappa, A. M., R. Rao, J. D. Long, J. A. Widness and M. K. Georgieff (2007). "The assessment of newborn iron stores at birth: a review of the literature and standards for ferritin concentrations." Neonatology 92(2): 73-82.

Singh, R. R., K. M. Moritz, J. F. Bertram and L. A. Cullen-McEwen (2007). "Effects of dexamethasone exposure on rat metanephric development: in vitro and in vivo studies." American Journal of Physiology-Renal Physiology 293(2): F548-F554.

Song, S., T. Christova, S. Perusini, S. Alizadeh, R.-Y. Bao, B. W. Miller, R. Hurren, Y. Jitkova, M. Gronda and M. Isaac (2011). "Wnt inhibitor screen reveals iron dependence of β-catenin signaling in cancers." Cancer research: canres. 2745.2011.

Steel, N. (2017). "Global, regional, and national age-sex specific mortality for 264 causes of death, 1980–2016: a systematic analysis for the Global Burden of Disease Study 2016." Lancet 390(10100): 1151-1210.

Sternberg, N. and D. Hamilton (1981). "Bacteriophage P1 site-specific recombination: I. Recombination between loxP sites." Journal of molecular biology 150(4): 467-486.

Stevenson, R. E. (2015). Human malformations and related anomalies, Oxford University Press.

Styrud, J., L. Thunberg, O. Nybacka and U. J. Eriksson (1995). "Correlations between maternal metabolism and deranged development in the offspring of normal and diabetic rats." Pediatric research 37(3): 343.

Sun, M. Y., J. C. Woolley, S. E. Blohowiak, Z. R. Smith, A. M. Siddappa, R. R. Magness and P. J. Kling (2017). "Dietary-induced gestational iron deficiency inhibits postnatal tissue iron delivery and postpones the cessation of active nephrogenesis in rats." Reproduction, Fertility and Development 29(5): 855-866.

Swali, A., S. McMullen, H. Hayes, L. Gambling, H. J. McArdle and S. C. Langley-Evans (2012). "Processes underlying the nutritional programming of embryonic development by iron deficiency in the rat." PLoS One 7(10): e48133.

Sweet, D., G. Savage, T. Tubman, T. Lappin and H. Halliday (2001). "Study of maternal influences on fetal iron status at term using cord blood transferrin receptors." Archives of Disease in Childhood-Fetal and Neonatal Edition 84(1): F40-F43.

Swetha, K., P. Tarakeswararao and M. Saisunilkishore (2017). "Relationship between maternal iron and cord blood iron status: A prospective study." Indian Journal of Child Health 4(4): 595-598.

Taricco, E., T. Radaelli, G. Rossi, M. Nobile de Santis, G. Bulfamante, L. Avagliano and I. Cetin (2009). "Effects of gestational diabetes on fetal oxygen and glucose levels in vivo." BJOG: An International Journal of Obstetrics & Gynaecology 116(13): 1729-1735.

Thesleff, I. and P. Ekblom (1984). "Role of transferrin in branching morphogenesis, growth and differentiation of the embryonic kidney." Development 82(1): 147-161.

Tran, S., Y.-W. Chen, I. Chenier, J. S. Chan, S. Quaggin, M.-J. Hébert, J. R. Ingelfinger and S.-L. Zhang (2008). "Maternal diabetes modulates renal morphogenesis in offspring." Journal of the American Society of Nephrology 19(5): 943-952.

Trowell, O. (1954). "A modified technique for organ culture in vitro." Experimental cell research 6(1): 246-248.

Van Zutphen, A. R., S. Lin, B. A. Fletcher and S.-A. Hwang (2012). "A population-based case–control study of extreme summer temperature and birth defects." Environmental health perspectives 120(10): 1443.

Waller, D. K., S. S. Hashmi, A. T. Hoyt, H. T. Duong, S. C. Tinker, M. S. Gallaway, R. S. Olney, R. H. Finnell, J. T. Hecht and M. A. Canfield (2018). "Maternal report of fever from cold or flu during early pregnancy and the risk for noncardiac birth defects, National Birth Defects Prevention Study, 1997–2011." Birth defects research 110(4): 342-351.

Wang, X. and M. R. Garrett (2017). "Nephron number, hypertension, and CKD: physiological and genetic insight from humans and animal models." Physiological Genomics 49(3): 180-192.

Warkany, J. (1986). "Hyperthermia." Teratology 33(3): 365-371.

White, S. L., V. Perkovic, A. Cass, C. L. Chang, N. R. Poulter, T. Spector, L. Haysom, J. C. Craig, I. Al Salmi and S. J. Chadban (2009). "Is low birth weight an antecedent of CKD in later life? A systematic review of observational studies." American Journal of Kidney Diseases 54(2): 248-261.

Xu, J., H. Liu, J.-S. Park, Y. Lan and R. Jiang (2014). "Osr1 acts downstream of and interacts synergistically with Six2 to maintain nephron progenitor cells during kidney organogenesis." Development 141(7): 1442-1452.

Zhang, C. (2014). "Essential functions of iron-requiring proteins in DNA replication, repair and cell cycle control." Protein & cell 5(10): 750-760.

Zhang, S.-L., Y.-W. Chen, S. Tran, I. Chenier, M.-J. Hebert and J. R. Ingelfinger (2007). "Reactive oxygen species in the presence of high glucose alter ureteric bud morphogenesis." Journal of the American Society of Nephrology 18(7): 2105-2115.

Zhao, X.-P., M.-C. Liao, S.-Y. Chang, S. Abdo, Y. Aliou, I. Chenier, J. R. Ingelfinger and S.-L. Zhang (2014). "Maternal diabetes modulates kidney formation in murine progeny: the role of hedgehog interacting protein (HHIP)." Diabetologia 57(9): 1986-1996.

Ziaei, A., M. R. P. Ardakani, M.-S. Hashemi, M. Peymani, K. Ghaedi, H. Baharvand and M. H. Nasr-Esfahani (2015). "Acute course of deferoxamine promoted neuronal differentiation of neural progenitor cells through suppression of Wnt/β-catenin pathway: a novel efficient protocol for neuronal differentiation." Neuroscience letters 590: 138-144.

Zoetis, T. and M. E. Hurtt (2003). "Species comparison of anatomical and functional renal development." Birth Defects Research Part B: Developmental and Reproductive Toxicology 68(2): 111-120.

# 13. Erklärung des Eigenanteils

Die Forschungsarbeit „Effects of Environmental Conditions on Nephron Number: Modeling Maternal Disease and Epigenetic Regulation in Renal Development“ wurde im April 2021 im International Journal of Molecular Sciences veröffentlicht. Die Eigenanteile der veröffentlichten Arbeit verteilten sich wie folgt:

Die Konzeption der Forschungsarbeit erfolgte durch Dr. rer. nat. Nicola Wanner, Lars Fuhrmann und Prof. Dr. med. Tobias Huber. Eigenanteil: Konzeption im Bereich der Modellierung von Hyperthermie und Eisenmangel.

Die Versuchsplanung, Durchführung und Auswertung erfolgte durch Saskia Lindner, L. Fuhrmann, Clemens Höse, Priv.-Doz Dr. med. Oliver Kretz, N. Wanner und T. Huber. Eigenanteil: Planung, Durchführung und Auswertung im Bereich der Modellierung von Diabetes (geteilt mit S.Lindner), Hyperthermie und Eisenmangel.

Die Resourcenaquise für die Versuche erfolgte durch Dr. Alexander Hauser, Dr. Manfred Jung, Priv. Doz. Dr. rer. nat. Maja Lindenmeyer, Prof. Dr. Wolfgang Sippl und Prof. Dr. med. Clemens Cohen.

Das Schreiben des ersten Manuskripentwurfs erfolgte durch N. Wanner und L. Fuhrmann. Eigenanteil: Anteiliges Schreiben der Einleitung, des Ergebnisteils und der Diskussion im Bereich der Modellierung von Diabetes, Hyperthermie und Eisenmangel

Die Weiterentwicklung des Manuskriptentwurfts erfolgte durch T. Huber, L. Fuhrmann, O. Kretz, M. Lindenmeyer, W. Sippl und N. Wanner. Eigenanteil: Weiterentwicklung der Bereiche wie zuvor für den ersten Manuskriptentwurf genannt.

Die Erstellung der Visualisierungen erfolgte durch S. Lindner, L. Fuhrmann, C. Höse, O. Kretz und N. Wanner. Eigenanteil: Erstellung der Bilder und Diagramme im Bereich der Modellierung von Hyperthermie und Eisenmangel.

Die Supervision und Betreuung erfolgten durch T. Huber und N. Wanner.

Die Förderungsaquise erfolgte durch T. Huber, O. Kretz, M. Jung, M. Lindenmeyer und N. Wanner.

# 14. Lebenslauf

**Lebenslauf wurde aus datenschutzrechtlichen Gründen entfernt**

# 15. Danksagung

**Ohne die Unterstützung vieler Personen wäre diese Arbeit nicht möglich gewesen. Ich danke an dieser Stelle besonders herzlich:**

Meinem Doktorvater Prof. Dr. Tobias Huber für die kraftvolle Unterstützung dieser Arbeit in jeglicher Hinsicht – insbesondere für seine ansteckende Begeisterung, seine Offenheit für neue Vorhaben innerhalb des Projektes, seinen Einsatz bezüglich meines Stipendiums und der nahtlosen Begleitung der Arbeit nach seinem Ruf nach Hamburg.

Meiner Betreuerin Dr. rer. nat. Nicola Wanner, deren detaillierte und andauernde Beratung und Hilfe in Wort und Tat sich jeder Aufzählung entzieht und für diese Arbeit unentbehrlich war.

Saskia Lindner für ihre exzellente Vorarbeit im Bereich der Nierenkultur und ex vivo Diabetesmodellierung.

Allen Kolleginnen und Kollegen der AG Huber für die vielseitige Hilfe und die angenehme Arbeitsatmosphäre.

Prof. Dr. Lutz Hein für seinen enge Auseinandersetzung mit dem Projekt und seine fundierten Ratschläge, die uns geholfen haben wichtige Weichenstellungen richtig zu treffen.

Prof. Dr. Manfred Jung und den Mitarbeiterinnen und Mitarbeitern seiner Arbeitsgruppe für ihre Kooperation im Bereich der epigenetischen Veränderungen in den Nierenkulturen.

Prof. Dr. Heike L. Pahl und Prof. Dr. Robert Thimme für die Förderung und Begleitung im Rahmen des MOTIVATE-Promotionskollegs der Universität Freiburg.

Dr. Andreas Eizinger für die lehrreichen Kollegs-Seminare und vielen guten Rat.

Des Weiteren danke ich: Käthe, meinen Eltern und meinem Bruder Arne.

# 16. Eidesstattliche Versicherung

Ich versichere ausdrücklich, dass ich die Arbeit selbständig und ohne fremde Hilfe verfasst, andere als die von mir angegebenen Quellen und Hilfsmittel nicht benutzt und die aus den benutzten Werken wörtlich oder inhaltlich entnommenen Stellen einzeln nach Ausgabe (Auflage und Jahr des Erscheinens), Band und Seite des benutzten Werkes kenntlich gemacht habe.

Ferner versichere ich, dass ich die Dissertation bisher nicht einem Fachvertreter an einer anderen Hochschule zur Überprüfung vorgelegt oder mich anderweitig um Zulassung zur Promotion beworben habe.

Ich erkläre mich einverstanden, dass meine Dissertation vom Dekanat der Medizinischen Fakultät mit einer gängigen Software zur Erkennung von Plagiaten überprüft werden kann.

Unterschrift: .....